AD-A069 004 CASE WESTERN RESERVE UNIV CLEVELAND OHIO DEPT OF MET--ETC F/G 11/2
USE OF NUCLEARMICROANALYSIS. PART II. NUCLEAR MICROANALYSIS OF --ETC(U)
AUG 78 A R COOPER, L D MAJOR F33615-74-C-4029
UNCLASSIFIED AFML-TR-78-119-PT-2 NL

1 OF 3
AD
AD-A069004

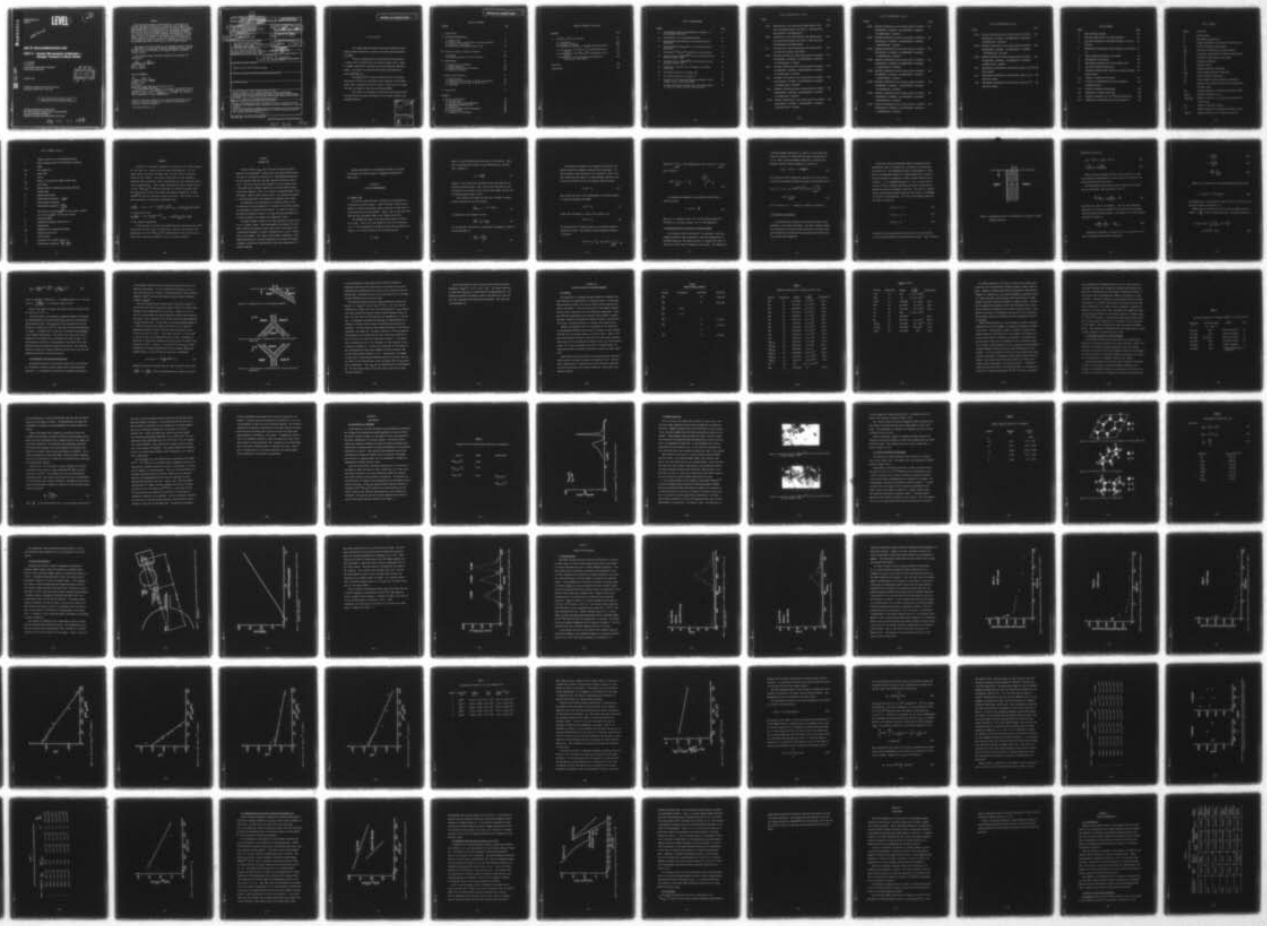

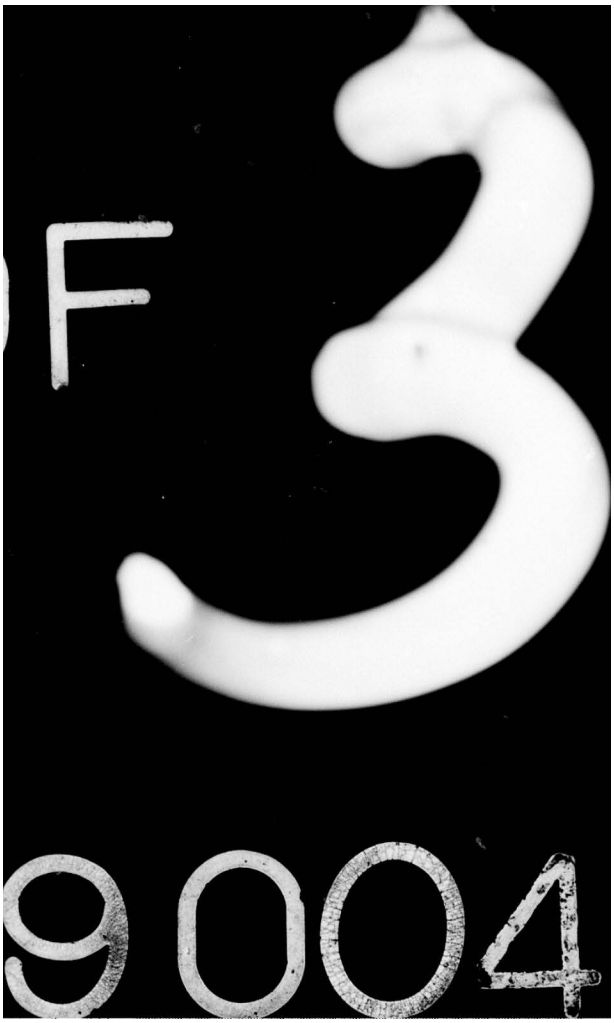
F
3
9004

AFML-TR-78-119
Part II

LEVEL III

2

A069003

USE OF NUCLEARMICROANALYSIS

PART II — Nuclear Microanalysis of Materials — Nitrogen Transport in Silicon Nitride

A. R. COOPER
L. E. MAJOR
CASE WESTERN RESERVE UNIVERSITY
CLEVELAND, OHIO 44106

AUGUST 1978

TECHNICAL REPORT AFML-TR-78-119, Part II
Final Report, October 1973 – June 1977

AIR FORCE MATERIALS LABORATORY
AIR FORCE WRIGHT AERONAUTICAL LABORATORIES
AIR FORCE SYSTEMS COMMAND
WRIGHT-PATTERSON AIR FORCE BASE, OHIO 45433

NOTICE

When Government drawings, specifications, or other data are used for any purpose other than in connection with a definitely related Government procurement operation, the United States Government thereby incurs no responsibility nor any obligation whatsover; and the fact that the government may have formulated, furnished, or in any way supplied the said drawings, specifications, or other data, is not to be regarded by implication or otherwise as in any manner licensing the holder or any other person or corporation, or conveying any rights or permission to manufacture, use, or sell any patented invention that may in any way be related thereto.

This report has been reviewed by the Information Office (OI) and is releasable to the National Technical Information Service (NTIS). At NITS, it will be available to the general public, including foreign nations.

This technical report has been reviewed and is approved for publication.

Henry C. Graham

HENRY C. GRAHAM
Project Engineer

FOR THE COMMANDER

Norman M. Geyer

NORMAN M. GEYER
Acting Chief
Processing & High Temperature Materials Branch
Metals and Ceramics Division

"If your address has changed, if you wish to be removed from our mailing list, or if the addressee is no longer employed by your organization please notify AFML/LLM, W_PAFB, OH 45433 to help us maintain a current mailing list".

Copies of this report should not be returned unless return is required by security considerations, contractual obligations, or notice on a specific document.

AIR FORCE/56780/11 May 1979 — 100

SECURITY CLASSIFICATION OF THIS PAGE (When Data Entered)

REPORT DOCUMENTATION PAGE

READ INSTRUCTIONS BEFORE COMPLETING FORM

1. REPORT NUMBER: AFML-TR-78-119 PART II
2. GOVT ACCESSION NO.
3. RECIPIENT'S CATALOG NUMBER

4. TITLE (and Subtitle): USE OF NUCLEARMICROANALYSIS - PART II. NUCLEAR MICROANALYSIS OF MATERIALS-NITROGEN TRANSPORT IN SILICON NITRIDE.
5. TYPE OF REPORT & PERIOD COVERED: Final Report. 1 Oct 73-30 Jun 77
6. PERFORMING ORG. REPORT NUMBER

7. AUTHOR(s): A. R. Cooper, Leslie Dean Major, Jr
8. CONTRACT OR GRANT NUMBER(s): F33615-74-C-4029

9. PERFORMING ORGANIZATION NAME AND ADDRESS: Case Western Reserve University, Department of Metallurgy & Materials Sci., Cleveland, Ohio 44106
10. PROGRAM ELEMENT, PROJECT, TASK AREA & WORK UNIT NUMBERS: 2306-P3-02 P3

11. CONTROLLING OFFICE NAME AND ADDRESS: Air Force Materials Laboratory (LLM), Air Force Wright Aeronautical Laboratories (AFSC), Wright-Patterson AF Base, Ohio 45433
12. REPORT DATE: August 1978
13. NUMBER OF PAGES: 209

14. MONITORING AGENCY NAME & ADDRESS (if different from Controlling Office)
15. SECURITY CLASS. (of this report): Unclassified
15a. DECLASSIFICATION/DOWNGRADING SCHEDULE

16. DISTRIBUTION STATEMENT (of this Report)

Approved for public release; distribution unlimited.

17. DISTRIBUTION STATEMENT (of the abstract entered in Block 20, if different from Report)

18. SUPPLEMENTARY NOTES

19. KEY WORDS (Continue on reverse side if necessary and identify by block number)

Nitrogen diffusion, grain boundary diffusion, Nuclear Microanalysis, Silicon Nitride, Particle Induced X-Ray Emission, Rutherford Backscattering, Channeling, Particle Induced Nuclea-Reactions, Nuclear Reaction Cross Section, Nitriding, $^{15}N(p,\alpha_0)\,^{12}C$ differential cross section.

20. ABSTRACT (Continue on reverse side if necessary and identify by block number)

Nitrogen self-diffusiuitres have been measured in both the grains and grain boundaries of hot-pressed silicon nitride by the direct observation of a nuclear reaction.

Nuclear microanalytical techniques and their utilization in the field of materials, and the calculation and measurement of a nuclear differential reaction cross section are also included.

DD FORM 1 JAN 73 1473 EDITION OF 1 NOV 65 IS OBSOLETE

SECURITY CLASSIFICATION OF THIS PAGE (When Data Entered)

405 321

F O R E W O R D

This report describes part of the study conducted at Case Western Reserve University, Cleveland, Ohio under Contract F33615-74-C-4029.

The work reported herein was performed during the period 1 October 1973 to 30 June 1977, the contract moniter was Dr. Henry C. Graham, Acting Chief, Processing and High Temperature Materials Branch. The report is essentially the doctoral Dissertation of Leslie Dean Major, Jr.

The authors wish to thank Professors Philip R. Bevington and Harvey B. Willard for assistance in the reduction of the experimental data. We would also like to thank H. Yinnon and K.P.R. Reddy for their assistance in carrying out the experiments.

This report is the second of a two part series dealing with the application of nuclear microanalysis for studying oxidation and nitrogen diffusion.

TABLE OF CONTENTS

TABLE OF CONTENTS (continued)

LIST OF ILLUSTRATIONS

List of Illustrations (con't)

LIST OF ILLUSTRATIONS (cont'd)

LIST OF ILLUSTRATIONS (cont'd)

LIST OF TABLES

LIST OF SYMBOLS

SYMBOL	DEFINITION
A	Nucleon number
C	Fractional concentration
$\bar{C}$	Average fractional concentration with respect to y
C_0	Initial fractional concentration
C_{GB}	Fractional concentration in grain boundary
C_V	Fractional concentration in volume (within grains)
C_e	Fractional concentration in gas phase
D	Diffusion coefficient
D_0	Frequency factor
D_C	Chemical diffusion coefficient
D_{GB}	Grain boundary diffusion coefficient
D_T	Tracer diffusion coefficient
D_V	Volume (single crystal) diffusion coefficient
E	Energy of the incident particle in the appropriate reference frame
E_0	Resonant energy in the laboratory reference frame
$E_i(x_j)$	Energy of particle i at x_j
$E_i(x_j,x_k)$	Energy of particle i at x_j which was scattered or created at x_k
E_S	Energy of scattered particle
E_λ	Channel energy in the laboratory reference frame
$F_\ell(\eta,\rho)$	Regular solution to the radial wave equation

$G_\ell(\eta,\rho)$	Irregular solution to the radial wave equation
I,I'	Intrinsic spin of the target nucleus and recoil nucleus respectively
J	Total angular momentum
J_0	Total angular momentum of a particular nuclear energy level
$\vec{J}$	Flux of diffusing species
$K(m,m_1,\theta),K_{m_1}$	Kinematic factor for scattering a particle of mass m from a target of mass m_1 at a laboratory scattering angle θ
K_S	Surface-exchange coefficient
N	Number density
N_0	Number of observed counts
$[N_0]$	Distorted spectrum
$P(E_i,E_j)$	Spreading function
P_A	Applied stress
$P_L(\text{Cos }\theta)$	Legendre polynomial
Q	Energy equivalent to the rest mass difference between the reactant and product nuclei
Q^*	Activation energy
R	Gas constant = 8.31434 J-mole^{-1}-K^{-1}
S	Scattering matrix
T	Temperature
V	Volume transported per atom
Z	Atomic number

a	Grain size
a	Activity of i
b	Penetration depth
$\frac{d\rho}{dt}$	Rate of densification
$(\frac{d\sigma(\theta)}{d\Omega})_{lab}$	Differential cross section
g_α	Real quantity related to the partial width of channel α
i,i'	Intrinsic spin of the incident and emitted particle
j	Integrated flux of particles
k	Wave number
k_{eg}	Equilibrium constant for reaction
m_i	Atomic mass of species i in u
n	Principal Quantum Number
p	Density
r	Interparticle separation
r_0	1.3×10^{-15} m
r_α	Screening radii for the Coulomb field in channel α
s,s'	Incoming and outgoing channel spins respectively
t	Time
w	Dummy variable of integration
x	Distance perpendicular to sample surface
y	Distance parallel to sample surface
z	Distance parallel to sample surface
ℓ,ℓ'	Orbital angular momentum of the incoming and outgoing channels respectively

ν	Relative velocity of the colliding particles
Γ	Total resonance width in the laboratory reference frame
ΔG_i	Free energy of i
Δ_λ	Level shift
π	Parity
π_0	Parity of a particular nuclear energy level
Ω	Solid angle
α,α'	Channel index of incoming and outgoing channels respectively.
β	Resonant phase shift
γ	Dimensionless parameter $= \frac{x}{(D_v t)^{\frac{1}{2}}}$
δ	Grain boundary thickness
ρ	Dimensionless parameter $= \frac{y-\frac{1}{2}\delta}{(D_v t)^{\frac{1}{2}}}$
η	Term equal to $0.1574\ Z_a Z_\chi m_a^{\frac{1}{2}} E^{-\frac{1}{2}}$ for the incident channel and $0.1574\ Z_b Z_\gamma (\frac{\mu}{E'})^{\frac{1}{2}}$ for the exit channel
θ	Scattering angle
$\lambda\!\!\!^{-}$	deBroglie wavelength (divided by 2π)
μ	Reduced mass
ξ_ℓ	Phaseshift for potential scattering
ρ	Parameter given as kr
σ	Cross section
σ_ℓ	Phaseshift for Coulomb scattering
τ	Dimesnionless parameter $= \frac{D_{GB}}{D_v} \frac{\frac{1}{2}\delta}{(D_v t)^{\frac{1}{2}}}$

SUMMARY

Studies of nitrogen transport in materials has been limited by the lack of a long-lived nitrogen radioisotope. Of the seven known nitrogen isotopes only two are found in nature, and both are stable. The short half-lives of the unstable isotopes have prevented their utilization in the standard radiotracer experiments. This study utilized the direct observation of the $^{15}N(p,\alpha_0)^{12}C$ nuclear reaction to obtain nitrogen self-diffusivities in both the grains and grain boundaries of NORALIDE^{TM} NC-132 hot pressed silicon nitride. The values of the self-diffusion coefficients measured were:

$$D_v\left(\frac{m^2}{sec}\right) = 2.02 \times 10^{-11} \left(^{+4.90 \times 10^{-9}}_{-2.01 \times 10^{-11}}\right)_{exp} - \frac{(3.17 \pm 0.74) \times 10^5}{RT}$$

in the grains, and

$$D_{GB}\left(\frac{m^2}{sec}\right) = 4.09 \left(^{+2.34 \times 10^{6}}_{-4.09}\right)_{exp} - \frac{(5.09 \pm 1.77) \times 10^5}{RT}$$

in the grain boundaries.

A discussion of nuclear microanalytical techniques and their utlization in the field of materials, and the calculation and measurement of the $^{15}N(p,\alpha_0)^{12}C$ differential cross section at a laboratory scattering angle of 165° is also included.

SECTION I

INTRODUCTION

Silicon nitride, Si_3N_4, one of the most interesting ceramic materials to be developed in recent years, has attracted much attention due to its possible utilization as a high-temperature material for gas turbines, bearings, and other advanced structural applications. Silicon nitride has good strength in its hot pressed form, a low coefficient of thermal expansion, and a high thermal conductivity which combine to give it a virtually unsurpassed thermal shock resistance. While it does oxidize readily, its oxidation resistance is relatively good due to the adherent silica-based layer formed.

To date most of the information (1) available about silicon nitride deals with the production of a material with optimum mechanical properties or with the microstructure. In order to better understand the processing kinetics of Si_3N_4, detailed measurements of nitrogen transport are valuable, but incomplete to date.

Nitrogen transport studies in nitrides have been limited by the lack of isotopic tracers. Most measurements (see Chapter III) have been inferred from reaction kinetic data, while a few studies have followed the decrement in isotopic concentration of a gas in contact with a solid sample. This study, to the author's knowledge, is the second application of a nuclear technique to the study of nitrogen transport, and the first application of the direct observation of a nuclear reaction.

Because the author has a considerable interest in nuclear microanalysis and nuclear physics, Appendices are devoted to these topics.

SECTION II

DIFFUSION PHENOMENOLOGY

2.1 General Laws

For the case considered here, diffusion can be regarded as a concentration-leveling process. Tracer diffusion involves the exchange of a marked and unmarked species and hence at least two diffusion equations can be considered. However, due to coupling of the equations only one species needs to be looked at explicity.

The mathematical basis for the diffusion process is found in Fick's laws. Fick's First Law relates the flux of diffusing species, $\vec{J}$ to the concentration gradient of the diffusing species, ∇C, (where C is in atom fraction) by the following equation:

$$\vec{J} = -pD\nabla C \qquad (1)$$

where D is the diffusion coefficient and p is the density. Often one is concerned with diffusion in one direction only, and Equation 1 reduces to:

$$J_x = -pD\left(\frac{\partial C}{\partial x}\right) \tag{2}$$

Equation 1 and 2 agree with the empirical fact that when the concentration gradient goes to zero, the driving force goes to zero. and there are no external forces acting on the sample, the net flux of diffusing species goes to zero.

Fick's Second Law relates the time rate of change in concentration with the flux by the following:

$$\left(\frac{\partial C}{\partial t}\right)_{x,y,z} = -\nabla\vec{J} = \nabla(D\nabla C)_t \tag{3}$$

and reduction to one dimension yields:

$$\left(\frac{\partial C}{\partial t}\right)_x = \frac{\partial}{\partial x}\left(D\,\frac{\partial C}{\partial x}\right)_t \tag{4}$$

If the diffusion coefficient is concentration independent, Equation 4 can be rewritten as:

$$\left(\frac{\partial C}{\partial t}\right)_x = D\left(\frac{\partial^2 C}{\partial x^2}\right)_t \tag{5}$$

The solution of Equation 5 will depend on the initial and boundary conditions imposed by the particular experiment. For the case where a semi-infinite solid is exposed to a gas of constant composition and there is no phase boundary reaction at the surface the following initial and boundary conditions apply:

$$C(x,0) = C_o \tag{6}$$

which states that the initial concentration of diffusing species is constant throughout the sample,

$$C(\infty,t) = C_o \tag{7}$$

states that the sample is a semi-infinite medium, and

$$C(0,t) = C_e \tag{8}$$

The concentration of diffusing species at the sample surface is constant with time. The solution to the differential equation is given by:

$$C(x,t) = C_o + (C_e - C_o)\ \mathrm{erfc}\left(\frac{x}{2(Dt)^{\frac{1}{2}}}\right) \tag{9}$$

where erfc $\left(\frac{x}{2(Dt)^{\frac{1}{2}}}\right)$ is the complementary error function of $\left(\frac{x}{2(Dt)^{\frac{1}{2}}}\right)$ and is given by:

$$\text{erfc}\left(\frac{x}{2(Dt)^{\frac{1}{2}}}\right) = 1 - \frac{2}{\pi^{\frac{1}{2}}} \int_0^{\frac{x}{2(Dt)^{\frac{1}{2}}}} e^{-w^2}\, dw \qquad (10)$$

The temperature dependence of the diffusion coefficient is usually given by:

$$D = D_o \exp - \frac{Q^*}{RT} \qquad (11)$$

where D_o is a frequency factor, Q* is the activation energy for diffusion, R is the gas constant, and T is the temperature.

2.2 Diffusion with a Finite Rate of Surface Exchange

The situation often arises where it is necessary to relax the boundary condition given by Equation 8, that the concentration of diffusing species at the sample surface is a constant with time, to allow for a finite rate of exchange at the surface. The presence of

a surface-exchange coefficient, K_s, which is a first-order reaction-rate constant will effect both the shape and magnitude of $C(x,t)$. When a surface-exchange coefficient is required, the boundary condition given by Equation 8 is written as:

$$K_s(C_e - C(0,\tau) = - D\left(\frac{\partial C(0,\tau)}{\partial x}\right) \tag{12}$$

The solution to Fick's Second Law, Equation 5, for this new set of initial and boundary conditions has been given by Robin (2) as:

$$C(x,t) = C_o - (C_e - C_o)\left\{\exp\left(\frac{K_s(x + K_s t}{D} - \frac{K_s}{}\right) \operatorname{erfc}\left(\frac{x + 2K_s t}{2(Dt)^{\frac{1}{2}}}\right)\right.$$

$$\left. - \operatorname{erfc}\left(\frac{x}{2(Dt)^{\frac{1}{2}}}\right)\right\} \tag{13}$$

As can be seen if $K_s \to \infty$ Equation 13 reduces to Equation 9.

2.3 Diffusion in Bicrystals

In polycrystalline materials high diffusivity paths, grain boundaries, exist within the sample. One should therefore expect the concentration profiles obtained to be due to diffusion along grain boundaries and diffusion into the grains from both the surface and the grain boundaries.

Solutions to the grain boundary diffusion problem have been presented by Fisher (3), Whipple (4), and Suzuka (5) and analyzed by LeClaire (6). The configuration used in the mathematical treatment of grain-boundary diffusion is shown schematically in Figure 1. The grain boundary is treated as a slab of uniform composition and thickness δ. It is assumed that $D_{GB} >> D_V$. Fick's Laws can now be solved in the grain boundary and within the grains by applying the appropriate initial and boundary conditions. The case of a constant surface concentration has been treated by both Fisher (3) and Whipple (4) and will be examined here. The initial and boundary conditions that apply are given by:

$$C(x,y,0) - C_o = 0 \tag{14}$$

$$C(\infty,y,t) - C_o = 0 \tag{15}$$

$$C(0,y,t) = C_e \tag{16}$$

Continuity of both concentration and flux must also be maintained at the interface between the grain boundary and grain. These continuity

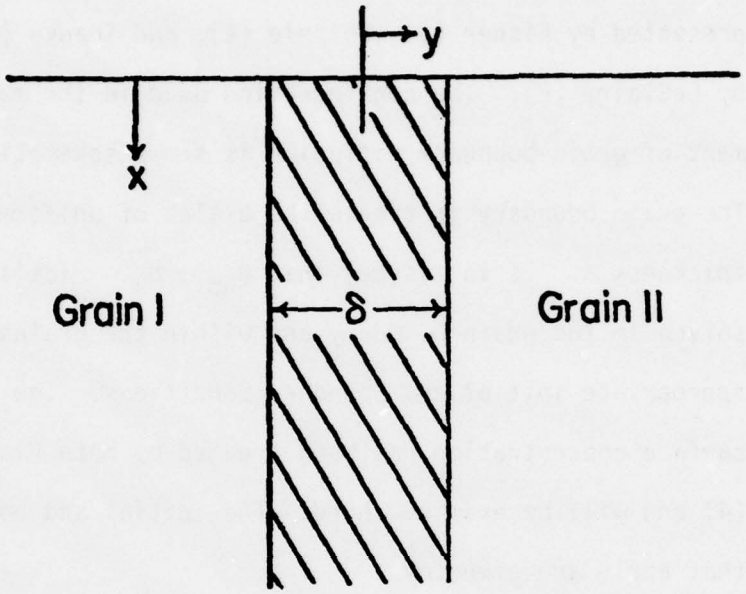

Figure 1: Configuration Used in the Mathematical treatment of Grain-boundary Diffusion.

conditions are given by:

$$C_v(x, \pm \frac{1}{2}\delta, t) = C_{GB}(x, \pm \frac{1}{2}\delta, t) \tag{17}$$

$$D_v(\frac{\partial C_v}{\partial y})_{\frac{1}{2}\delta} = D_{GB}(\frac{\partial C_{GB}}{\partial y})_{\frac{1}{2}\delta} \tag{18}$$

Within the grain boundary C will be an even function of y and can therefore be approximated by a power series in y^2 with the constants being functions of x and t.

From the boundary conditions and Fick's Second Law the following can be obtained, ignoring terms of order δ^2:

$$\frac{2D_v}{\delta}(\frac{\partial C}{\partial y})_{\frac{1}{2}\delta} + D_{GB}(\frac{\partial^2 C}{\partial x^2})_{\frac{1}{2}\delta} = \frac{\partial C}{\partial t} \tag{19}$$

which must be solved at the boundary. The first term represents diffusion out of the grain boundary and the second term represents diffusion along the grain boundary. The equation to be solved within the grains is given by:

$$D_v(\frac{\partial^2 C}{\partial x^2} + \frac{\partial^2 C}{\partial y^2})_t = (\frac{\partial C}{\partial t})_{x,y} \tag{20}$$

Following the derivation of Whipple (4) it is convenient to convert to dimensionless variables, defined by:

$$\gamma = \frac{x}{(D_v t)^{\frac{1}{2}}} \tag{21}$$

$$\zeta = \frac{y - \frac{1}{2}\delta}{(D_v)^{\frac{1}{2}}} \tag{22}$$

$$\tau = \frac{D_{GB}}{D_v} \frac{\frac{1}{2}\delta}{(D_v t)^{\frac{1}{2}}} \tag{23}$$

Fisher (3) has obtained the following approximate solution for C:

$$C = C_e \exp(-\pi^{\frac{1}{4}} \gamma \tau^{-\frac{1}{2}}) \operatorname{erfc}(\tfrac{1}{2} \zeta) \tag{24}$$

by assuming that γ is sufficiently large and that only diffusion from the grain boundary contributes to C.

Whipple (4) has provided the exact solution to Equation 20 providing $\gamma > \frac{D_{GB}}{D_v}$, which is usually the case. The exact solution is:

$$C = C_e[\operatorname{erfc}(\tfrac{1}{2}\gamma) + \frac{\gamma}{2\pi^{\frac{1}{2}}} \int_w^\infty \frac{1}{w^{3/2}} \exp(-\frac{\gamma^2}{4w}) \operatorname{erfc} \frac{1}{2}(\frac{w-1}{\tau} + \zeta) dw] \tag{25}$$

where w is a dummy variable of integration. The first term in Equation 25 is the direct volume diffusion contribution to C and is the one-dimensional solution to the diffusion equation. The second term gives the contribution to C from diffusion out of the grain boundaries.

If $\tau > 1$, the second term in Equation 25 can be rewritten as (4):

$$C = C_e\left[\frac{1.159}{(\gamma\tau^{-\frac{1}{2}})^{2/3}} \exp\{-0.473(\gamma\tau^{-\frac{1}{2}})^{4/3} + 0.396\,\frac{(\gamma\tau^{-\frac{1}{2}})^{2/3}}{\tau}\,(1-\tau\zeta)\}\right] \qquad (26)$$

Equation 26 is known as Whipple's asymptotic solution. If the quantity $\gamma\tau^{-\frac{1}{2}} >> 1$ then the first term in Equation 25, that due to direct volume diffusion, can be neglected and C will be given by Equation 26.

From Equations 21 and 23 the following can be obtained:

$$D_{GB}\delta = \left(\frac{\partial \ln \bar{C}}{\partial x}\right)^{-2} \left(\frac{4D_v}{t}\right)^{\frac{1}{2}} \left(\frac{\partial \ln \bar{C}}{\partial(\gamma\tau^{-\frac{1}{2}})}\right)^2 \qquad (27)$$

The bar indicates average concentration with respect to y; and it is understood that differentiation with respect to $\gamma\tau^{-\frac{1}{2}}$ is with t and D_v held constant.

The last term of Equation 27, $\left(\frac{\partial \ln \bar{C}}{\partial(\gamma\tau^{-\frac{1}{2}})}\right)^2$ is a constant as can be seen by integration of the Fisher solution, Equation 24, with respect to ζ(6):

$$\exp(-\pi^{-\frac{1}{4}}\gamma\tau^{-\frac{1}{2}}) \qquad (28)$$

Here the last term is simply $\pi^{-\frac{1}{2}}$ and is independent of $\bar{C}$ and x.

Similarly, it is possible to obtain an expression for $(\frac{\partial \ln \bar{C}}{\partial(\gamma\tau^{-\frac{1}{2}})})^2$ from Whipple's asymptotic solution, Equation 26:

$$(\frac{\partial \ln \bar{C}}{\partial(\gamma\tau^{-\frac{1}{2}})})^2 = [-\frac{4}{3}(\gamma\tau^{-\frac{1}{2}})^{-1} - 0.6307(\gamma\tau^{-\frac{1}{2}})^{1/3} + 0.264\frac{(\gamma\tau^{-\frac{1}{2}})^{-1/3}}{\tau}] \qquad (29)$$

1) It should be noted that Equations 28 and 29 apply only to regions where direct volume diffusion can be neglected. 2) The asymptotic solution is a good approximation if the value of $\gamma\tau^{-\frac{1}{2}} > 9$. 3) The asymptotic solution is not a constant. However for most experimental data the midpoint of the range of $\gamma\tau^{-\frac{1}{2}}$ can be used due to the low curvature. 4) Equation 27 will give values of $D_{GB}\delta$ approximately three times too small if the Fisher solution is used and approximately 10% too large if Whipple's asymptotic solution is used when $\gamma\tau^{-\frac{1}{2}}$ falls between 4 and 8(6).

Levine and MacCallum (7) noted that the quantity $\frac{\partial \ln \bar{C}}{\partial(\gamma\tau^{-\frac{1}{2}})}^{6/5}$ was essentially independent of $(\gamma\tau^{-\frac{1}{2}})$ over the approximate range $2 < \gamma\tau^{-\frac{1}{2}} < 10$. The quantity $D_{GB}\delta$ can then be calculated from:

$$D_{GB}\delta = \left(\frac{\partial \ln \bar{C}}{\partial x^{6/5}}\right)^{-5/3} \left(\frac{4D_v}{t}\right)^{1/2} \left(\frac{\partial \ln \bar{C}}{\partial (\gamma\tau^{-1/2})^{6/5}}\right)^{5/3} \qquad (30)$$

which is analogous to Equation 27. For large values of $\tau(\tau > 10)$ the value of $\frac{\partial \ln \bar{C}}{\partial (\gamma\tau^{-1/2})^{6/5}}$ is a constant equal to 0.78.

Borisov and Lyubov (8) report this ratio to have a value of 0.99 for values of $(\gamma\tau^{-1/2}) < 1$.

Lundy and Federer (9) presented a graphical method for obtaining the grain-boundary and volume diffusivities given the concentration versus-depth profile. The logarithm of the concentration is first plotted as a function of $x(x^{6/5}$ if the model of Levine and MacCallum is used). A straight line is then fit to the points corresponding to the deepest penetrations. The slope of this line can be used in Equation 27 (or Equation 30) to determine the value of $D_{GB}\delta$. The concentration distribution corresponding to the linear fit is then subtracted from the measured concentration profile. The resulting profile is then due to volume diffusion only and can be fit with the appropriate solution to Fick's Second Law.

2.4 Extension to the Polycrystalline Case

The equations derived in the previous section are for diffusion in a bicrystal however we wish to apply them to polycrystalline materials. It is therefore of importance to examine what meaning

the calculated diffusiuities will have when these equations are applied to polycrystals. If it is assumed that the grain size is a, then this value can be related to the characteristic volume diffusion distance, $2(D_v t)^{\frac{1}{2}}$, and the characteristic grain boundary diffusion distance, $2(D_{GB} t)^{\frac{1}{2}}$.

The first possible case is when $2(D_v t)^{\frac{1}{2}} < \frac{1}{2} a$ and $2 (D_{GB} t)^{\frac{1}{2}} < a$. In this case the value of D_{GB} and D_v will be correct if all the grain boundaries are perpendicular to the surcase. However, as is the case for real materials the grain boundaries intersect the surface at all angles. Use of Equation 27 or 30 will lead to an underestimation of D_{GB} by factor of $\frac{2}{3}$. If the plane of the grain boundary makes an ϕ with the surface of the sample, see Figure 2a, the measured penetration distance in the x direction will be given by b sin ϕ. As can be seen if ϕ is 90^o x will equal b and if ϕ is 0^o or 180^o x will be 0, that is, no penetration will be seen. According to Equations 27 and 30 the calculated value of D_{GB} will be directly proportional to $(\partial x)^2$. To determine the amount by which D_{GB} is underestimated for a uniform distribution of grain boundary angles the average value of $(b \sin \phi)^2$ must be found over a hemisphere:

$$\langle (b \sin \phi)^2 \rangle = \frac{\int (b \sin \phi)^2 d\Omega}{\int d\Omega} = \frac{2}{3} \qquad (31)$$

Because the process of subtracting the values associated with either $(\frac{\partial \ln \bar{C}}{\partial x})$ or $(\frac{\partial \ln \bar{C}}{\partial x^{6/5}})$ from the experimental data removes the contri

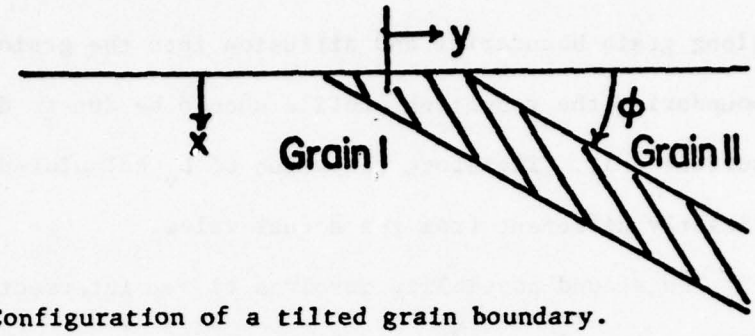

Figure 2a: Configuration of a tilted grain boundary.

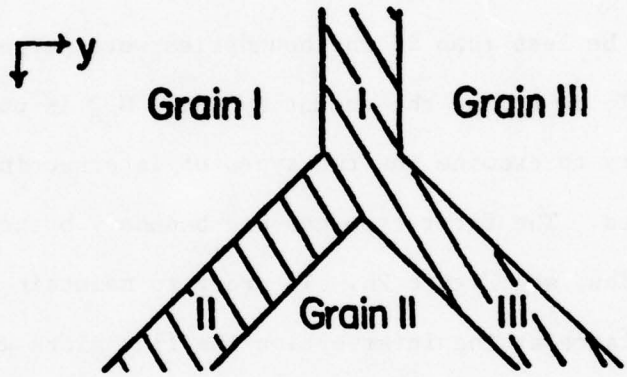

Figure 2b: First possible configuration for intersecting grain boundaries.

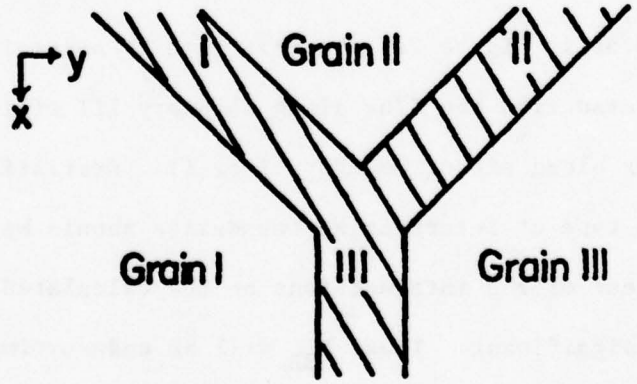

Figure 2c: Second possible configuration for intersecting grain boundaries.

to the concentration versus depth profile from both diffusion along grain boundaries and diffusion into the grains from the grain boundaries the resulting profile should be due to diffusion from the surface only. Therefore the value of D_v calculated will not be significantly different from the actual value.

The second possiblity involves tilted intersecting grain boundaries, i.e. $2(D_{GB}t)^{\frac{1}{2}} > a$ while $2(D_v t)^{1/2} < \frac{1}{2}\ a$. The fact that the boundaries are tilted will lead to an underestimation of D_{GB}, because the actual penetration distance along the grain boundaries will appear to be less than if the boundaries were perpendicular to the surface. To determine the amount by which D_{GB} is underestimated it is necessary to examine the two types of intersecting boundaries encountered. The first type has one boundary branching to form two new boundaries, see Figure 2b. In order to maintain a diffusing species flux balance at the intersection the flux along grain boundaries II and III will be less than that along grain boundary I. The second type of intersection is for two boundaries to come together to form a third as in Figure 2c. In this case to maintain a flux balance at the intersection the flux along boundary III will be greater than the flux along either boundary I or II. Statistically, the number of each type of intersecting boundaries should be the same, thus the net effect of the intersections on the calculated value of D_{GB} should not be significant. Thus, D_{GB} will be underestimated by approximately $\frac{2}{3}$. For the reasons given in the first case D_v will not be significantly affected.

The final possibility also involves tilted intersecting grain boundaries, $2(D_{GB}t)^{\frac{1}{2}} > a$, but $(D_v t)^{\frac{1}{2}} > \frac{1}{2} a$. For reasons identical to those above D_{GB} will be underestimated by approximately $\frac{2}{3}$. The diffusion profiles from opposite sides of the grains will now overlap, thus, decreasing the concentration gradient. This will tend to overestimate D_v.

Section III

PREVIOUS STUDIES OF NITROGEN TRANSPORT

3.1 General

The possibility of studying nitrogen transport in materials has been limited by the availability of isotopic tracers. Of the seven known nitrogen isotopes, only two are found in nature and both are stable, see Table 1. The short half-lives of the unstable isotopes prevents their utilization in usual radiotracer experiments. Nitrogen diffusion measurements have therefore been confined to gaseous exchange, studied by following the change in isotopic concentration of the gas, activation analysis, or inferred from reaction data.

Smeltzer and Desmaison (10) in an appraisal of the literature on the measured diffusion coefficients of nitrogen in metal nitrides conclude that the studies remain at an infancy state. Table 2 (10) gives the available diffusion coefficients for some binary nitrides. The scatter in both the measured frequency factor, D_o, and activation energy, Q^*, can be attributed to the lack of suitable single crystals and the lack of suitable techniques to measure nitrogen transport.

Most studies have been carried out on polycrystalline materials which often have unknown structures and impurity levels. This has led to difficulties in separating the volume diffusion coefficient from the contributions due to grain boundaries, dislocations, and impurity effects.

TABLE 1

KNOWN NITROGEN ISOTOPES

Isotope	% Abundance	Decay Mode	Half-Life
$^{12}_{7}N$		β^+	0.011 Sec
$^{13}_{7}N$		β^+	599.4 Sec
$^{14}_{7}N$	99.63		
$^{15}_{7}N$	0.37		
$^{16}_{7}N$		β^-	7.35 Sec
$^{17}_{7}N$		β^-	4.14 Sec
		n	
$^{18}_{7}N$		β^-	0.63 Sec

TABLE 2

Diffusion Coefficients for Binary Nitrides (10)

Nitride	Diffusivity	Temp(K)	$D_o (\frac{m^2}{sec})$	Q^* (kJ-Mole^{-1})
TiN	D_c	1173-1843	5.4×10^{-7}	217.7
TiN	D_c	1573-1873	4.4×10^{-4}	304.7
TiN	D_c	1623-1973	2.0×10^{-3}	376.8
TiN	D_c	1473-1723	5.8×10^{-5}	279.2
TiN	D_c	1573-1943	2.3×10^{-7}	210.1
TiN	D_c	1223-1773	2.1×10^{-7}	199.2
ZrN	D_c	923-1123	7.9×10^{-9}	150.3
ZrN	D_c	1623-1973	6.0×10^{-6}	251.2
ZrN	D_c	1533-1993	1.7×10^{-6}	224.4
ZrN	D_c	1073-1373	2.5×10^{-6}	185.0
ZrN	D_c	1473-1773	3.1×10^{-4}	332.4
$ZrN_{0.76}$	D_c	1873-2473	7.5×10^{-5}	327.8
$ZrN_{0.68}$	D_c	2823-2973	3.5×10^{8}	1025.7
$ZrN_{0.86}$	D_c	2673-3023	7.9×10	628.0
$ZrN_{0.96}$	D_c	2673-2873	2.6×10^{-2}	406.1
$ZrN_{0.93}$	D_c	1273-1473	4.1×10^{-10}	153.2
$ZrN_{0.75}$	D_c	1273-1473	3.0×10^{-14}	96.2
VN	D_c	1723	$D = 2.5 \times 10^{-12}$	
NbN	D_c	1783-2308	2.1	468.9

Table 2 (Con't)

Nitride	Diffusivity	Temp(K)	$D_o(\frac{m^2}{sec})$	Q^* (kJ-mole^{-1})
Cr_2N	D_c	1473	$D = 4.2 \times 10^{-12}$	
Fe_4N	D_c	777	$D = 3.2 \times 10^{-16}$	
εFe_4N	D_c	853-1003	4.4×10^{-7}	113.4
ThN	D_c	2173-2673	2.5×10^{-2}	416.1
UN	D_T	1773-2173	2.6×10^{-8}	230.2
UN	D_T	2065	$D = 8.1 \times 10^{-15}$	
UN	D_T	1973-2273		~234.4
UN	D_c	2073-2673	1.2×10^{-3}	502.4
αSi_3N_4	D_T	1473-1683	1.2×10^{-16}	233.2
β-Si_3N_4	D_T	1473-1683	5.8×10^{2}	777.4
Si_3N_4	D_c	1763-2023	10^{6}	778.7

As already pointed out, the lack of a long lived nitrogen radiotracer has led to difficulties in making nitrogen transport measurements. Chemical nitrogen diffusivities (calculated by following the changes in a property), D_c, have been determined by exposing a sample to a fixed environment and following either the kinetics of weight change, electrical conductivity change, or density change. By applying the appropriate equations (11-14) the diffusivity can be calculated assuming the mechanism of the process is known exactly. These methods are subject to considerable question due to the influence of grain boundary diffusion contributions and the assumptions required by the model.

Tracer diffusivities, D_T, can be obtained by forming a diffusion couple where one of the segments is enriched in nitrogen-15 related to the other. Alternatively a sample is placed in a gaseous environment enriched in nitrogen-15 and the decrement of nitrogen-15 in the gas phase during the exchange is determined. This method can give erroneous results due to exchange with the containment vessel. If the sample is polycrystalline a way of separating the contribution of grain boundary diffusion from the volume diffusion must be developed. It is also possible to obtain a tracer diffusivity by measuring the nitrogen-15 concentration versus depth profile after exchange. The concentration versus depth profile can either be obtained by mass spectrometry or activation analysis. To analyze a sample by mass spectrometry, the sample must first be sectioned and converted to a gaseous phase where the ^{14}N - ^{15}N ratio is measured.

This procedure has two possible sources of error, which become increasingly important when attempting to measure small penetrations. These are in determining the exact amount of material contained in each section and in determining the degree of conversion to a gaseous phase. Activation analysis can be performed either by induced radioactivity or the direct observation of a nuclear reaction. (The direct observation of a nuclear reaction technique is discussed in Appendix A.) In 1967 Condit, Holt, and Himmel (15) suggested an activation analysis technique for detecting nitrogen-15 in solids using the $^{15}N(\alpha,n)^{18}F$ reaction. The reaction product Fluorine-18 is radioactive, which decays by emission of a 0.67 MeV β^+ with a half-life of 6732 seconds. The β^+ particles are then detected by autoradiography. This technique was applied by Holt and Almassy (16) to study nitrogen diffusion in uranium nitride in 1969.

3.2 Nitrogen Transport in Silicon Nitride

To date there have been few studies which have allowed determinations of nitrogen diffusivities in silicon nitride. Table 3 (17) tabulates the activation energies reported to date for nitrogen transport in silicon nitride and the method by which it was obtained. The large variations in activation energies can possibly be attributed to differences in the impurity levels in the samples.

Kijima and Shirasaki (17) obtained tracer diffusion coefficients for both α- and β-Si_3N_4 by gas-solid exchange techniques. The decrement in nitrogen-15 isotope in the gas phase was followed as a function of time during the exchange and the data reduced using the

TABLE 3

Activation Energies for Nitrogen Transport in Silicon Nitride

Temp Range (K)	Activation Energy ($kJ \cdot mole^{-1}$)	Method	Ref
1243-1873	141.5	Nitriding Kinetics	18
1473-1683	233.2	Isotopic Exchange	17
1533-1683	418.6-837.3	Nitriding Kinetics	19
1623-1683	661.5	Nitriding Kinetics	20
1473-1683	777.4	Isotopic Exchange	17
1763-2023	778.7	Thermal Decomposition Kinetics	21

method of Carmon and Haul. Their samples were prepared by nitriding high purity silicon pellets to produce pure α-Si_3N_4. The β-Si_3N_4 was produced by firing the α-Si_3N_4 at 1653 K for 4.32×10^4 seconds. The two types of Si_3N_4 are reported to have similar densities, 55% theoretical, but to have different grain sizes. The average grain size for the α-Si_3N_4 was 50.0nm and was 150.0nm for the β-Si_3N_4. The pellets were crushed to form powders with average particle sizes of 75μm and 1.0mm which were used for the exchange. It was necessary to substitute the average grain size for the average sphere size in the equation for the early stages of exchange between a sphere and a well-stirred solution of limited volume in order to obtain agreement between the diffusivities calculated for the two particle sizes. The measured diffusivities, corrected for grain size, for the temperature range 1473 to 1673 K are:

$$\left[1.2 \times 10^{-16} \exp - \left(\frac{2.33 \times 10^5 J}{RT}\right)\right] \frac{m^2}{sec} \tag{32}$$

for α-Si_3N_4 and:

$$\left[5.8 \times 10^{2} \exp -\left(\frac{7.77 \times 10^5 J}{RT}\right)\right] \frac{m^2}{sec} \tag{33}$$

for β-Si_3N_4.

Kijima and Shirasaki report that minimal experimental error was introduced by reactions (thermal decomposition, oxidation, reaction between the sample and crucible and nitriding of the crucible or

suscepter). This was determined by monitoring the relative pressure of nitrogen against a standard of argon by mass spectrometry and also checking for weight change of the nitride powder, crucible, and susceptor during a 3.6×10^3 second anneal at 1623 K. It would seem doubtful that either mass spectrometry or weight change measurements would be sensitive enough to detect the presence of a reaction during an anneal of this length. Because no reference is made as to sample size or to the amount of gas present the following assumptions will be made: particle size = 75 μm spheres, initial mass of Si_3N_4 = 10 mg, and volume of gas present = 1 liter. Assuming that 1.0nm of SiO_2 forms on each particle the weight change would be 0.1 μg and the volume of nitrogen would change by 2×10^{-5}%. Since all the particles will not be equally exposed to the nitrogen these changes will probably be even smaller.

It is also emphasized that Kijima and Shirasaki's technique allowed nitrogen diffusivities less than 10^{-21} m^2 - sec^{-1} to be determined. The diffusion times quoted by Kijima and Shirasaki are of the order of 5×10^3 seconds. This corresponds to a maximum penetration distance of 2 nm and to 0.07 nm for their lowest diffusivity ($\sim 10^{-24}$ m^2 - sec^{-1}) which is considerably less than a unit cell dimension of β-Si_3N_4. It seems improbable that any technique would allow the measurement of diffusion coefficients corresponding to penetration distances on the order of a unit cell. Even if it were possible to measure penetration distances to a unit cell dimension or even several unit cells, the calculated diffusivity would not be

one representative of the bulk diffusivity (22), but will be characteristic of the sample's surface. For penetrations this small the measurement is probably only representative of a phase boundary reaction.

Wuensch and Vasiles (23) proposed to study both silicon and nitrogen self-diffusion in silicon nitride by ion microprobe spectrometry, but were unsuccessful due to charge buildup on the sample surface while sputtering. They therefore microchemically separated the silicon and nitrogen, and finally analyzed the separated components for isotopic ratio by mass spectrometric techniques. Due to carbon contamination during sectioning, nitrogen isotopic gradients were "not as satisfactory as hoped" and no self-diffusion coefficient for nitrogen was obtained.

Brook, et.al. (24) calculated a process diffusion coefficient from densification rates of Si_3N_4 containing 5 w/o MgO during hot pressing at 21 MN-m^2. They assumed that the hot pressing model proposed by Coble (14) could be used where the rate of densification is controlled by grain boundary diffusion. The model has been modified for liquid-phase sintering to allow use of the following simplified rate equation:

$$\frac{d\rho}{dt} = \frac{47V\delta D_{GB}}{k\ Ta^3} P_A \qquad (34)$$

where $\frac{d\rho}{dt}$ is the densification rate, V is the volume transported by

each atom of the least mobile species, and P_A is the applied stress. The grain-boundary thickness, δ, was calculated from the grain size and the amount of MgO added (it was assumed all of the MgO combined with SiO_2 to form grain boundaries) on the basis of a uniform boundary film. Using this model they found an activation energy for nitrogen grain-boundary diffusion of 4.5×10^5 J-mole^{-1} for the temperature range 1823-2023K and 6.95×10^5 J-mole^{-1} for the temperature range 1723-1823K. They interpret the break at 1823 K as being due to the solidus of the $MgSiO_3$ - SiO_2 system (1916K) with diffusion being in the second phase boundary either containing or not containing a liquid phase.

It would appear as if the diffusivities calculated by this model (10^{-16} - 10^{-14} m^2-sec^{-1}) are several orders of magnitude too low considering they represent diffusion in either a liquid phase or a phase that is almost at its melting point. There is no data available for nitrogen diffusion in molten silicates, however one can assume it should be of approximately the same order of magnitude as other diffusivities in molten silic tes. Oishi, et.al. (25) have quoted diffusivities for oxygen, calcium, aluminum, and silicon in molten silicates to be of the order of 10^{-10} m^2-sec. The reason for the low diffusivities can possibly be attributed to two equilibrium assumptions required to use the model. The first assumption involves the grain size of the hot pressed material; the diffusivity is proportional to the cube of the grain size. During the hot pressing

process considerable grain growth occurs as the Si_3N_4 density increases. The model requires knowledge of the grain size at the time the measurement is made and could be rapidly changing. The diffusion coefficient is inversely proportional to the grain boundary thickness which has been calculated from the grain size and the equilibrium phase diagram for the $MgSiO_3$ - SiO_2 system. In making this calculation it is therefore necessary to know the grain size, which is not known exactly as discussed above, and to assume all of the MgO added goes to the grain boundaries where it combines with SiO_2. Even if all of the MgO does go to the grain boundaries the grain boundary film is probably far from being in equilibrium.

SECTION IV

Experimental

4.1 Selection of a Technique

It was desired to be able to measure the self-diffusion coefficient for nitrogen in both grains and grain boundaries of silicon nitride. The stable isotope, nitrogen-15, was used as a tracer and detected by the direct observation of a nuclear reaction. The nuclear micro-analytical technique eliminates the need for serial sectioning which would create a serious problem if Kijima and Shirasaki's (17) measured diffusivity is correct. The technique also eliminates the problem encountered by Wuensch and Vasiles (23) of efficiently converting each section to a gaseous phase, free of contaminants, suitable for measuring the nitrogen isotopic ratios.

There are three nuclear reactions available for the detection of nitrogen-15, these are given in Table 4 along with the Q value (Q is the energy equivalent to the mass difference between the reactant and product nuclei) and the possible interfernces. The deuteron induced reaction on nitrogen-15 was eliminated due to nitrogen-14 interference reactions. Of the two possible proton induced reactions on nitrogen-15 the $^{15}N(p,\alpha_o)^{12}C$ reaction was selected because of the high Q value and the virtually background free, sharp resonance at 1.210 MeV. The reaction also has a broad resonance which could be used for the single spectrum technique, see Figure 3.

TABLE 4

Charged Particle Induced Nuclear Reactions on Nitrogen-15

Reaction	Q(MeV)	Interferences
$^{15}N(p,\alpha_0)^{12}C$	4.964	
$^{15}N(p,\alpha_1)^{12}C^*$	0.531	
$^{15}N(d,\alpha)^{12}C$	7.683	$^{14}N(d,\alpha_0)^{12}C$
		$^{14}N(d,\alpha_1)^{12}C^*$

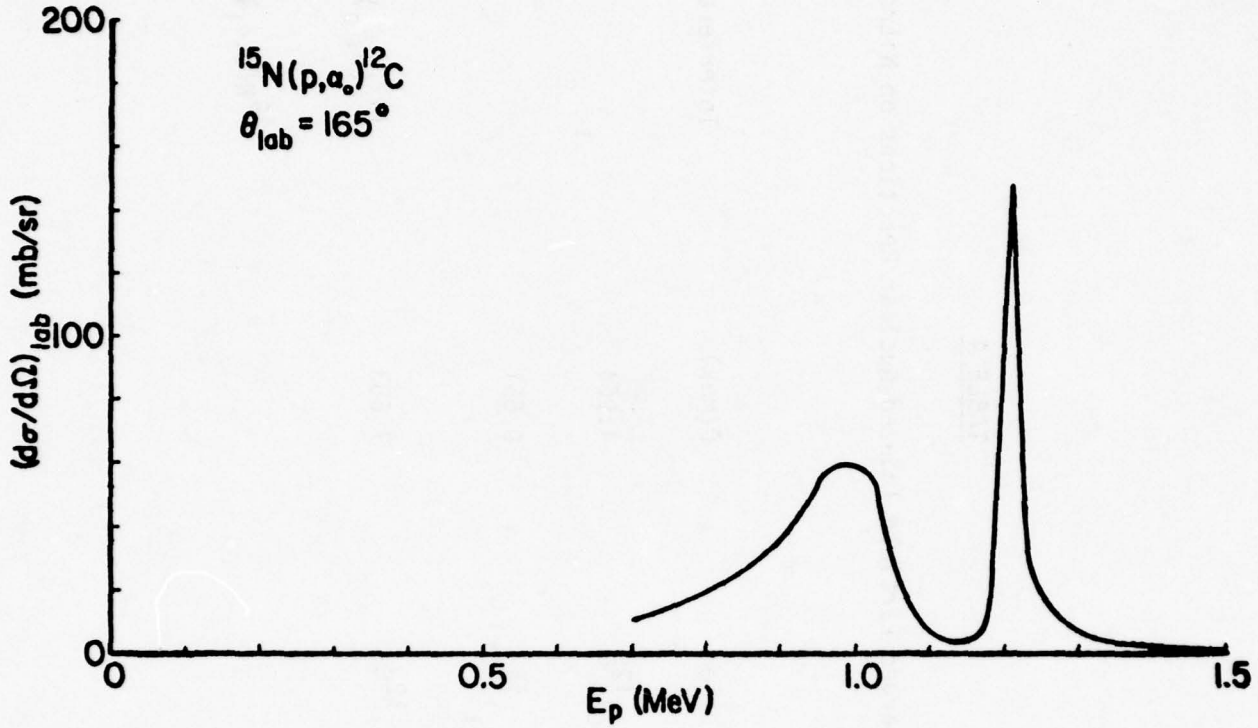

Figure 3: Experimental $^{15}N(p,\alpha_0)^{12}C$ differential cross section.

4.2 Sample Selection

Due to the fact that large single crystals of high purity, theoretically dense, dislocation free silicon nitride are not presently available, commercial grade silicon nitride was used in these studies. It was initially thought that CVD silicon nitride would make the best samples. These samples would have been thin films, therefore making the selection of the substrate material important to prevent reaction with or contamination of the film. It was determined that silicon would make the best substrate, but it was found that deposition was not uniform and there was an adhesion problem with some of the samples.

Next attention was turned to a piece of Norton reaction bonded silicon nitride. The reaction-bonded sample, while having a high purity, was fine grained and was not uniformly dense. Due to the complex structure (small grains, high porosity, and nonuniform density), the models presently available and those that could possibly be derived were not able to reduce the corcentration versus depth profile. For this reacon the reaction-bonded samples were not used.

It was finally decided to use a sample of fully dense NORALIDE ™ NC-132 hot pressed silicon nitride cut from billet number 122072A. Electron microscopy studies (26) showed the sample to be composed of a statistical mixture of ∿95% 0.5 μm grains of β-silicon nitride and ∿5% 0.5 μm grains of silicon oxynitride surrounded by a continous glassy phase, presumably a silica rich magnesium oxide glass (27-29), approximately 3 nm wide (29). See Figure 4 (26). The dark spots in

Figure 4a: Microstructure of NORALIDE™ NC-132 hot-pressed silicon nitride, 10,000 x (26).

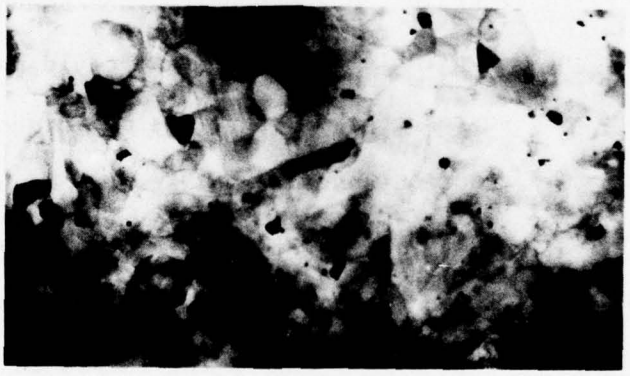

Figure 4b: Microstructure of NORALIDE™ NC-132 hot-pressed silicon nitride, 30,000 x (26).

the micrographs are tungsten carbide (26). A typical chemical analysis of the material is given in Table 5 (31).

The β form of silicon nitride is composed of SiN_4 tetrahedra sharing corners, with each nitrogen corner being common to three tetrahedra. The tetrahedra are arranged in a hexagonal structure as shown in Figures 5a and 5b (32).

Silicon oxynitride, Si_2N_2O, is composed of SiN_3O tetrahedra arranged so that parallel sheets of silicon and nitrogen atoms are joined by Si-O-Si bonds. The crystal structure of silicon oxynitride is shown in Figure 5c (32).

4.3 Sample Preparation and Exchange

The samples were diamond machined from the billet to a nominal size of 7mm x 10mm x 2mm. The samples were then mechanically polished using an alumina slurry.

Thermodynamic calculations show that at 1600 K an oxygen partial pressure less than 7.0×10^{-19} atmosphere must be maintained at the silicon nitride surface in order to prevent the thermal oxidation of the surface while exchanging with one atmosphere of nitrogen. The thermodynamic calculations considered are given in Table 6. In order to assure that this oxygen partial pressure was maintained at the sample surface, the sample was placed in a tungsten sample basket and completely surrounded by powdered carbon. A tungsten sample basket was used instead of alumina for two reasons. First the tungsten will act as an oxygen getter and second the possiblity of reactions.

TABLE 5

Typical Chemical Analysis of the Samples

Element	Maximum w/o	Typical w/o
O		3.07%
Mg	1.0%	0.4 - 0.6%
Al	0.5%	0.18 - 0.30%
Ca	0.05%	0.006 - 0.03%
F	0.75%	0.16 - 0.35%
W	3.0%	1.5 - 2.0%

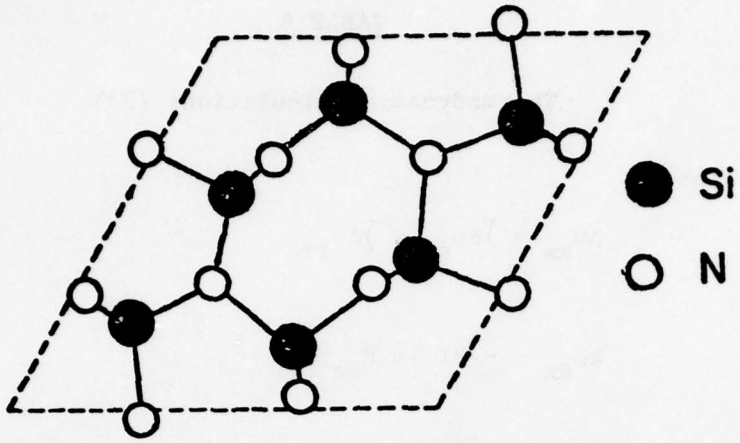

Figure 5a: Projection of the unit cell of β-Si_3N_4 in the basal plane (32).

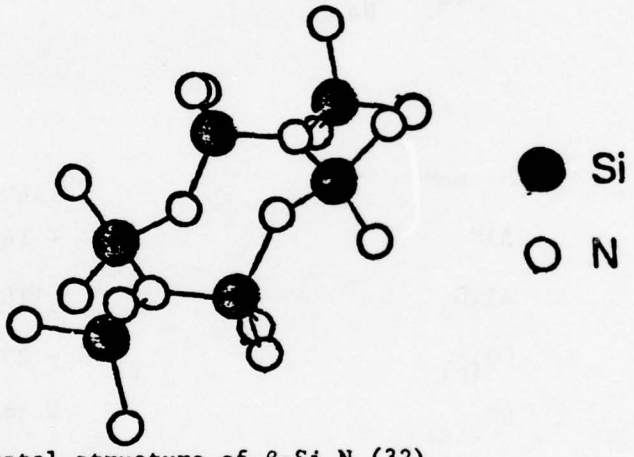

Figure 5b: The crystal structure of β-Si_3N_4(32).

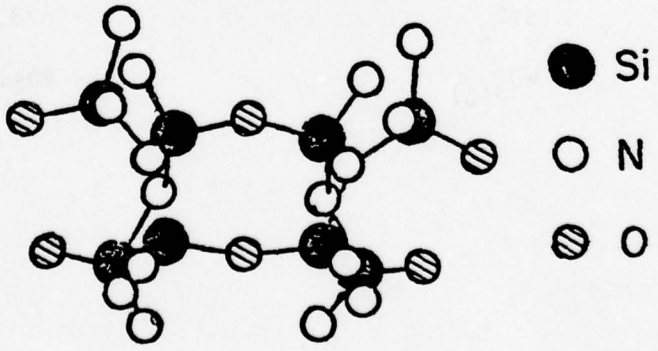

Figure 5c: The crystal structure of Si_2N_2O (32).

TABLE 6

Thermodynamic Calculations (33)

Equations:

$$\Delta G_{Rx} = \sum \Delta G_{fp} - \sum \Delta G_{fr} \tag{35}$$

$$\Delta G_{Rx} = - RT \ln K_{eq} \tag{36}$$

$$K_{eq} = \frac{\Pi a_p}{\Pi a_p} \tag{37}$$

Substance	ΔG_{f1600} (kJ-mole^{-1})
AlN	- 142.209
Al_2O_3	-1166.219
$CO_{(g)}$	- 252.590
$CO_{2(g)}$	- 396.956
Si_3N_4	- 217.252
SiO_2	- 628.613
$WO_{3(g)}$	- 204.577

TABLE 6 (Con't)

Reaction	$G_{Rx\ 1600}$ (kJ-mole^{-1})	Equilibrium $p(O_2)_{1600}$ at 1 atm N_2 (atm)
1) $Si_3N_4 + 3O_2 \rightleftarrows 3SiO_2 + 2N_2$	-1668.587	7.0×10^{-19}
2) $W + \frac{3}{2} O_2 \rightleftarrows WO_3$	- 204.577	$3.5 \times 10^{-5} (p(WO_3)_{1600})^{2/3}$
3) $Al_2O_3 + N_2 \rightleftarrows 2AlN + \frac{3}{2} O_2$	+ 881.801	6.4×10^{-20}
4) $2Al_2O_3 + Si_3N_4 \rightleftarrows 4AlN + 3SiO_2$	+ 95.015	
5) $Al_2O_3 + Si_3N_4 \rightleftarrows SiAlON$		
6) $C + \frac{1}{2} O_2 \rightleftarrows CO$	- 252.590	$3.2 \times 10^{-17} (p(CO)_{1600})^2$
7) $C + O_2 \rightleftarrows CO_2$	- 396.956	$1.1 \times 10^{-13} (p(CO_2)_{1600})$
8) $CO + \frac{1}{2} O_2 \rightleftarrows CO_2$	- 144.366	$4.0 \times 10^{-10} (\frac{p(CO_2)_{1600}}{p(CO)_{1600}})^2$
9) $C + CO_2 \rightleftarrows 2CO$	- 108.224	

There are three reactions that were considered (reactions 3-5 in Table 6), while equilibrium thermodynamics will not allow enough oxygen to be present when Al_2O_3 is exposed to an atmosphere of N_2 at 1600 K the errors in G_{f1600} could allow the oxygen partial pressure to exceed 7.0×10^{-19} atmosphere. The other two reactions which involve the chemical reaction between Si_3N_4 and Al_2O_3 were of primary importance when considering the use of thin film CVD Si_3N_4. As can be seen from reactions 6-9 in Table 6 as long as $p(CO_2)_{1600} < 6.4 \times 10^{-6}$ atmosphere and $p(CO)_{1600} < 1.5 \times 10^{-1}$ atmosphere carbon will serve as an adequate getter to prevent the thermal oxidation of the silicon nitride surface. Mass spectrometric analysis of the ambient gas showed no mass 44 peak and no increase in the mass 28 peak (it was possible to use the mass 28 peak since the ambient was 99.13% ^{15}N thus giving a low $^{14}N_2$ peak) verifying that carbon was an adequate getter.

Each sample was heated in vacuum to the diffusion temperature and maintained in vacuum until a pressure of 10^{-6} atmosphere was obtained. Oxygen free, research-grade nitrogen (0.37% ^{15}N) was then introduced to the system to obtain a pressure of one atmosphere. The sample was preannealed in this atmosphere for a period of time equal to or greater than twice the planned diffusion time. At the conclusion of the preanneal the ambient was changed to a 99.13% enriched nitrogen-15 gas. At the end of the diffusion time the nitrogen-15 was removed via zeolite and the sample cooled to room temperature.

The temperature range investigated was from 1506 K to 1723 K with diffusion times ranging from 5.4×10^3 seconds to 8.64×10^4 seconds.

4.4 Activation Analysis

Following the diffusion anneal the samples were mounted in aluminum sample holders, which were mounted on a movable target holder in the scattering chamber capable of holding five samples at a time. The samples were positioned so that the incident proton beam made an angle of 7.5° with the sample normal. (This geometry was chosen to prevent channelling when analyzing single crystals). The energetic alpha particles were observed at a laboratory scattering angle of 165°; after they passed through a magnetic spectrometer, a momentum analyzer (designed by Lindstrom and Hever (34)), by a conventional silicon surface barrier detector. The magnetic spectrometer eliminates the need for mylar to separate the alphas from the backscattered protons, which is an advantage since one does not have to worry about the uniformity or stopping power of the mylar film. A schematic of the scattering chamber and magnetic spectrometer is shown in Figure 6.

Each sample was bombarded with a monoenergetic beam of protons and the resulting alpha spectrum recorded. By systematically varying the incident proton energy upward from 1.205 MeV the 1.210 MeV resonance could be moved deeper into the sample. Figure 7 shows the

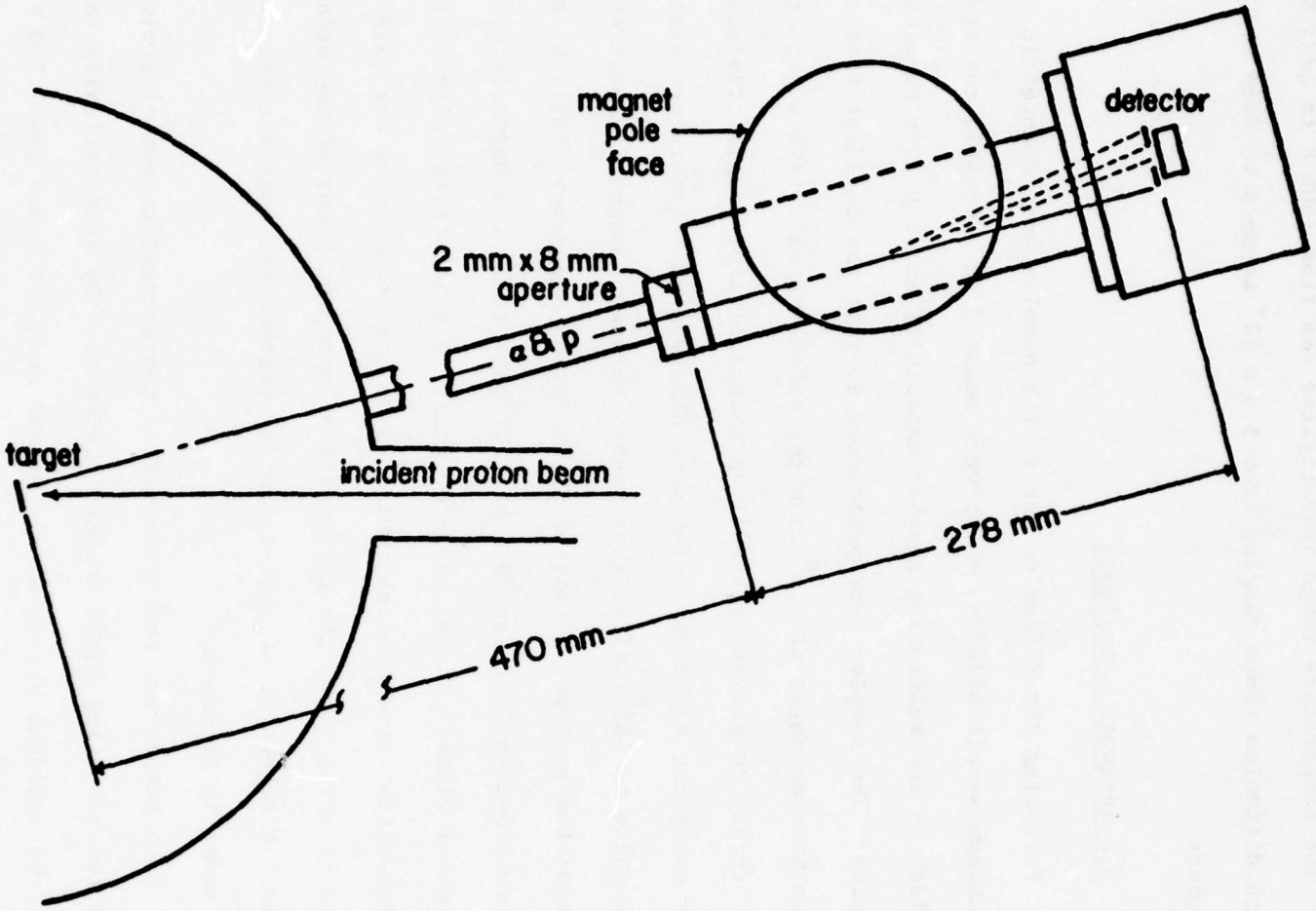

Figure 6. Schematic of the scattering chamber and magnetic spectrometer used in these experiments.

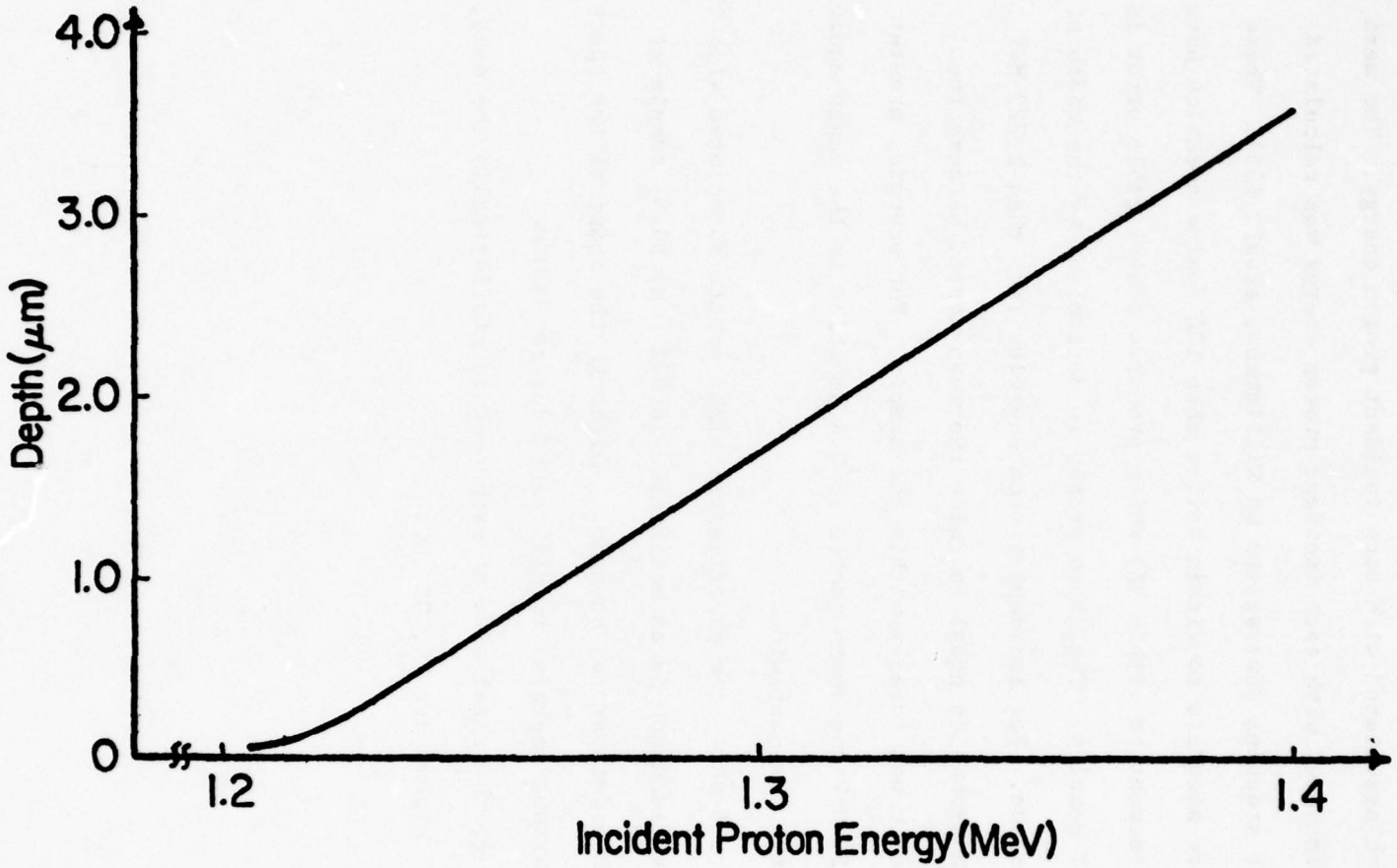

Figure 7: The mean depth associated with the 1.210 MeV resonance in Si_3N_4 for various incident proton energies.

mean depth associated with each incident proton energy. The mean depth associated with each incident proton energy was calculated using the stopping powersgiven by Williamson, et.al. (35). These values are accurate to within better than 10% (oxide ceramics have shown agreement to within 5%) which produces a negligible error in the final results. The depth probed is determined by the width of the resonance. For incident proton energies less than 1.223 MeV the depth probed is equal to twice the mean depth, because the resonance is not totally within the sample. For energies greater than 1.223 MeV the depth probed is 0.4 μm which is the depth equivalent to the resonant width.

Figure 8 shows the experimental alpha specta associated with the 1.210 MeV resonance in an undiffused (0.37% ^{15}N) Si_3N_4 sample at various incident proton energies. Although the shape of the spectra at the various energies is different, due to alpha straggling, the total area of each peak is statistically the same, 4360 ± 67 alphas per 10,000 μC.

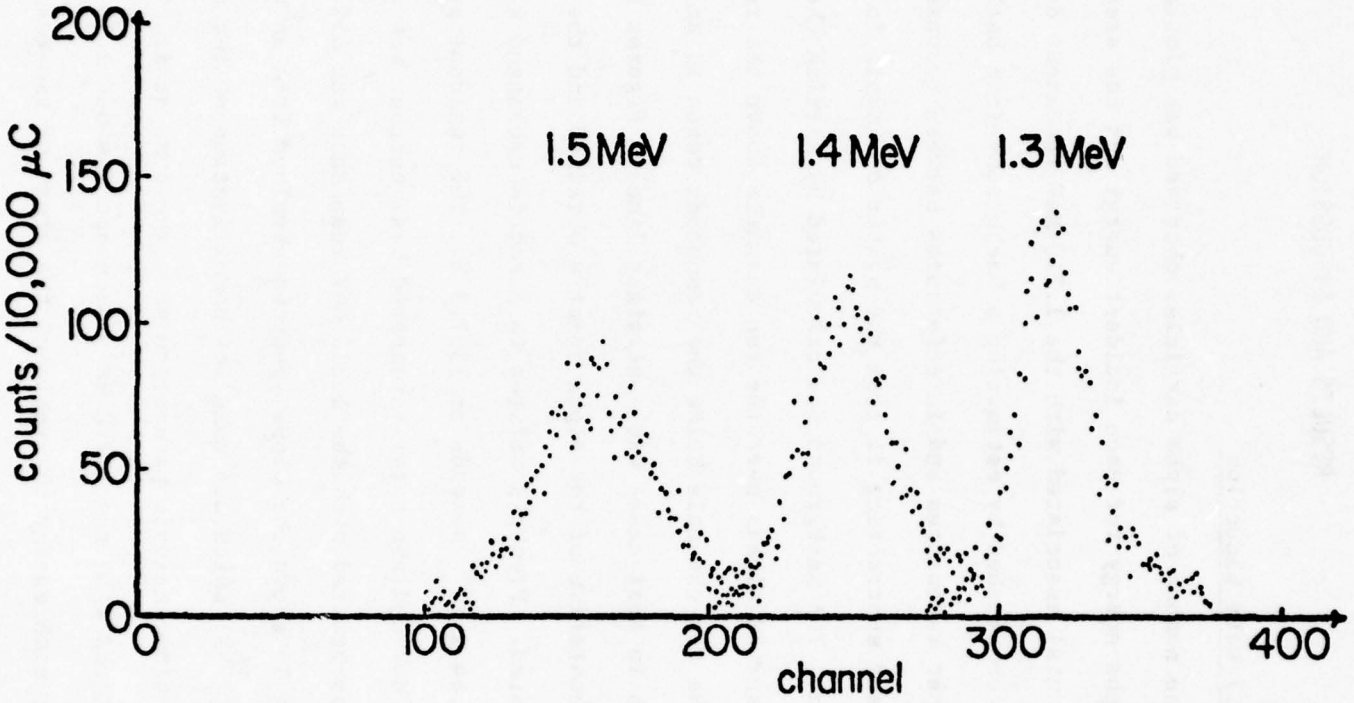

Figure 8: Alpha spectra from the 1.210 MeV resonance from an undiffused Si_3N_4 sample for three incident proton energies.

SECTION V

RESULTS AND DISCUSSION

5.1 Data Reduction

The number of alpha particles observed was plotted as a function of alpha energy for each incident energy and the area (total number of counts) associated with the 1.210 MeV resonance determined. This was accomplished by estimating a background (the background is due to other resonances and interferences between resonances, see Section B.4) and subtracting it from the number of counts in the resonance region. The background was calculated by fitting the average number of observed alphas over the ten channels above the resonance region and the ten channels below the resonance regon to an appropriate curve (which in most cases was a straight line). Figures 9 and 10 are representative of the alpha spectra obtained and the background estimated. Figure 9 relates to a sample exchanged with nitrogen-15 for 8.64×10^{14} seconds at 1507.5 K. The incident proton energy was 1.300 MeV and the total integrated beam current was 2×10^{3} μC. The area associated with the 1.210 MeV resonance was 1357 ± 37 counts. Figure 10 shows the alpha spectrum obtained from an undiffused sample (0.37% ^{15}N) which was used for normalization of the data. The proton activation analysis parameters were the same as in Figure 9. The area associated with the 1.210 MeV resonance was 664 ± 26 counts.

At each energy the ratio of the areas of the resonance region of the diffused sample to the undiffused sample was calculated and multiplied by 3.7×10^{-3}, the natural abundance of nitrogen-15, to

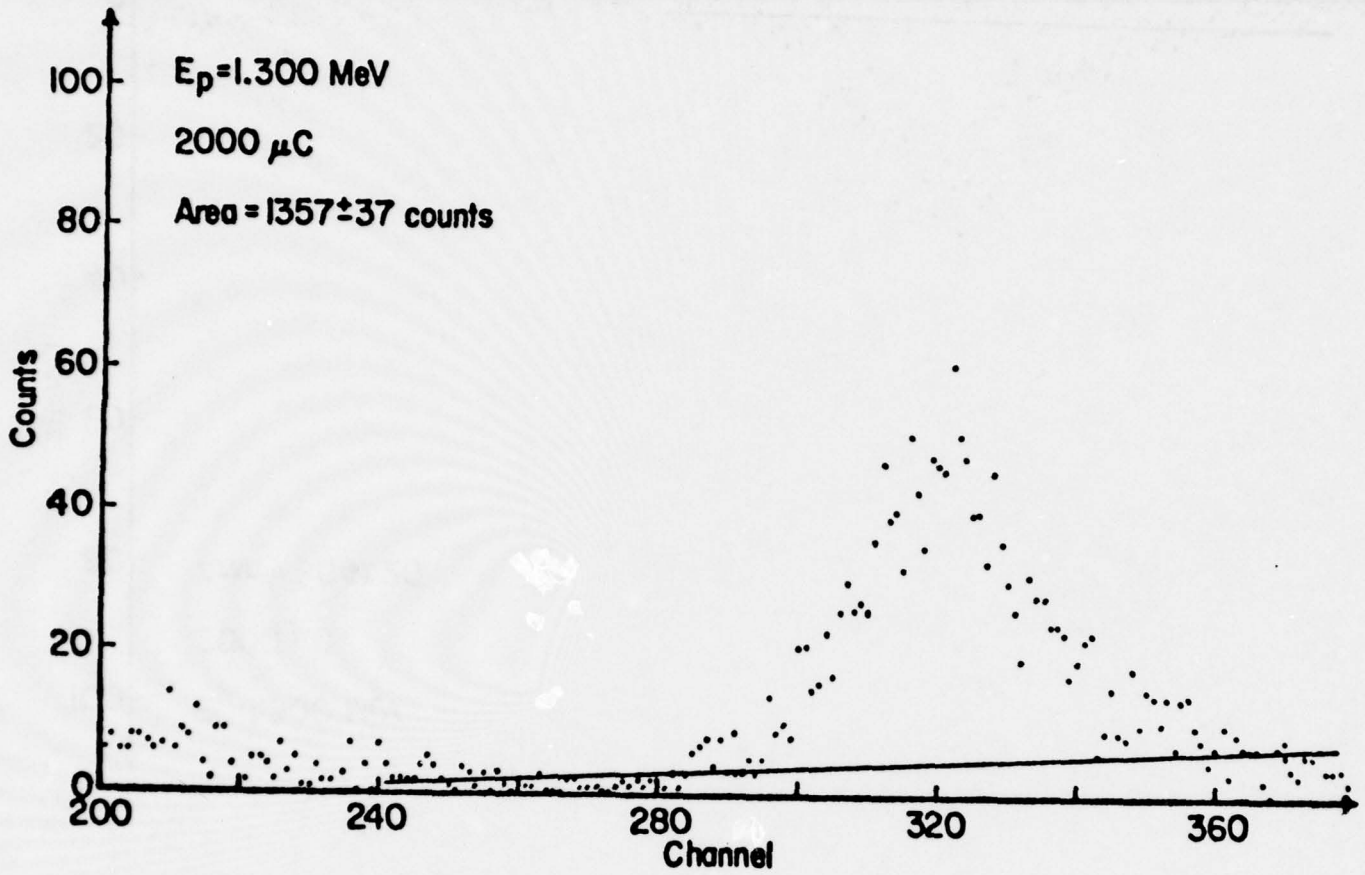

Figure 9: Observed alpha spectrum for a sample exchanged with nitrogen-15 for 8.64×10^4 seconds at 1507.5 K.

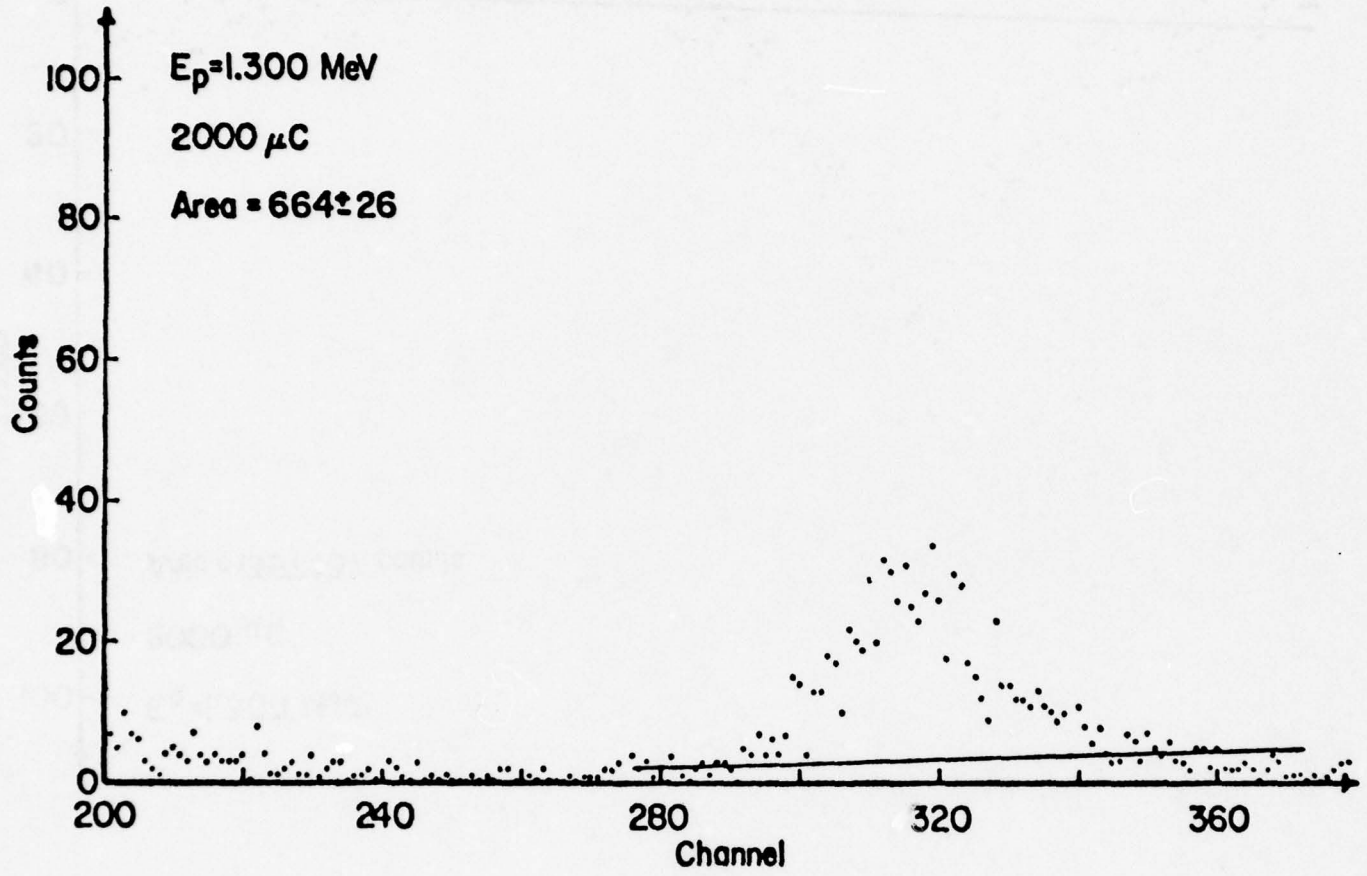

Figure 10: Observed alpha spectrum for an undiffused sample.

determine the nominal average fractional concentration of nitrogen-15, in each depth interval. Figures 11-14 show the nominal average fractional concentration versus "mean depth" profiles for representative samples. The "mean depth" associated with each incident proton energy was obtained from Figure 7.

In order to obtain the true average fractional concentration, $\bar{C} + C_o$, from the nominal average fractional concentration it is necessary to look at the variation in the concentration profile over the depth probed by the resonance. Since the yield from the resonance region is proportional to the integral of the product of the concentration and the differential cross section over the depth interval associated with the depth of the resonance (see Equation 38), the nominal average fractional concentration and true average fractional concentration will be exactly equal if the concentration profile in the interval is constant. If the concentration profile varies slowly in a uniform manner over the depth interval then the nominal average fractional concentration will be a reasonable estimate of the true average fractional concentration. This is the case for the points corresponding to "mean depths" greater than 0.25 μm in Figures 11-14. However, if the concentration profile varies rapidly or in a nonuniform manner across the depth interval the nominal average fractional concentration and the true average fractional concentration can be drastically different. This is the case for the first four points in Figures 11-14. The analysis of the concentration profile in this region will be treated later.

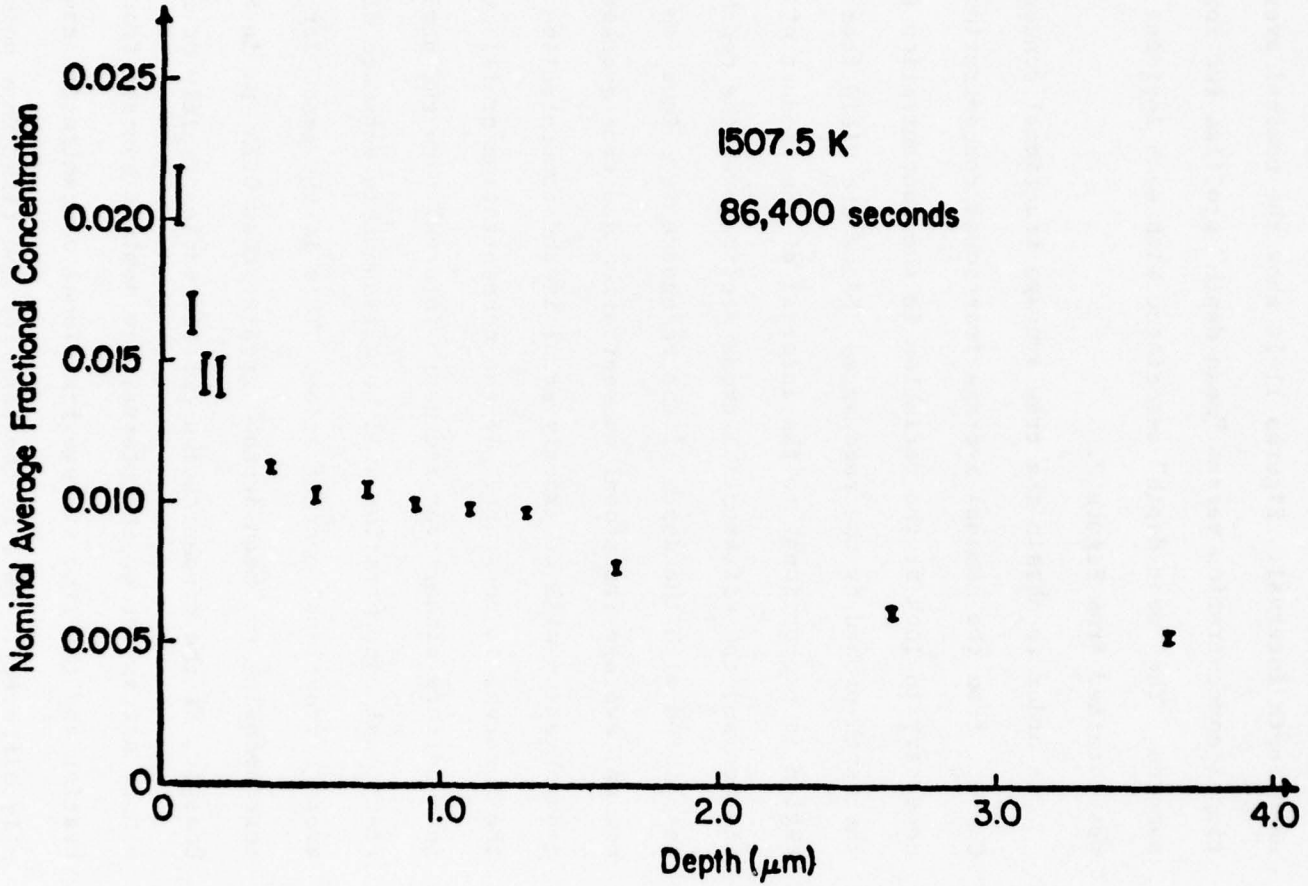

Figure 11: Nominal average fractional concentration versus depth profile for Sample 1.

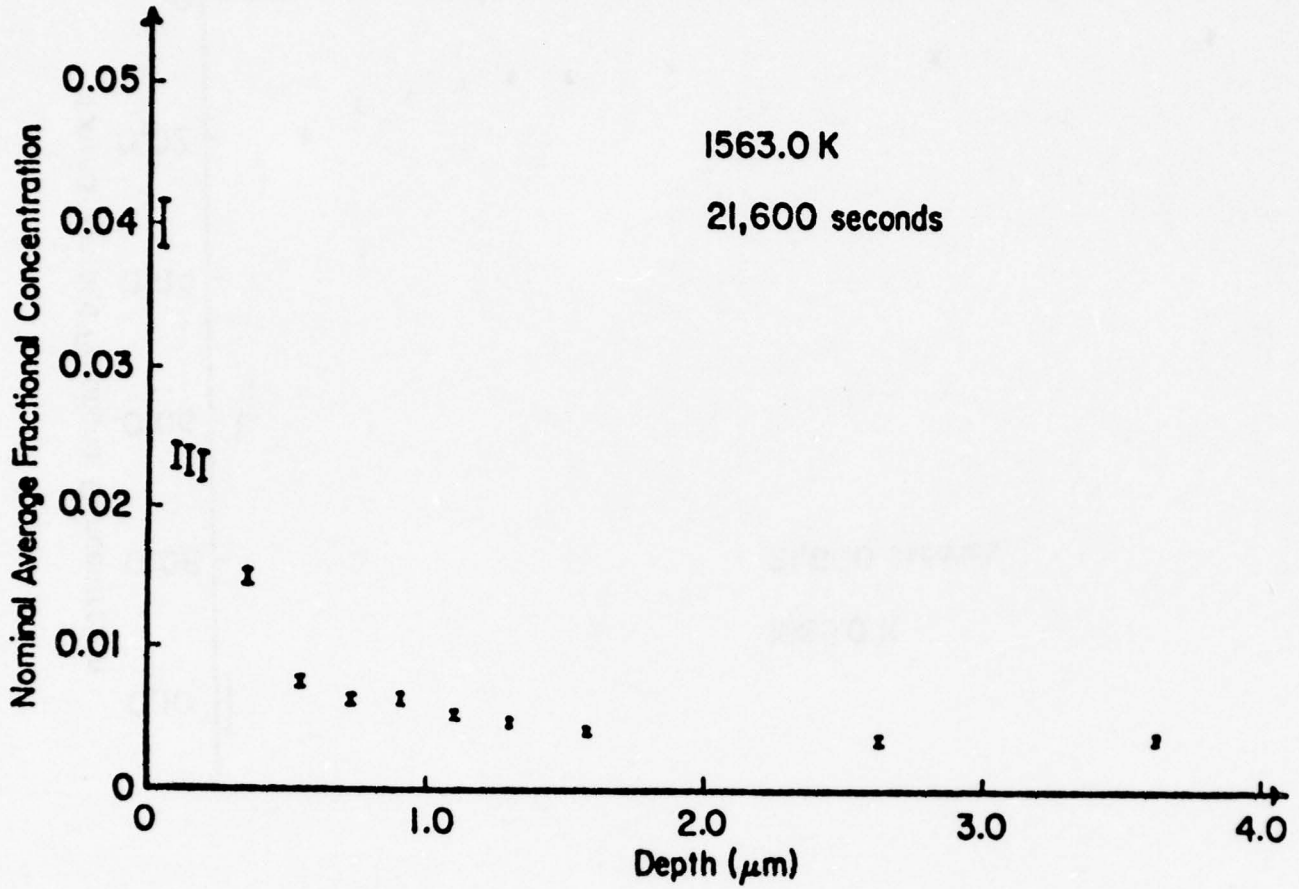

Figure 12: Nominal average fractional concentration versus depth profile for Sample 3.

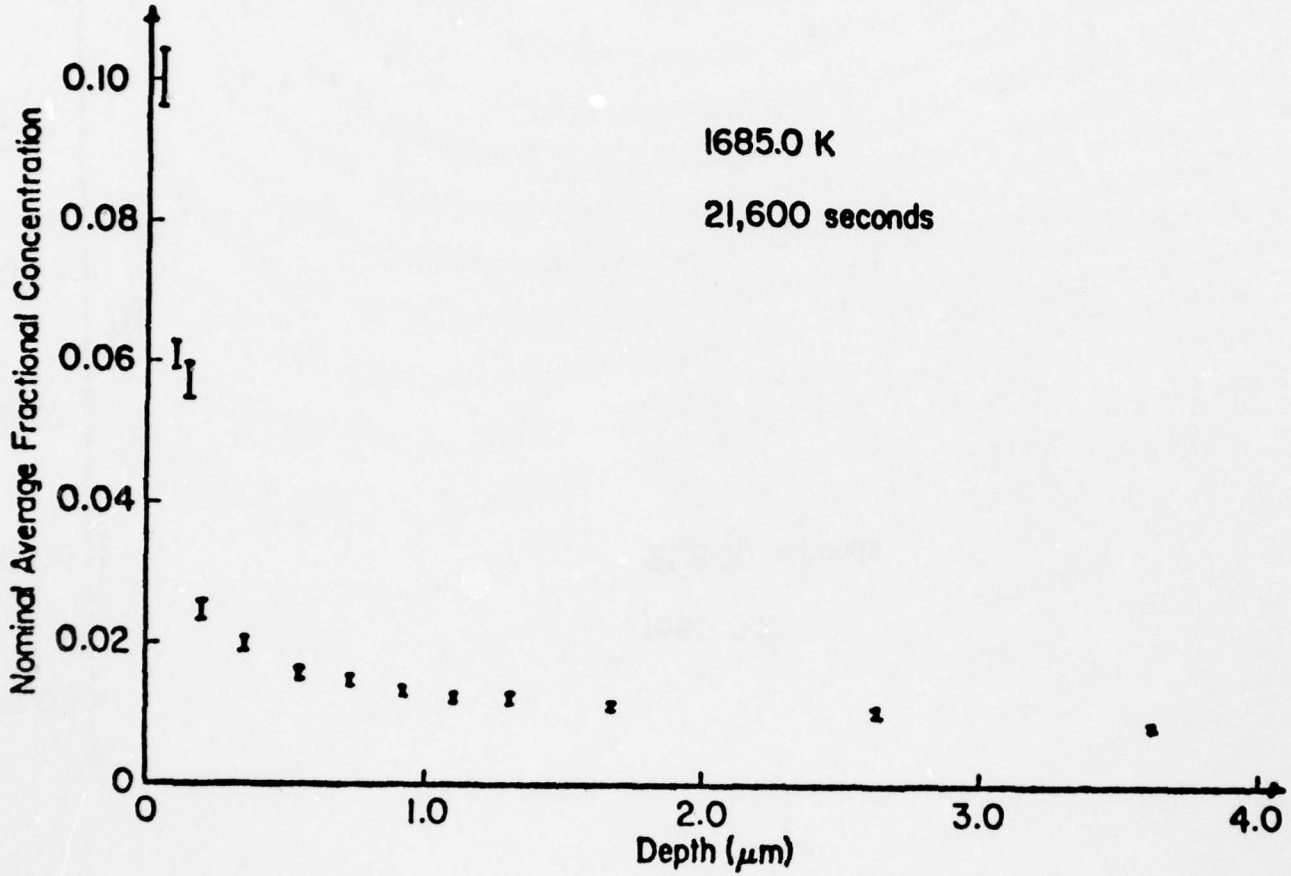

Figure 13: Nominal average fractional concentration versus depth profile for Sample 6.

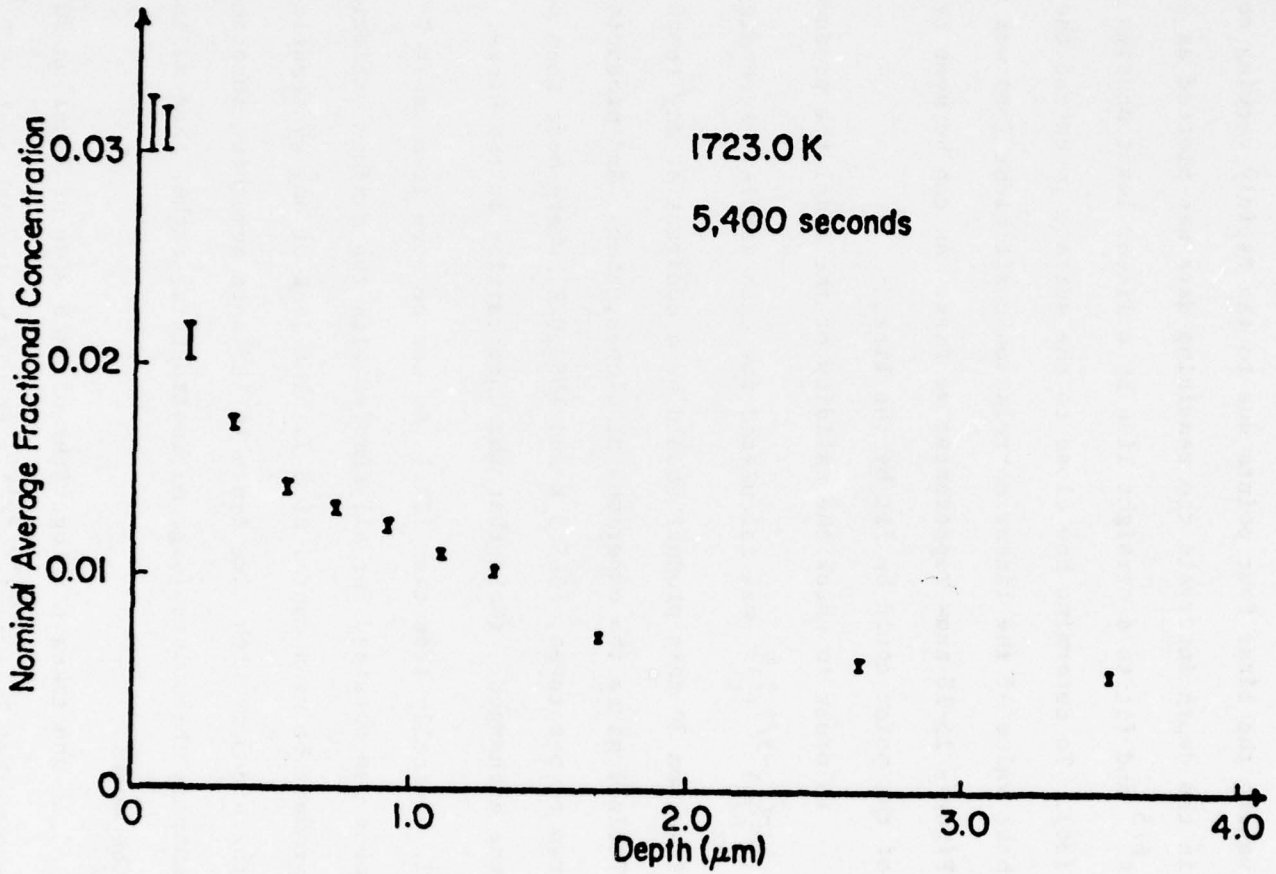

Figure 14: Nominal average fractional concentration versus depth profile for Sample 7.

According to Levine and MacCallum (7), a plot of ln $\bar{C}$ versus $x^{6/5}$, see Equation 30, should be linear at deep penetrations. After eliminating the first four points due to the rapidly varying concentration in the depth intervals the remaining data was plotted as ln $\bar{C}$ versus $x^{6/5}$ and fit to a straight line by a linear least squares procedure (36). To determine how close to the surface to extend the fit the best value of the linear correlation coefficient (36) was used. Figures 15-18 show representative fits. As can be seen typically all of the point could be fit by the line.

In order to check the validity of the model the product $(\frac{\partial \ln \bar{C}}{\partial x^{6/5}})^{-5/3}(\frac{1}{t})^{\frac{1}{2}}$ was calculated for each sample. According to Equation 30 this product should be a constant at any temperature. Table 7 gives the experimental slopes, times, and products for the two temperatures, 1565.5 K and 1683.0 K, where more than one sample was exchanged. (Note that the uncertainity in the slope, $\frac{\partial \ln \bar{C}}{\partial x^{6/5}}$ is typically less than 12%.) As can be seen from Table 7 fair agreement was obtained for all samples with the maximum variation in the product being a factor of 6.7. The lack of any systematic trend in the products with time tends to indicate something inherent in the samples themselves (e.g. microstructure) rather than an inadequacy in the model.

If one takes the logarithm of each side of Equation 30 it can be shown that $\ln[(\frac{\partial \ln \bar{C}}{\partial x^{6/5}})^{-5/3}(\frac{1}{t})^{\frac{1}{2}}]$ should be proportional to T^{-1}.

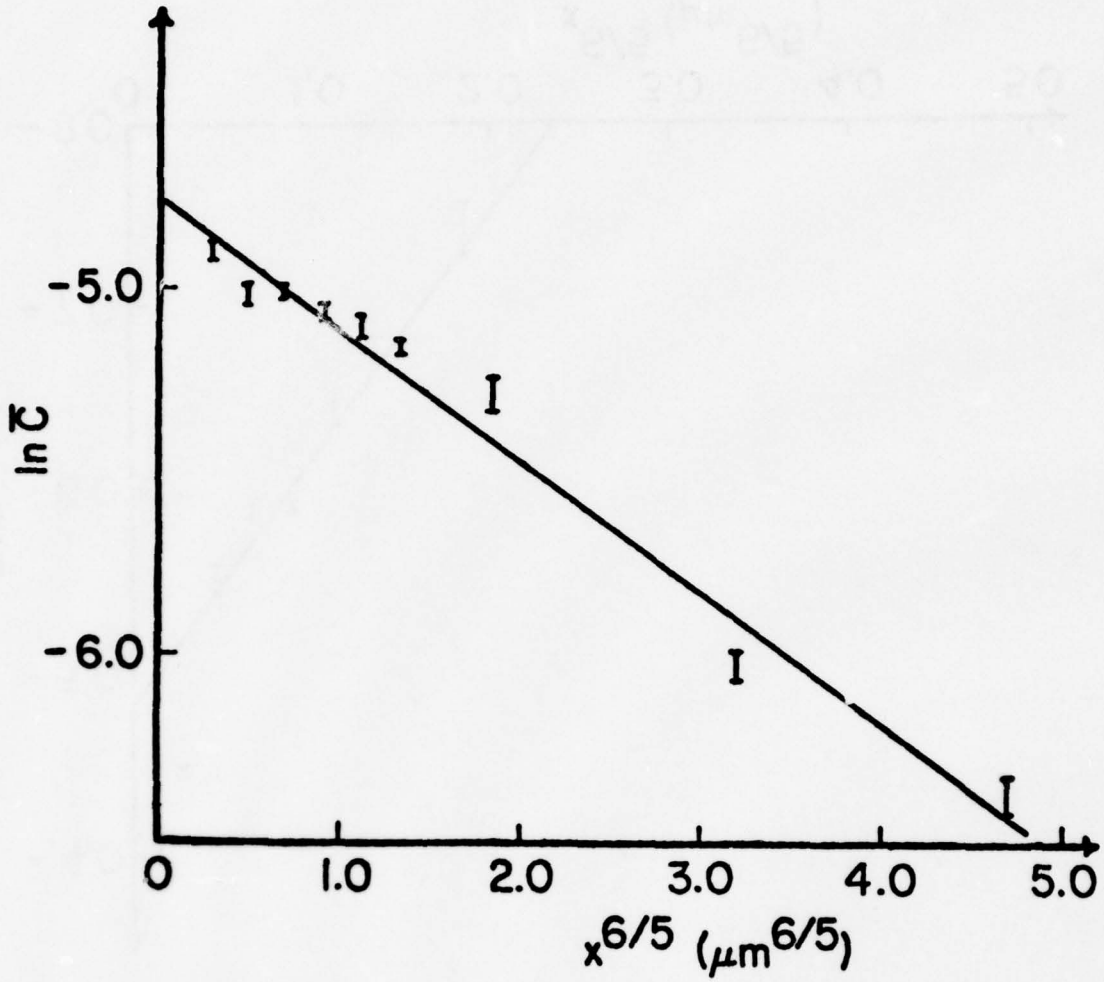

Figure 15: Plot of $\ln\bar{C}$ versus $x^{6/5}$ for Sample 1.

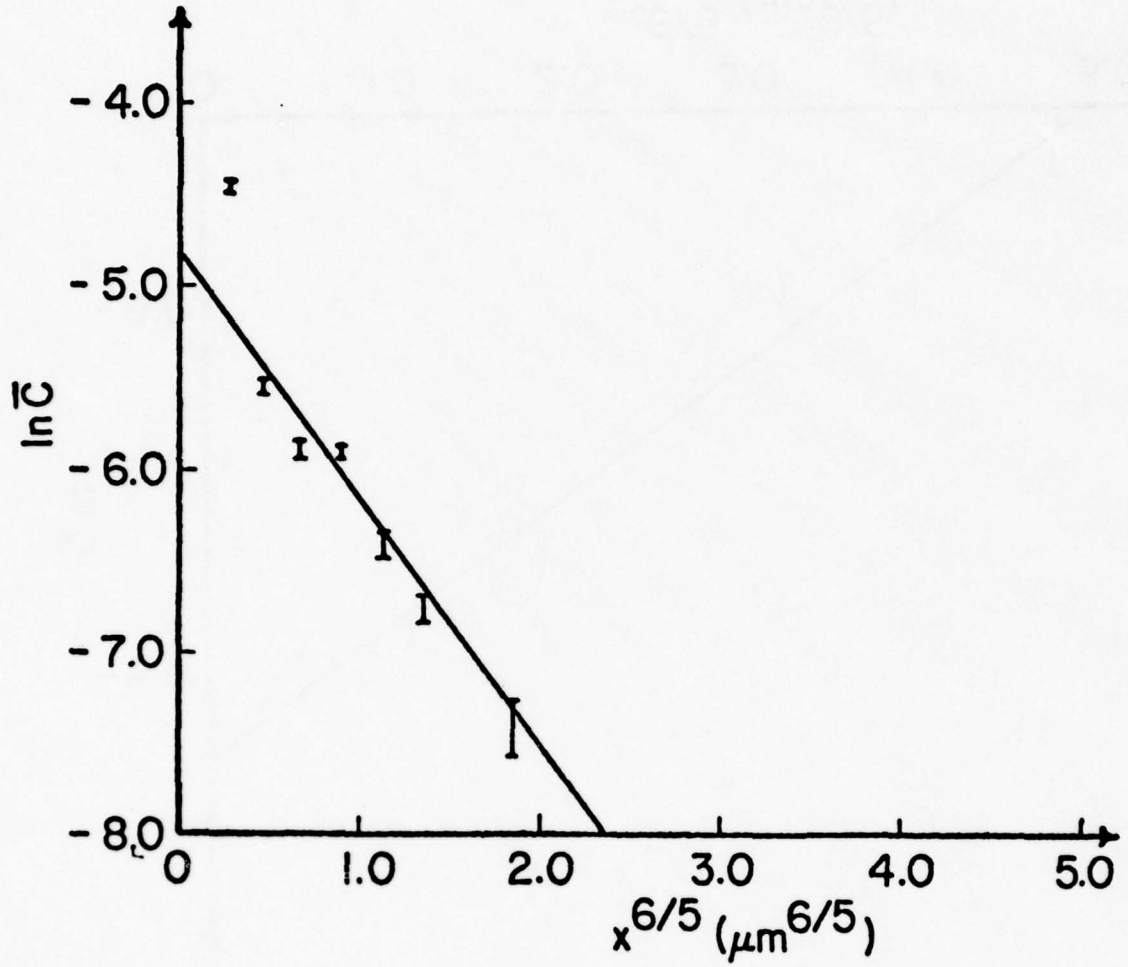

Figure 16: Plot of $\ln \bar{C}$ versus $x^{6/5}$ for Sample 3.

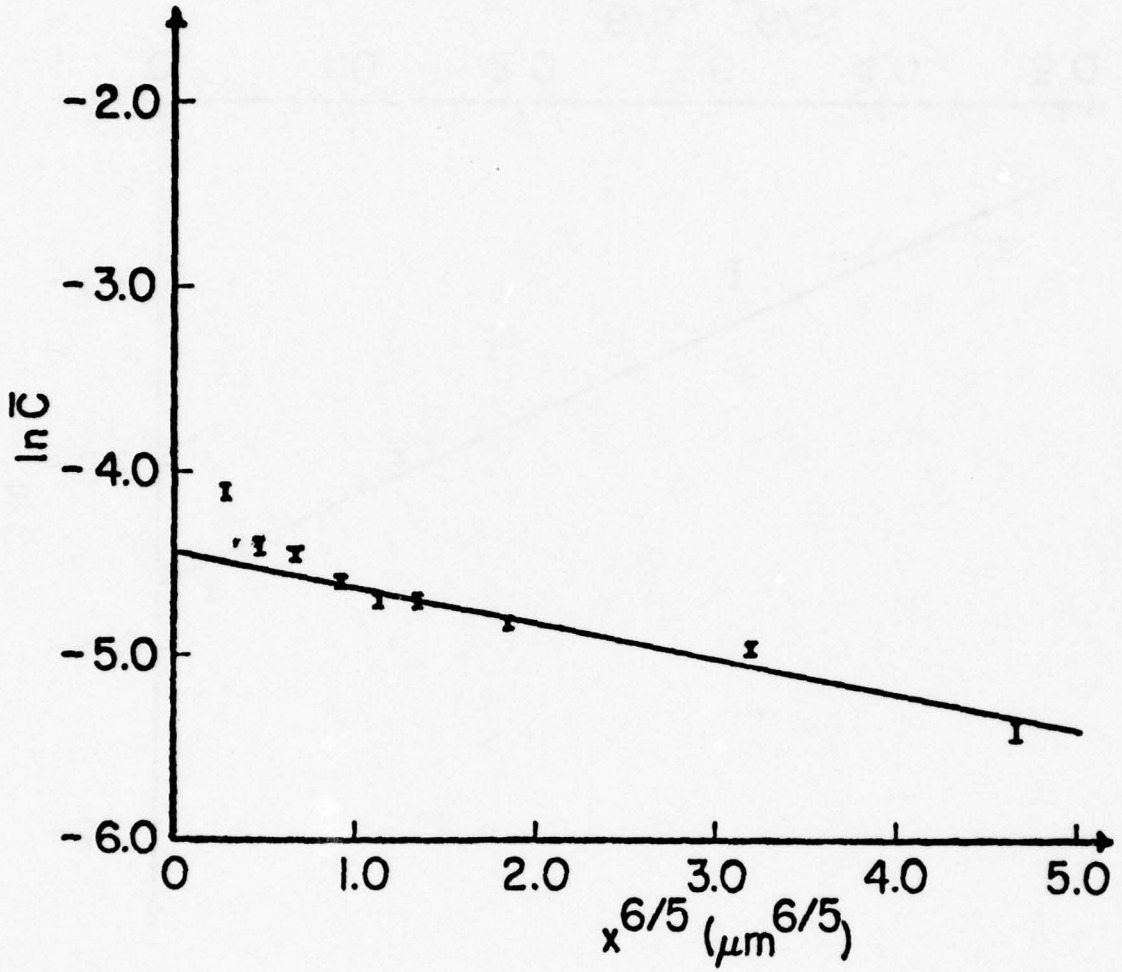

Figure 17: Plot of $\ln\bar{C}$ versus $x^{6/5}$ for Sample 6.

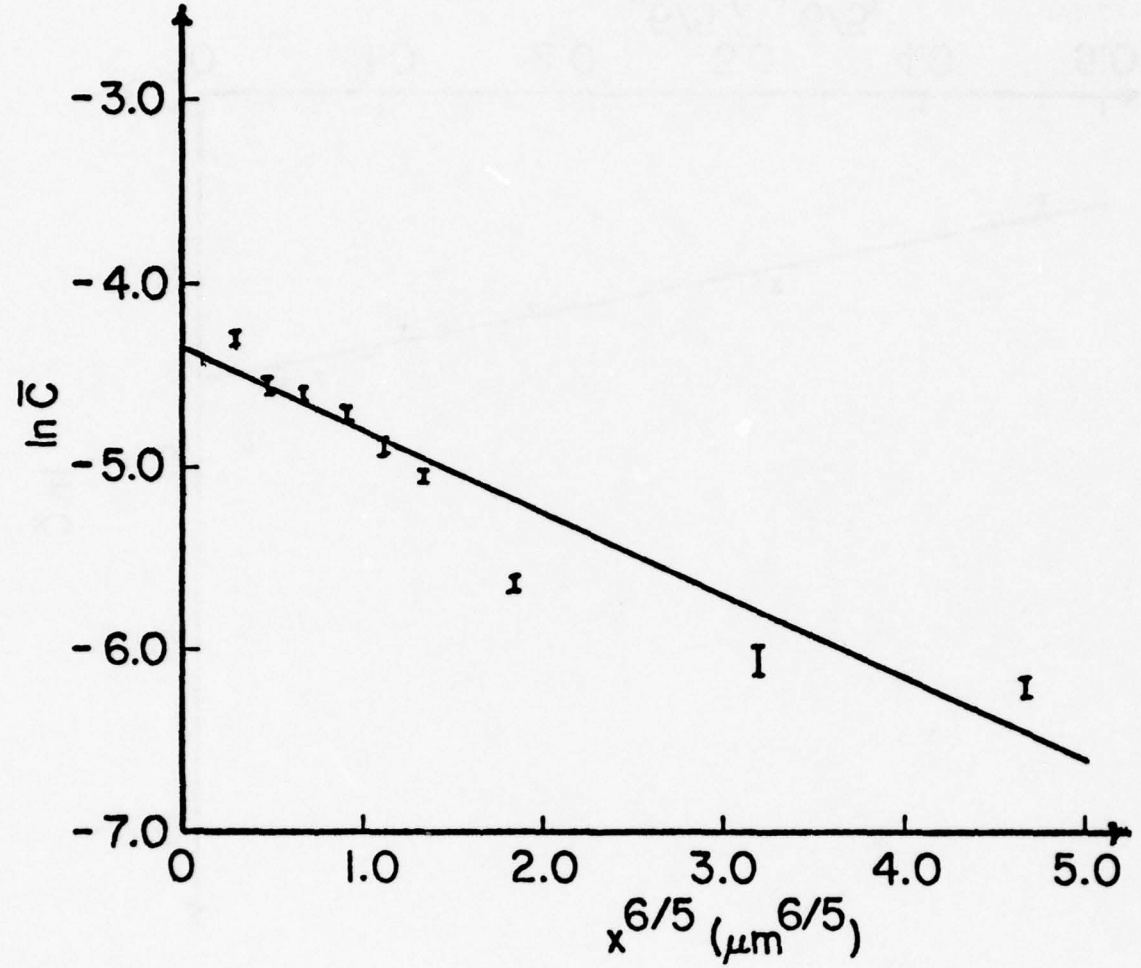

Figure 18: Plot of $\ln\bar{C}$ versus $x^{6/5}$ for Sample 7.

TABLE 7

Experimental Parameters for Grain Boundary Fits

Sample	Temperature (K)	$\left(\frac{\partial \ln \bar{C}}{\partial x^{6/5}}\right)$	Time (Sec)	$\left(\frac{\partial \ln \bar{C}}{\partial x^{6/5}}\right)^{-5/3} \left(\frac{1}{t}\right)^{1/2}$
2	1568.0	-2.072 ± 0.212	0.54×10^{4}	$(4.04 \pm 0.69) \times 10^{-3}$
3	1563.0	-1.387 ± 0.090	2.16×10^{4}	$(3.94 \pm 0.43) \times 10^{-3}$
4	1565.5	-0.292 ± 0.032	8.64×10^{4}	$(2.65 \pm 0.48) \times 10^{-2}$
5	1681.0	-0.123 ± 0.009	0.54×10^{4}	$(4.47 \pm 0.55) \times 10^{-1}$
6	1685.0	-0.188 ± 0.021	2.16×10^{4}	$(1.10 \pm 0.21) \times 10^{-1}$

This being the case, a graph of this function versus T^{-1} should be a straight line, however as can be seen in Figure 19,there is a fair amount of scatter in the points. This scatter can be attributed to either nonuniformity in the samples, or the inability of the model to adequately treat the case of intersecting grain boundaries or possibly the presence of a phase boundary reaction.

Because of the rapidly varying concentration of nitrogen-15 at the sample surface the number of counts obtained in the resonance region for the first four depth intervals may be almost entirely due to this surface concentration. For this reason the volume diffusivity was estimated using the total number of counts obtained in the resonance region. The use of only the total number of counts to estimate D_v requires three assumptions to be made. First it is necessary to decide if a phase boundary reaction plays any part in the profiles obtained.Because of the inability to determine uniquely both a value of D_v and of K_s from the data available,it was decided to assume there was no phase boundary reaction thus giving the lowest possible value of D_v. This assumption was also made by Kijima and Shirasiki in their study.

It was also necessary to make some assumption regarding the contribution to the total number of counts from nitrogen-15 in the grain boundaries. It has been assumed for the purpose of calculation that the contribution is negligible,which is justified by the fact that the apparent surface contribution due to nitrogen-15 in the grain boundaries (see Figures 15-18) is approximately 1% while it has been

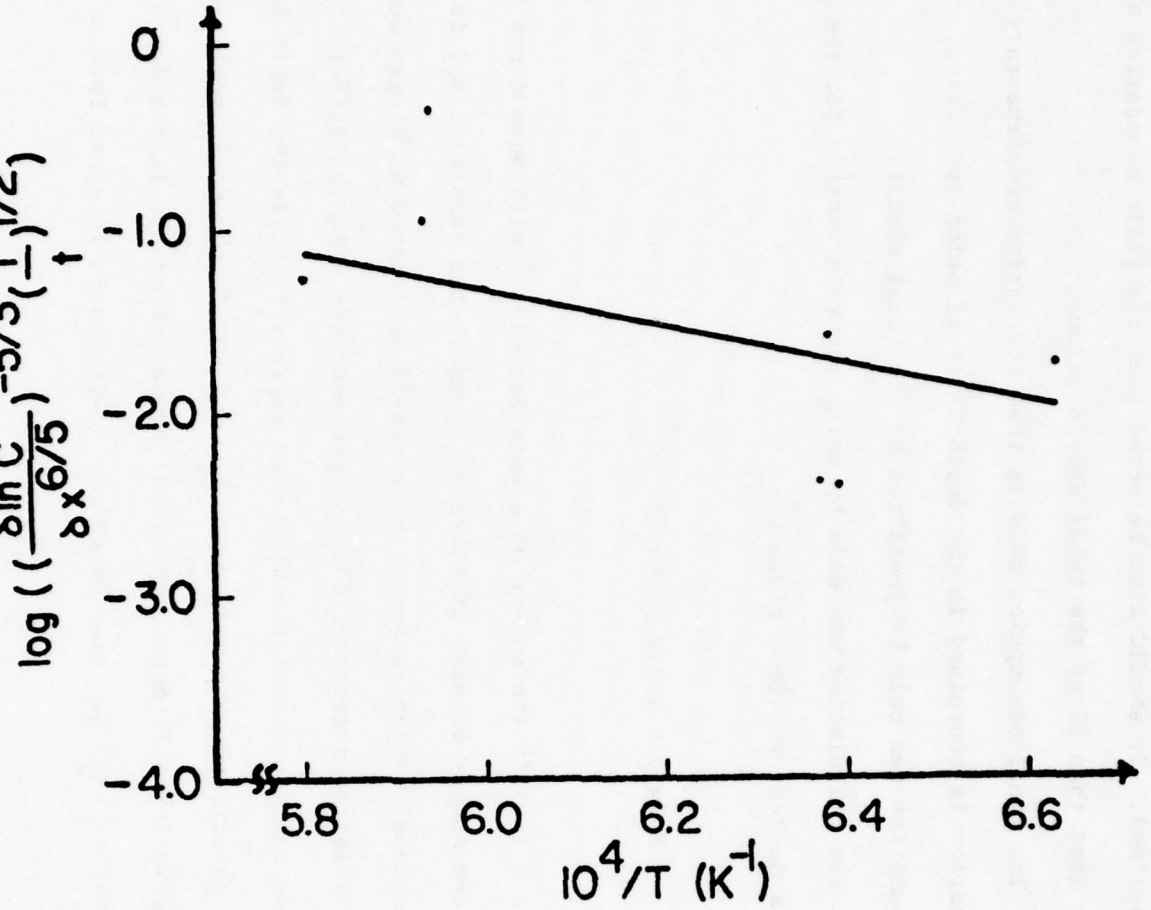

Figure 19: Plot of $\log\left[\left(\frac{\partial \ln \bar{C}}{\partial x^{6/5}}\right)^{-5/3}\left(\frac{1}{t}\right)^{\frac{1}{2}}\right]$ versus $\frac{1}{T}$.

assumed that the surface concentration is 100% (no phase boundary reaction). It should also be noted that the grain boundaries account for less than 2% of the total sample volume.

The final assumption made is that the entire complementary error function is contained in the depth interval being considered. This assumption can only be justified by the final result.

The calculation was made by using the relationship for the yield of a nuclear reaction given by:

$$N_o(x_i) = N\, C(x_i) j \sigma(x_i) \Delta x_i \Delta\Omega \tag{38}$$

Here $N_o(x_i)$ is the number of counts associated with mean depth x_i; N is the number density of nitrogen atoms in the sample; $C(x_i)$ is the fractional concentration of nitrogen-15 associated with mean depth x_i; j is the integrated flux of protons; $\sigma(x_i)$ is the differential cross section associated with mean depth x_i; Δx_i is the depth interval associated with mean depth x_i; and $\Delta\Omega$ is the solid angle of observation. To obtain the total number of counts in the depth interval (x_1, x_2) Equation 38 can be rewritten in integral form as:

$$N_o = Nj\, \Delta\Omega \int_{x_1}^{x_2} C(x)\sigma(x)dx \tag{39}$$

If the differential cross section does not drastically change over the depth interval (x_1,x_2) it can be replaced by an average cross section value, $\bar{\sigma}(x)$ and Equation 39 rewritten as:

$$N_o = Nj\Delta\Omega\bar{\sigma}(x)\int_{x_1}^{x_2} C(x)dx \tag{40}$$

For Si_3N_4 N is equal to 5.5×10^{28} nitrogens-m^{-3}. The total charge collected was 2 mC which corresponds to an integrated proton flux of 1.25×10^{16} protons and the solid angle of observation was 7.2×10^{-5} sr. Initially it was assumed that the entire complementary error function was contained within the interval $(x_1,x_2) = (0,20nm)$ which is the interval over which a proton loses 1 keV of energy in Si_3N_4. The integral in Equation 40 can then be replaced by (37):

$$\int_{x_1}^{x_2} C(x)dx = \int_{o}^{20nm} \operatorname{erfc} \frac{x}{2(D_v t)^{\frac{1}{2}}}\, dx = \int_{o}^{\infty} \operatorname{erfc} \frac{x}{2(D_v t)^{\frac{1}{2}}}\, dx$$

$$= 1.1284(D_v t)^{\frac{1}{2}} \tag{41}$$

This substitution can be made if the surface concentration is unity and the entire complementary error function is contained in the interval (0,20nm). Equation 40 can now be rewritten as:

$$N_o = (5.58 \times 10^{40}) \frac{sr}{m^3}\ \bar{\sigma}(x)(D_v t)^{\frac{1}{2}} \tag{42}$$

The values of $\bar{\sigma}(x)$ used (see Figure 3) were 114 mb, 157 mb, and 127 mb for incident proton energies of 1.205 MeV, 1.210 MeV, and 1.215 MeV respectively. The appropriate number of counts (observed-background-undiffused) and time were substituted in Equation 42 and the Equation solved for D_v. If it was found that the value of $2(D_v t)^{\frac{1}{2}}$ exceeded 20nm, as was the case for samples 4 and 6, it was necessary to increase the depth interval and hence use a slightly different differential cross section. This calculation was made for the first three points of each sample and the results tabulated in Table 8. As can be seen reasonable agreement was obtained between the values of D_v calcualted from the resonance yield in each of the first three depth intervals considering the fact that the cross section is known to ±5% at the resonant energy. The fact that the calculated value of D_v increases with increasing time at a given temperature (Samples 2, 3, & 4 and 5 & 6) is indicative of either the presence of a phase boundary reaction or the failure to account for the nitrogen-15 present in the grain boundaries. It can also be seen that the value of D_v calculated when the incident proton energy was 1.210 MeV is usually the lowest value of D_v. This can be attributed to the fact that the differential cross section is a maximum at this point and any deviation in machine energy will cause the differential cross section to decrease, thus decreasing the alpha yield.

Figure 20 shows a comparison of the number of counts observed in each of the first three depth intervals and the number of counts

TABLE 8

Calculated Volume Diffusivities

Sample	Temperature (K)	Time (Sec)	$D_v (m^2 - sec^{-1})$			
			1.205 MeV	1.210 MeV	1.215 MeV	Average
1	1507.5	8.64×10^4	6.19×10^{-23}	3.05×10^{-23}	5.33×10^{-23}	4.85×10^{-23}
2	1568.0	0.54×10^4	7.29×10^{-22}	3.28×10^{-22}	4.26×10^{-22}	4.91×10^{-22}
3	1563.0	2.16×10^4	1.10×10^{-21}	6.05×10^{-22}	7.31×10^{-22}	8.12×10^{-22}
4	1565.0	8.64×10^4	4.93×10^{-21}	3.62×10^{-21}	4.56×10^{-21}	4.37×10^{-21}
5	1681.0	0.54×10^4	6.71×10^{-21}	1.16×10^{-21}	2.22×10^{-21}	3.36×10^{-21}
6	1685.0	2.16×10^4	7.80×10^{-21}	2.34×10^{-21}	5.45×10^{-21}	5.19×10^{-21}
7	1723.0	0.54×10^4	2.56×10^{-21}	2.14×10^{-21}	2.03×10^{-21}	2.24×10^{-21}

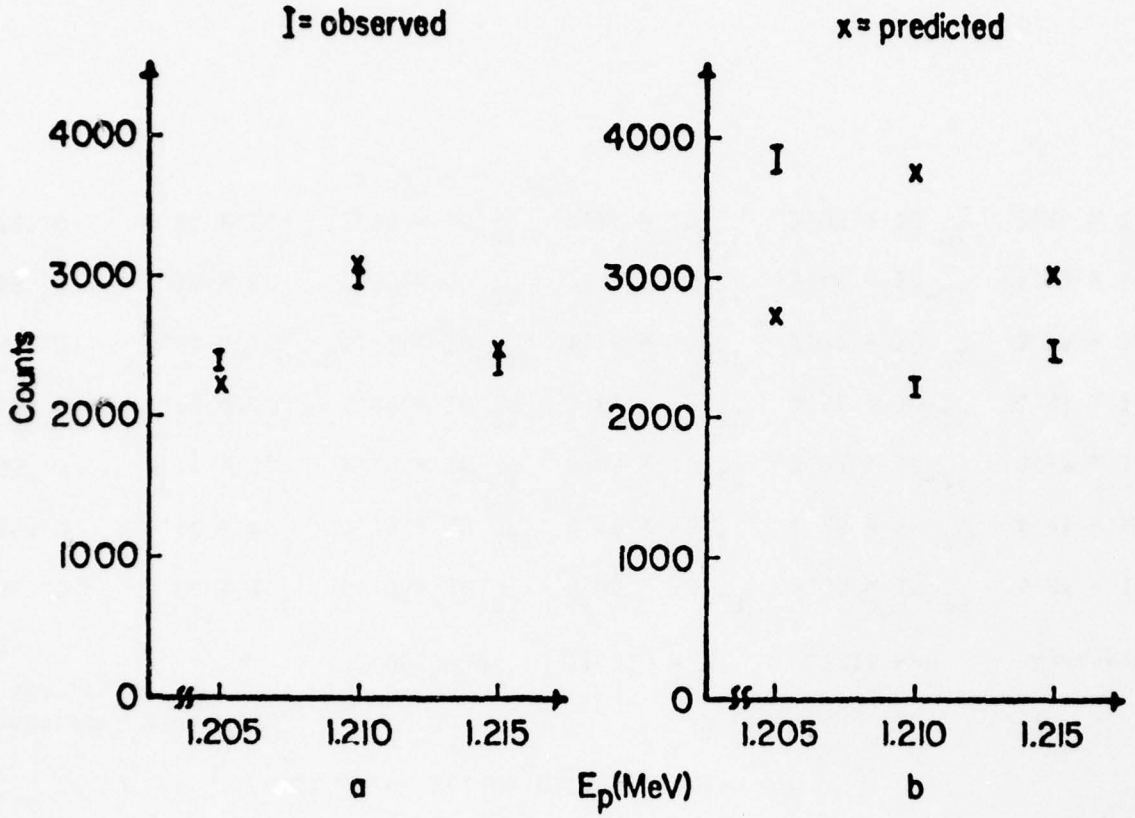

Figure 20: Comparison of the observed number of counts and predicted number of counts based on the average value of D_v given in Table 8 for (a) Sample 7 and (b) Sample 5.

observed in each of the first three depth intervals and the number of counts that would be predicted in the interval assuming the average diffusivity given in Table 8. Figure 20a is for the sample with the smallest spread in diffusivities (Sample 7) and Figure 20b for that with the largest spread in calculated diffusivities (Sample 5).

The temperature dependance of D_v is shown in Figure 21 and given by:

$$D_v\left(\frac{m^2}{sec}\right) = 2.02 \times 10^{-11}\left(^{+4.90 \times 10^{-9}}_{-2.01 \times 10^{-11}}\right)\exp - \frac{(3.17 \pm 0.74)\times 10^5}{RT} \qquad (43)$$

The relationship found by Levine and MacCallum (7), Equation 30, was used to obtain the value of $D_{GB}\delta$ for each sample. The value of D_v substituted in Equation 30 was the average value given in Table 8. Table 9 is a tabulation of the value of $\left(\frac{\partial \ln C}{\partial(\gamma\tau^{-\frac{1}{2}})}\right)^{6/5}$ used, the values of the dimensionless parameters γ, τ, and $\gamma\tau^{-\frac{1}{2}}$, and the calculated value of D_{GB} (with δ = 3.0 nm). The value of the grain boundary thickness used, δ = 3.0 nm, was measured by electron microscopy (26) and is in agreement with the value given in the literature, 3.0 ± 1.0 nm (28).

The temperature dependence of D_{GB} is shown in Figure 22 and given by:

$$D_{GB}\left(\frac{m^2}{sec}\right) = 4.09\left(^{+2.34 \times 10^6}_{-4.09}\right)\exp - \frac{(5.09 \pm 1.77)\times 10^5}{RT} \qquad (44)$$

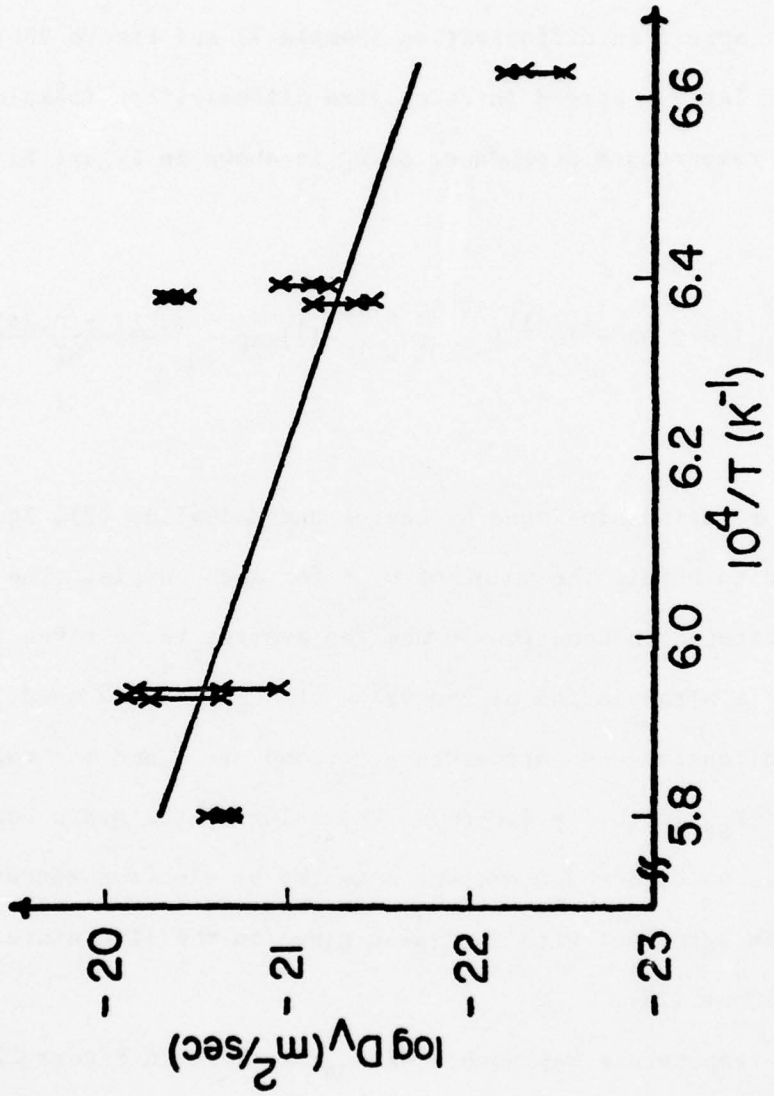

Figure 21: Temperature dependence of D_v.

TABLE 9

Calculated Dimensionless Parameters and Grain Boundary Diffusivities

Sample	Temperature (K)	Time (Sec)	$\frac{\partial \ln \bar{C}}{\partial (\gamma\tau^{-\frac{1}{2}})}_{6/5}$	γ	τ	$\gamma\tau^{-\frac{1}{2}}$	D_{GB} $(\frac{m^2}{sec})$
1	1507.5	8.64×10^4	0.78	9.8×10^2	2.2×10^5	2.1	1.45×10^{-17}
2	1568.0	0.54×10^4	0.78	1.2×10^3	1.9×10^4	8.7	9.88×10^{-18}
3	1563.0	2.16×10^4	0.78	4.8×10^2	5.4×10^3	6.5	1.23×10^{-17}
4	1565.0	8.64×10^4	0.78	1.0×10^2	3.4×10^3	1.7	1.92×10^{-16}
5	1681.0	0.54×10^4	0.99	4.7×10^2	4.5×10^5	0.7	4.25×10^{-15}
6	1685.0	2.16×10^4	0.99	1.9×10^2	3.5×10^4	1.0	$1.3- \times 10^{-15}$
7	1723.0	0.54×10^4	0.78	5.8×10^2	5.0×10^4	2.6	2.63×10^{-16}

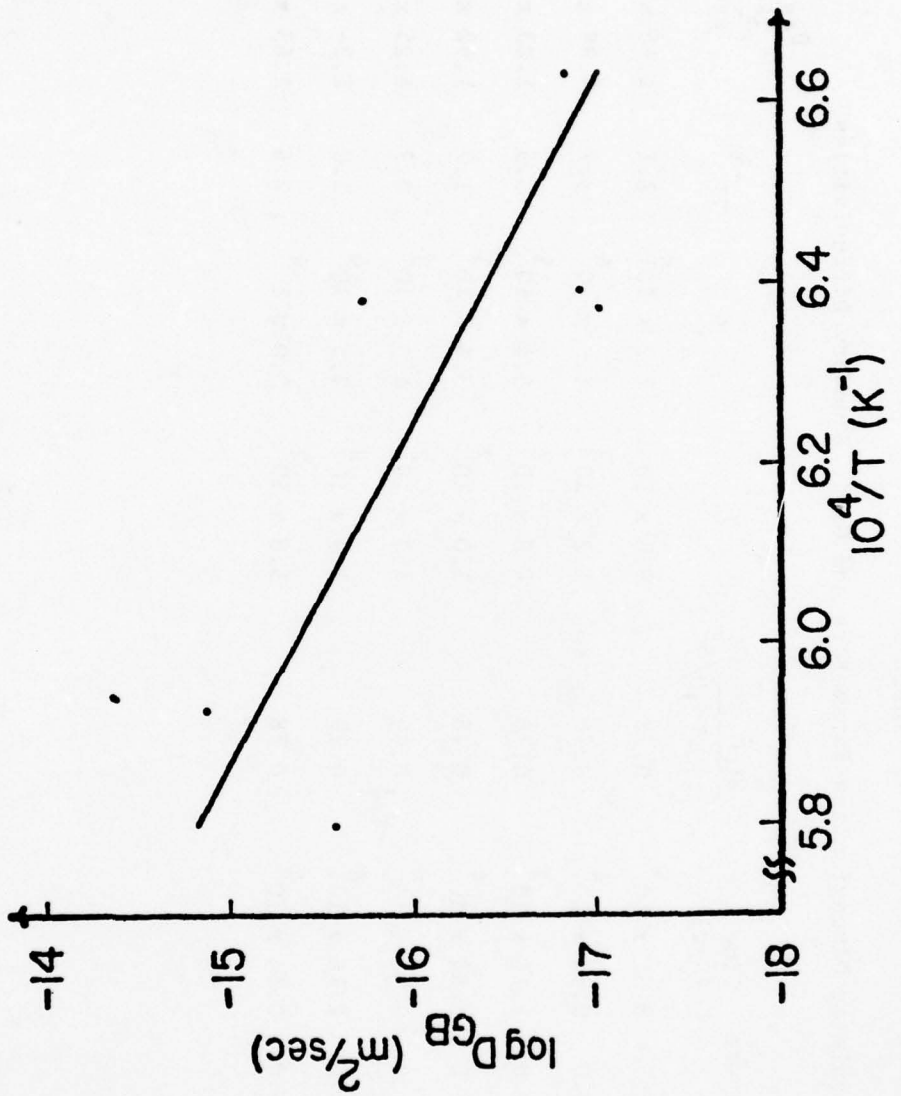

Figure 22: Temperature dependence of D_{GB}.

5.2 Comparison with the work of Kijima and Shirasaki (17).

Figure 23 shows a graphical comparison of Kijima and Shirasaki's results for nitrogen diffusion in β-Si_3N_4 and the results obtained in this study. As can be seen the value of D_v from this study is on the average 1½ orders of magnitude greater than that calculated by Kijima and Shirasaki while the activation energy is approximately $\frac{2}{5}$ that calculated by Kijima and Shirasaki.

The discrepancy in the magnitude of the measured diffusivities can be attributed to the difference in starting materials. Kijima and Shirasaki started with high purity, 55% theoretically dense, reaction sintered β-Si_3N_4 powders. The particle sizes in the powders were 75.0 μm and 1.0 mm with average grain sizes of 150 nm. The present study used a slab of commercial grade hot pressed Si_3N_4, NORALIDE^{TM} NC-132 , which contained a statistical mixture of 95% β -Si_3N_4 grains and 5% Si_2N_2O grains with an average grain size of 0.5 μm. The grains were surrounded by a 3.0 nm glassy phase. Gauckler and Lucas (38) have found that low concentrations of metal oxides will form single-phase solid solutions with β-Si_3N_4 without the production of extrinsic defects by maintaining a metal to non-metal ratio of 3 to 4. They argue that the high degree of covalency of the Si-N bond is responsible for the solid solution formation and the lattice not forming extrinsic defects upon the addition of metal oxides. (The justification for this is not obvious.) It has been found that the β-Si_3N_4 lattice expands when metal atoms larger than silicon dissolve in the lattice and contracts when metal atoms

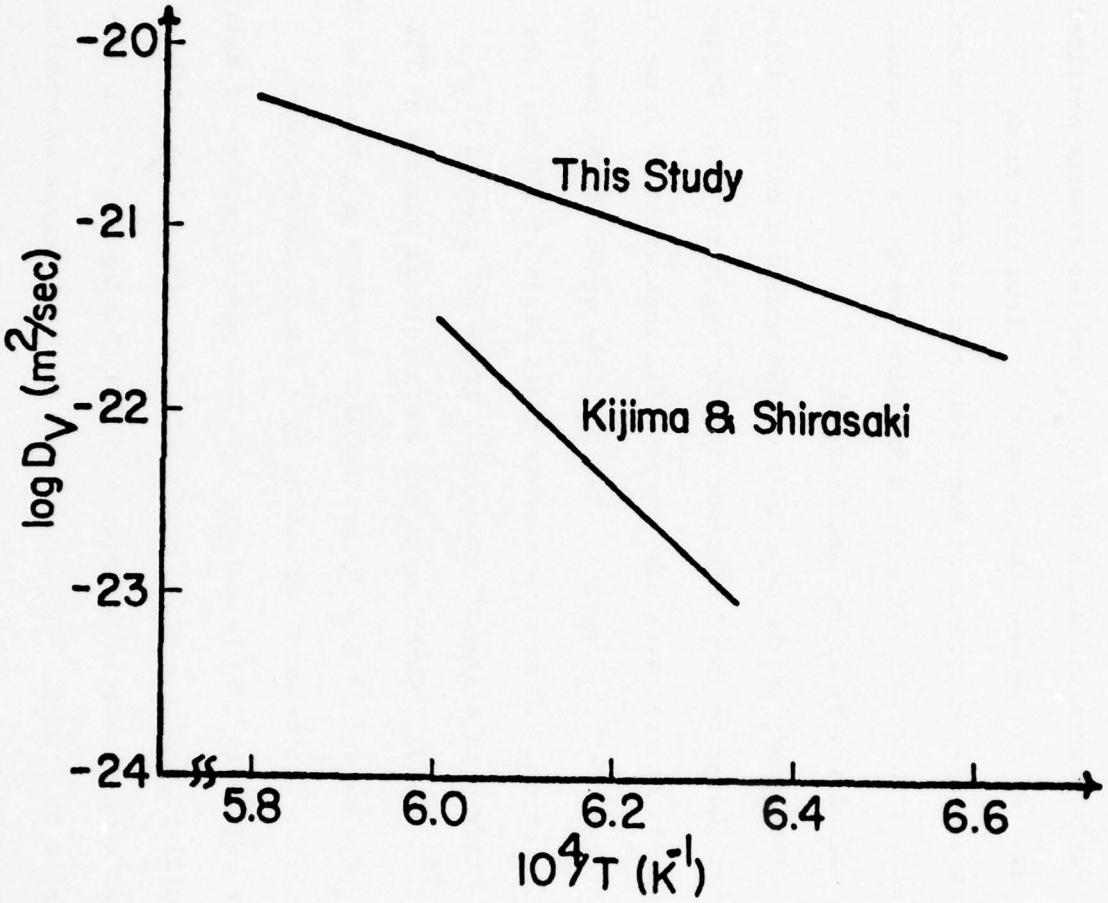

Figure 23: Comparison of D_v's obtained in this study and by Kijima and Shirasaki (17).

atoms smaller than silicon dissolve in the lattice. It would also be possible that the addition of MgO will create either magnesium interstitials or nitrogen vacancies. It is therefore reasonable to argue that based on either Gauckler and Lucas' argument (Mg covalent radii = 0.14 nm and Si covalent radii = 0.12 nm) or the formation of nitrogen vacancies that the rate of nitrogen diffusion will be enhanced by the addition of MgO.

5.3 Comparison with the Work of Brook, et.al. (24).

A comparison of the grain boundary diffusion coefficients calculated by Brook, et.al. and those measured in this study is shown in Figure 24. (Also shown is the value obtained if Kijima and Shirasaki's value of D_v is used in the calculation). The grain boundary diffusivity measured in this study is approximately $1\frac{1}{3}$ orders of magnitude larger than that measured by Brook, et.al. while the activation energy is in experimental agreement with that of Brook, et.al. Part of this discrepancy can be attributed to the materials used. Both studies used hot pressed silicon nitride, however the amount of MgO used as a hot pressing additive was different. Brook, et al's samples contained 5 w/O MgO and those in this study contained 0.5 w/O MgO.

Most of the discrepancy can be attributed to the models used to analyze the raw data. Brook, et.al. used a modified version of Coble's model (13) for densification during hot pressing which requires several assumptions (see Section 3.2) and to the author's knowledge results using the model have never been compared with other grain

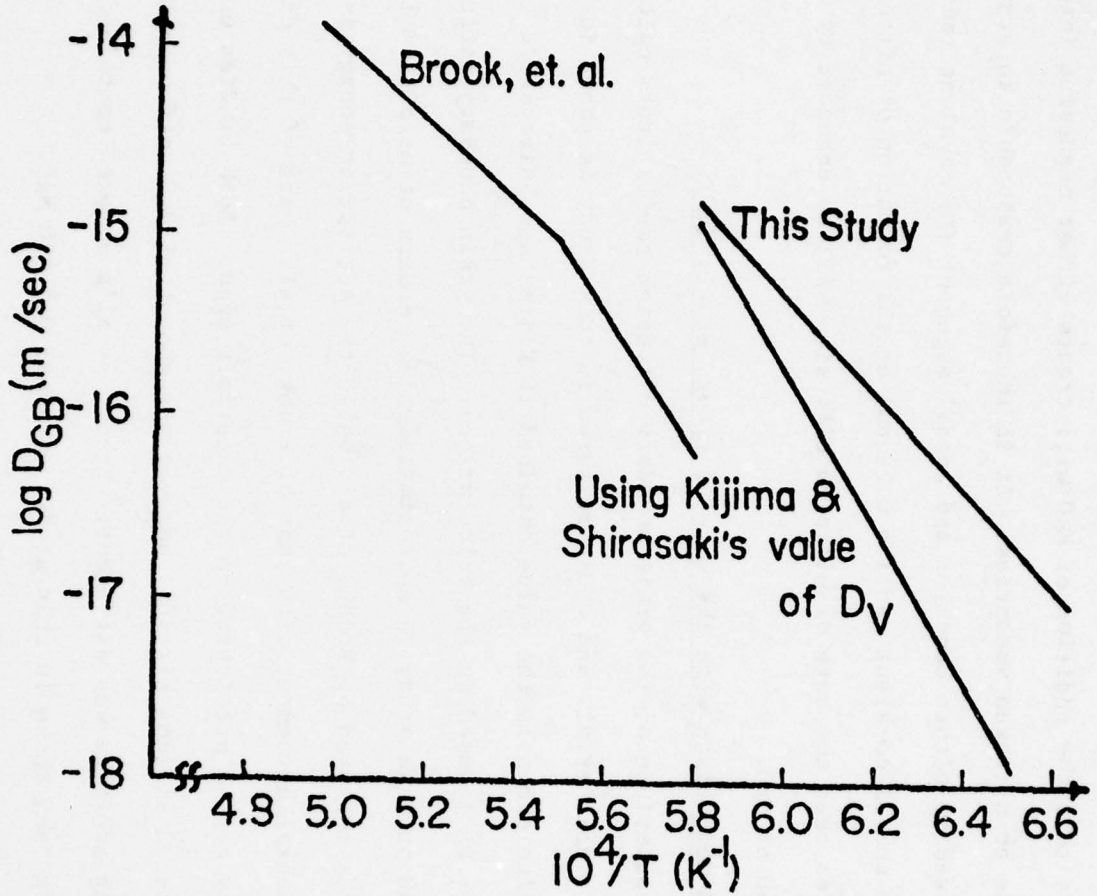

Figure 24: Comparison of D_{GB}'s obtained in this study and by Brook et.al. (24).

boundary diffusion data. Of the assumptions made several are subject to considerable question. First, is nitrogen grain boundary diffusion the rate controlling process in densification and if so, is the modified Coble model valid? The model used by Brook, et. al. also requires a knowledge of the grain size and the grain boundary thickness at the time of the measurement. Brook, et. al. do not state how they estimated their grain size especially since grain growth is occurring during the process. It was then assumed that by a knowledge of grain size, the amount of MgO added, and the $MgSiO_3$-SiO_2 equilibrium phase diagram the grain boundary thickness could be calculated. As can be seen from Equation 34 the grain boundary diffusivity is proportional to the cube of the grain size divided by the grain boundary thickness. Assuming a constant grain boundary volume, it can be shown that if the grain size is underestimated by a factor of 4 the grain boundary thickness will also be underestimated by a factor of 4 which will underestimate the grain broundary diffusion coefficient by a factor of 16.

In the present sutdy it is not known what effect a phase boundary reaction at either the grain boundary-surface or grain boundary-grain interface will have on the value of D_{GB}. It is also not known how the presence of 5% silicon oxynitride grains along with the β-Si_3N_4 grains will have on D_{GB}.

5.4 Conclusions

This study has shown that the direct observation of the $^{15}N(p,\alpha_0)^{12}C$ reaction can be used to measure nitrogen-15 concentration

versus depth profiles with submicron resolution and without the need for serial sectioning. The technique has been applied to the study of nitrogen diffusion in NORALIDE™ NC-132 hot pressed silicon nitride and values of both the volume and grain boundary diffusivities estimated.

SECTION VI

FUTURE WORK

The obvious extention of this work is to investigate nitrogen diffusion in both pure α- and pure β-Si_3N_4 over as large a temperature range as possible. Once a diffusion coefficient is obtained for the pure forms of silicon nitride the effect of impurities should be investigated, especially those added during hot pressing. If possible a glass of the same composition as that found in the grain boundaries should be produced to allow the study of nitrogen diffusion in a material with the same composition as the grain boundary.

In order to eliminate the question of a phase boundary reaction it would be advantageous to develop a method of producing layered samples of theoretically dense silicon nitride. By the samples being composed of a layer of $Si_3{}^{14}N_4$ followed by a layer of $Si_3{}^{15}N_4$ the possibility of a phase boundary reaction would be eliminated.

The proton activation technique should also be applied to the problem of the nitriding of silicon. By a method similar to the one used in this laboratory to study the mechanism of the thermal oxidation of silicon (37) it would be possible to determine the mechanism of the nitridation of silicon.

A deconvolution program would be valuable in allowing utilization of the 1.028 MeV resonance to obtain concentration versus depth profiles by the single spectrum technique.

The scattering chamber should also be modified to allow the incident beam to strike the sample surface at a shallow angle (38). This

would be especially useful for shallow penetrations, since the depth resolution could be reduced to 2-3 nm.

Finally, the proton activation technique should be applied to other nitrogen containing systems and also to some non-nitrogen systems which have a high nitrogen solubility at their forming temperatures.

APPENDIX A

NUCLEAR MICROANALYSIS

A.1. Introduction

During the past decade the use of low energy, less than 4 MeV, positive ion accelerators, both Cockroft-Waltons and Van de Graaffs has emerged as an important and powerful materials research tool. The role of the low energy accelerator has declined from its former place of prominence in nuclear physics research, but only after a wealth of information had been collected, waiting to be tapped by the materials scientist.

When an energetic ion impinges on the surface of a sample it can interact with the sample in a number of different ways. These interactions are summarized in Table A.1 (41). As one moves down the table, the amount of energy required for the process increases. Also, all process of lower required energy occur simultaneously for example, for coulomb excitation to occur both coulomb scattering and atomic ionization and excitation will occur.

The remainder of the appendix will be devoted to a discussion of the four major charged particle nuclear microanalytical techniques; Particle Induced X-Ray Emission (PIXE), Rutherford Backscattering (RBS), Channeling, and Particle Induced Nuclear Reactions.

A.2 Particle Induced X-Ray Emission

Introduction Particle Induced X-Ray Emission, PIXE, is the newest of the nuclear microanalytical techniques. The birth of X-ray

TABLE A.1

Summary of Possible Interactions

Incident Particle Interacts with	Type of Force	Effect on Energy of Particle	Effect on Nucleus			Name of Process
			Kinetic Energy	Internal Energy	Identity	
Atomic Electron	Coulomb	Slight Reduction	Unchanged	Unchanged	Unchanged	Atomic Ionization and Excitation
Nucleus	Coulomb	Reduced	Increased	Unchanged	Unchanged	Coulomb Scattering
Nucleus	Coulomb	Reduced	Increased	Increased	Unchanged	Coulomb Excitation
Nucleus	Nuclear	Reduced	Increased	Unchanged	Unchanged	Nucleus Elastic Scattering
Nucleus	Nuclear	Reduced	Increased	Increased	Unchanged	Nuclear Inelastic Scattering
Nucleus	Nuclear	Transmutated or Absorbed	Increased	Varies	Transmutated	Nuclear Reaction

AD-A069 004 CASE WESTERN RESERVE UNIV CLEVELAND OHIO DEPT OF MET--ETC F/G 11/2
USE OF NUCLEARMICROANALYSIS. PART II. NUCLEAR MICROANALYSIS OF --ETC(U)
AUG 78 A R COOPER, L D MAJOR F33615-74-C-4029
UNCLASSIFIED AFML-TR-78-119-PT-2 NL

2 OF 3
AD
A069004

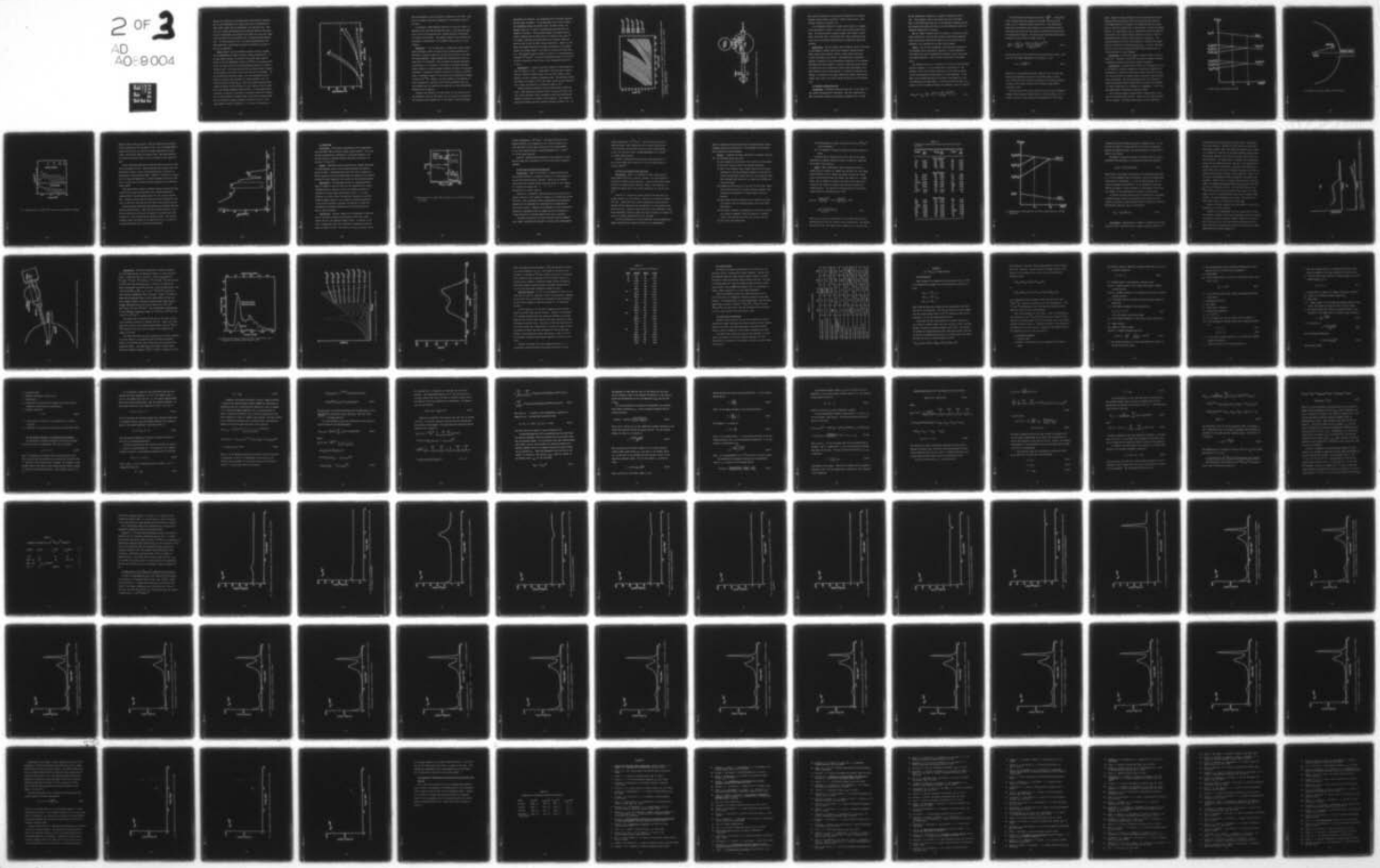

2 OF 3

AD

A069004

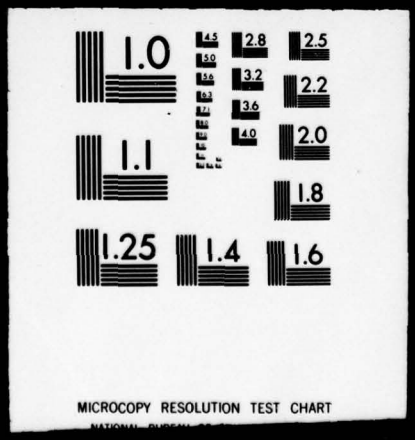

emission for qualitative and quantitative spectrochemical analysis was in 1913 when Moseley (42) showed there was a relationship between atomic number and the wavelength of the emitted X-ray. However, for a long time analytical x-ray emission analysis was mainly by x-ray fluorescence even though it was known that there was a high cross section for x-ray production due to charged particle bombardment. In 1970 Johansson, et.al. (43) showed experimentally that high sensitivity, multielement analysis was possible by proton induced x-ray emission.

Theory Valkovic (44) has probably provided the best treatment of the fundamentals of PIXE, the basis of which is given here. If by some means a vacancy is created in one of the inner electron shells it will be immediately filled (10^{-15}sec) by an electron from one of the outer shells with the simultaneous emission of a characteristic x-ray. The x-rays emitted when an electron fills a vacancy in the K-shell, n=1, result in the x-ray lines of the K-series. If the transition is from the L-shell, n=2, the associated x-ray is known as K_α and if the transition is from the M-shell, n=3, the associated x-ray is known as K_β. The x-ray energy increases, wavelength decreases, from the M-series to the L-series to the K series due to the energy difference between levels. As the atomic number increases, the energy of the same x-ray spectral line also increases due to the increase in nuclear charge, the electron binding energy and the increase in energy difference between the orbits. This relationship is shown in Figure A.1. It is also of importance to

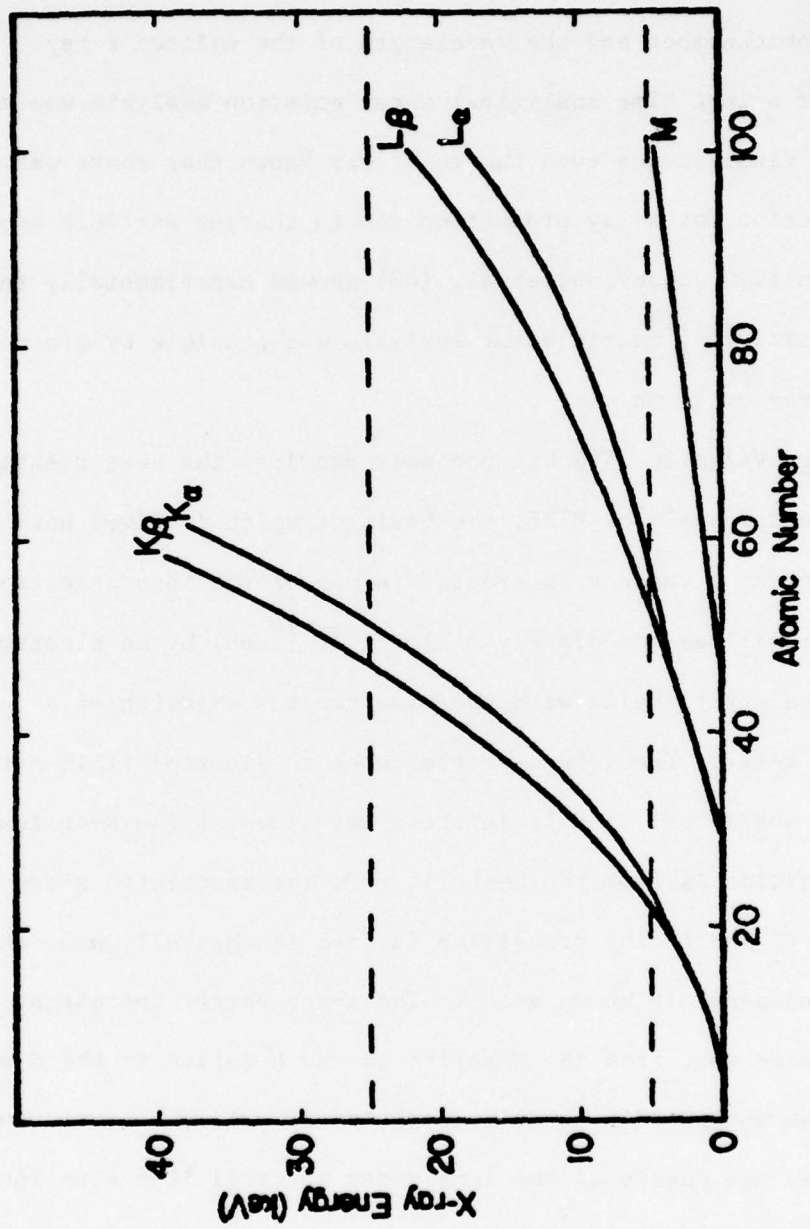

A.1 X-ray energy as a function of atomic number.

note this because as the x-ray spectra originates in the inner orbitals it is almost completely independent of the chemical state of the atom.

A continuous, bremsstrahlung, spectrum of x-rays will exist in addition to the line spectrum described above. The continuous spectrum is due to electrons and other charged particles slowing down in a step by step fashion. The highest energy of the continuum will correspond to deceleration of the highest energy particle to zero velocity.

Sensitivity It is of importance to examine how various experimental parameters effect the sensitivity, minimum detectable concentration, keeping in mind that the sensitivity refers to the sample being bombarded. Sample preparation techniques may allow the sensitivity to be enhanced. Once one knows the minimum detectable concentration, it is possible to calculate the minimum detectable absolute amount for various elements knowing the mass of the material irradiated. Assuming the incident particles are protons in the MeV range, a sufficient number of x-ray counts can be obtained for masses as small as 10^{-19}kg. However, the trace element to be measured is always contained in a matrix, and the counts associated with the trace element must be separated from these due to the bremsstrahlung background and the matrix.

Johansson and Johansson (45) have shown that the sensitivity of the experiment varies as the square root of the detector resolution and inversely as the square root of the product of the solid angle

subtended by the detector, the integrated flux of incident particles and the target thickness. In any experiment one is free to choose the bombarding energy, the particle type, the beam current, the analysis time, etc. in order to optimize the sensitivity for the elements of interest. For practical reasons the analysis time is usually minimized and the beam current is limited by the nature of the target, therefore one usually selects an incident energy and particle type to give the best overall sensitivity. Figure A.2 (45) shows the minimum detectable fractional concentration for incident protons of incident energy 1 to 10 MeV as a function of atomic number. The parameters used in Figure A.2 relate to a carbon matrix of thickness 10^{-3} mg-mm^{-2}, a detector subtending an angle at 3.8 x 10^{-2} sr with a resolution of 165 eV and a total integrated proton flux of 10 μC.

Experimental. A typical scattering chamber for PIXE analysis is shown in Figure A.3 (46). A monoenergetic particle beam is passed through a diffuser (usually havar foil) and then through a colliminator in order to produce a homogenous beam. The beam then strikes the sample at an angle of 45° to the sample normal and the characteristic x-rays are observed at a laboratory angle of 90°.

Sample preparation produces the most difficulties in PIXE analysis. Thin targets are desired in order to gain sensitivity, however certain materials such as biological tissue and metallurgical samples are difficult to obtain in thin sections. The problem of using thick targets has been treated by Patnaik and Dhere (47). In

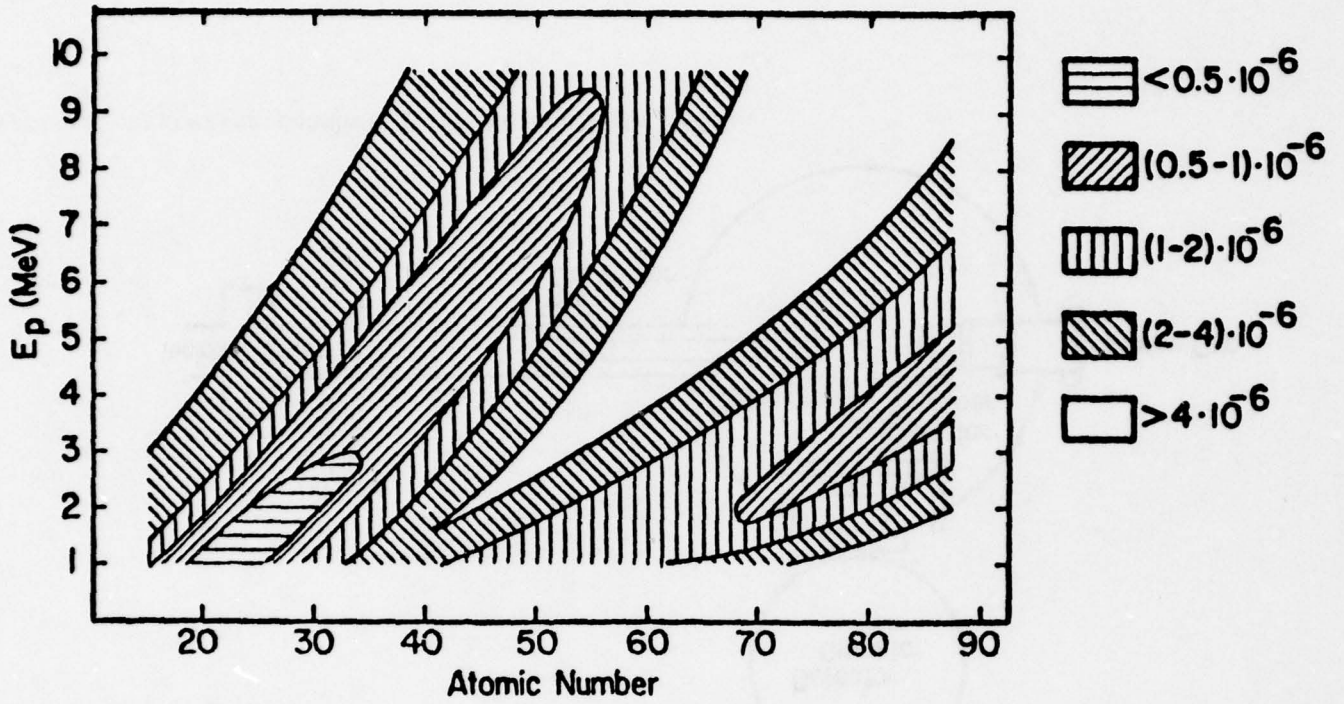

A.2 Minimum detectable concentration as a function of atomic number and bombarding energy (10^{-3} mg-mm^{-2} carbon matrix, $\Omega = 3.8 \times 10^{-2}$ sr, detector resolution = 165 eV, total charge = 10 μC) (45).

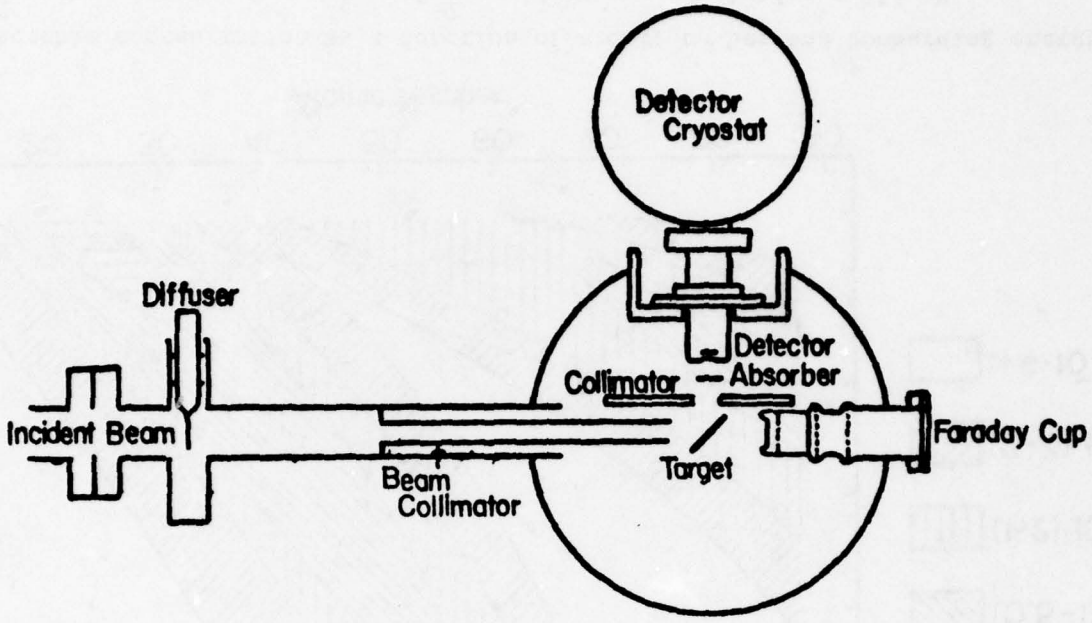

A.3 Typical scattering chamber for PIXE analysis (46).

most cases the material to be analyzed is deposited on a suitable backing, such as carbon, collodion, formuar, kapton, mylar, polystyrene, millipore, nuclopore, etc.

It is sometimes desirable to analyze liquid samples or samples which deteriorate in vacuum. In these cases external beams can be used. The particle beam is passed through a thin window, usually mylar (48) nickel (48), or beryllium (49), which sacrifices sensitivity due to increased bremsstrahlung, but simplifies sample preparation.

Applications. The two primary uses of PIXE have been in the areas of environmental studies (50-56) and biological systems (56-63) which include plant material (56-60), animal tissue and fluids (57-63), and medical uses (6-63). The application to materials systems is presently in the developmental stages due to the problems associated with thick samples. Research is presently being carried out which will allow concentration versus depth measurements to be made (64-66) by one of three methods 1) variation of incident ion energy; 2) variation of the angle between the incident beam and the target, and 3) use of the ratio between the K_β and K_α x-ray intensities.

A.3 Rutherford Backscattering

Introduction. Rutherford Backscattering, RBS, is the oldest of the nuclear microanalytical techniques. The first application of RBS to materials analysis was by Geiger and Marsden (67) in 1909

and was subsequently explained in a paper by Rutherford (68) in 1911. The technique was not well publicized until the 1960's when a 5 MeV alpha source was part of the Surveyer 5 payload (69,70). The backscattered alphas were used to provide information about the elemental composition of the moon.

RBS is a simple technique which is absolute, it requires no additional calibration, and will give reliable, quantitative elemental depth distributions provided the sample surface is smooth and the elelments to be considered do not have similar masses.

Theory. Chu (71) has divided RBS into three basic concepts: 1) the kinematic factor (qualitative analysis), 2) the differential scattering cross section (quantitative analysis), and 3) the energy loss (depth analysis). Each of these concepts will be discussed below.

The kinematic factor, K, is defined as the ratio of the scattered particle's energy, E_s, to its energy before scattering, E. The kinematic factor can be simply calculated from the laws of conservation of mass-energy and conservation of linear momentum. If the mass of the incident particle, m, the mass of the target, m_1, and the laboratory scattering angle, θ, are known and the process is assumed to be pure coulomb scattering; the kinematic factor is given by:

$$K(m,m_1,\theta) = K_{m_1} = \frac{E_s}{E} = \left[\frac{m\cos\theta + (m_1^2 - m^2\sin^2\theta)^{1/2}}{m + m_1}\right]^2 \qquad (A.1)$$

The differential scattering cross section, $\frac{d\sigma(\theta)}{d\Omega}$, arises from a pure coulomb interaction between the incident particle and the target and is a classical physics problem (72). The differential scattering cross section can be though of as the probability that a scattering event will occur and couples the backscattered yield with the quantitative analysis. The differential scattering cross section including the cor-ection for target recoil is:

$$\frac{d\sigma(\theta)}{d\Omega} = \left[\frac{ZZ_1e^2}{2E\sin^2\theta}\right]^2 \frac{\{\cos\theta + [1-(\frac{m}{m_1}\sin\theta)^2]^{\frac{1}{2}}\}^2}{[1-(\frac{m}{m_1}\sin\theta)^2]^{\frac{1}{2}}} \qquad (A.2)$$

The average value of the differential scattering cross section, $\sigma(\theta)$, over the solid angle subtended by the detector, Ω, is:

$$\sigma(\theta) = \frac{1}{\Omega}\int \frac{d\sigma(\theta)}{d\Omega}\, d\Omega \qquad (A.3)$$

Exceptions to the Rutherford formula, Equation A.2, occur when the energy of the incident particle is low and the target is heavy (e.g. 10 KeV He^+ on Au) and when the energy of the incident particle is high and the target is light (in this energy range reaction resonances occur).

The energy loss factor arises from the fact that when an energetic charged particle passes through matter it will lose energy in a ca - culable way due to atomic ionization and excitation of the target

atoms. Figure A.4 shows graphically how the observed energy can be associated with the depth at which the scattering event occurred. If an alpha particle is incident on the sample surface with energy $E_\alpha(0)$ it will have energy $E_\alpha(x)$ at some distance x beneath the sample surface. At some distance, say x_1, beneath the surface the particle will scatter from a target nucleus, assumed to be type 1, and the scattered particle will have energy $K_1E_\alpha(x)$ or $E_{\alpha_1}(x_1,x_1)$. The scattered particle will also lose energy as it traverses the sample and will be observed to have energy $E_{\alpha_1}(0,x_1)$. As can be seen there will be a one-to-one correlation between observed energy and the scattering depth for each component.

Experimental. A scattering chamber utilized for RBS is shown in Figure A.5. Typically, 2.0 MeV $^4He^+$ are used as incident particles to minimize Coulomb scattering and resonant scattering.

Applications. The applications of RBS are far reaching (72) due to the ability to measure composition variations and impurity distributions as a function of depth with a depth resolution of 10 nm over the first 300 nm of sample without the need for serial sectioning or sputtering. The other advantage of RBS is its ability to perform quantitative depth analysis without the need for standards of similar composition, the technique is is absolute. A few of the many applications of RBS will be discussed below.

One of the most important applications of RBS has been in the area of thin film studies (72-79). Figure A.6 (74) shows the power of the technique. The alpha spectrum shown is for a multilayer

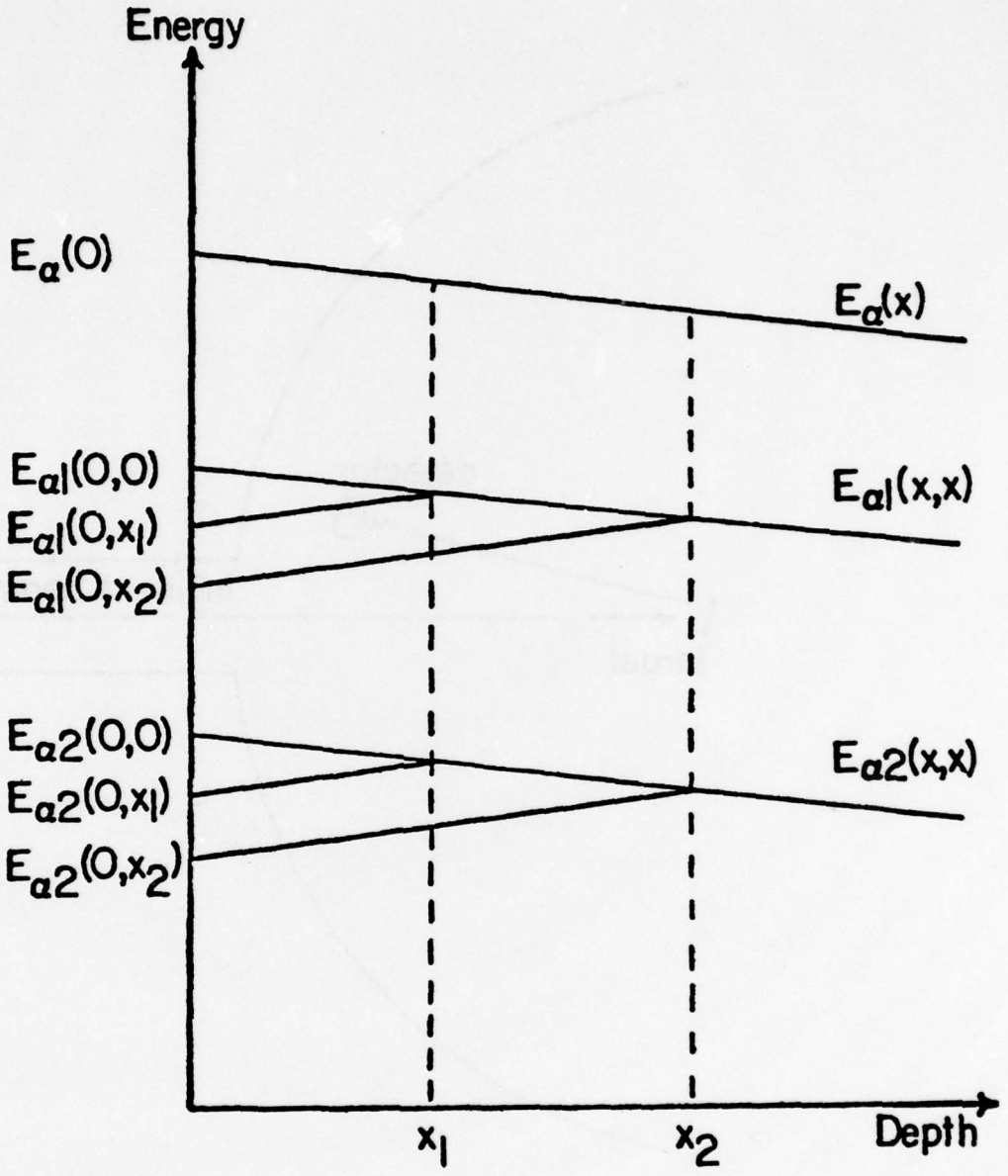

A.4 Depth-energy relationship for RBS.

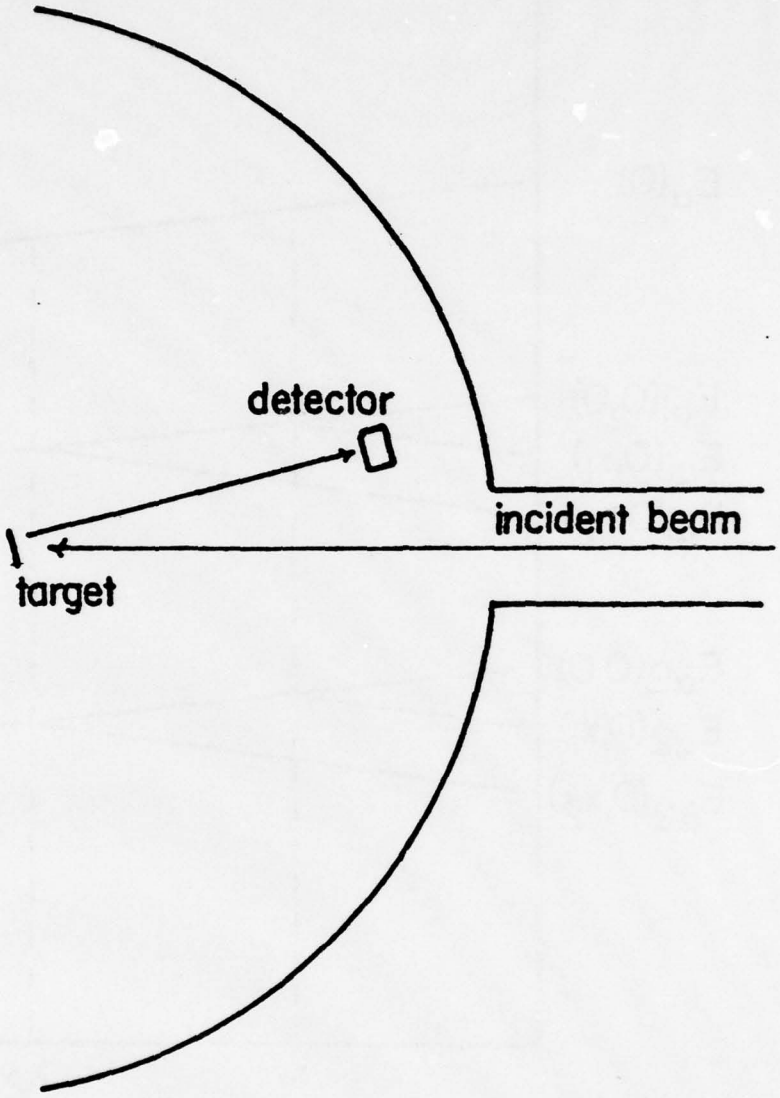

A.5 Typical scattering chamber for RBS analysis.

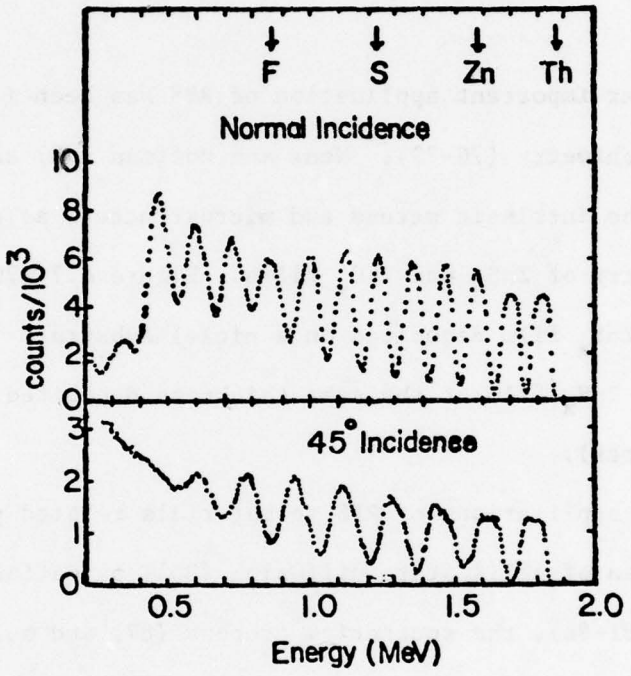

A.6 RBS spectra for 2.0 MeV $^{4}He^{+}$ incident on a multilayer coating.

sample of ZnS and ThF_4 on quartz, there are twelve 105.6 nm layers of ThF_4 separated by 67.0 nm layers of ZnS. Due to the high differential cross section for Thorium, the peaks associated with zinc, sulfur, and Fluorine cannot be directly seen. The arrows indicate the position the peaks should occur at if located at the sample surface.

Another important application of RBS has been in the area of thin film stoichimetry (76-79). Wenz and Hoffman (78) and Wenz (79) have studied the intrinsic stress and microstructure as a function of stoichimetry of ZnS_x and TiO_x films. Figure A.7 (79) shows a comparison of a ZnS_x film deposited on a nickel substrate (solid line) with that of a ZnS_x film of the same thickness deposited on a carbon substrate (dots).

Other applications of RBS to materials related problems have been in the area of solid state diffusion (80), oxidation mechanism studies (81-86), the sputtering process (87) and surface roughness (88). Schmid and Ryssel (88) have measured surface roughness of the order of 300 nm by observing the front edge of the observed spectra.

By using resonant backscattering Mackenzie and Armitage (89) have measured sample perosity. They used the 2.66 MeV resonance in the proton scattering cross section in oxygen-16 to measure pore sizes as small as 1.0 nm by obersving the resonance width. The observed resonance width will depend on the number and size of the pores encountered before and after resonant backscattering.

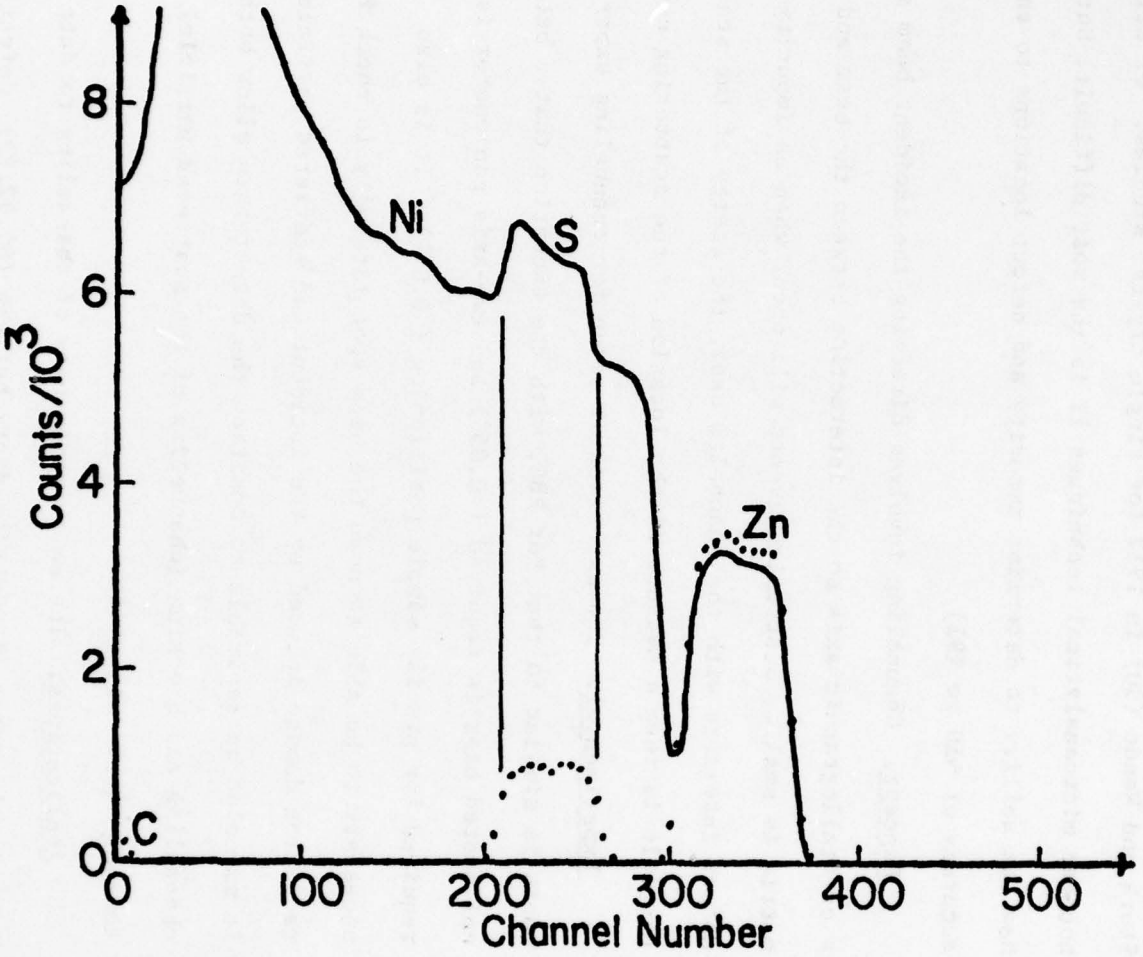

A.7 RBS spectra for simultaneously deposited ZnS films on Ni (solid line) and C (dots) (79).

A.4 Channeling

Introduction. Historically channeling was first suggested by Stork and Wendt (90) in 1912 for single crystal studies. Of all the nuclear microanalytical techniques it is the most difficult, but has the ability to determine impurity and defect locations to an accuracy of ∿10 pm (91).

Concept. Channeling involves directing the incident beam along a crystallographic axis so the interaction between the beam and matrix is small. Scattering events will occur when an impurity or defect interacts with the channeled beam, the energy of the scattered particle is then a measure of the location of the scattering center.

Experimental. The experimental setup for channeling experiments is similar to that for RBS, with the exception that a better collimated beam is required (<0.05°) and two-axis goniometer is required for precise sample positioning (<0.05°). It is also necessary to be able to move the beam spot laterally to check for radiation damage induced by the incident and scattered particles. It may also be desirable to position the detector to allow both channeling and blocking (channeling of the scattered particle) kown as double alinement.

Applications. The most common uses of channeling to date have been in the areas of impurity distributions (80,92,93), defect studies (94,95), and radiation damage (96,97). An example of the type of information that can be obtained by channeling studies is shown in Figure A.8 (93). The spectra are from an as-grown silicon

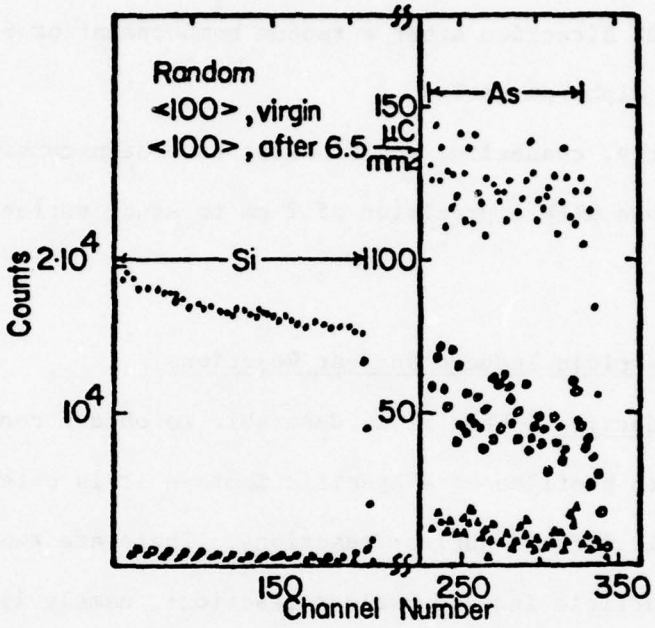

A.8 RBS spectra for 1.8 MeV $^{4}He^{+}$ incident on a 6 x 10^{25} As-m^{-3} doped Si crystal.

crystal containing 6×10^{25} As-m^{-3}. The solid circles are for a random direction, the triangles are for a crystal alined in the <110> direction, and the open circles are for an alined sample in the <110> direction after a random bombardment of 6.5 $\mu C\text{-}mm^{-2}$ of 1.8 MeV alpha particles.

Recently, channeling and blocking have been combined to locate surface atoms with a precision of 2 pm to study surface relaxation (98-100).

A.5 Particle Induced Nuclear Reactions

Introduction. When it is desirable to obtain concentration versus depth profiles of a specific isotope it is often possible to use particle induced nuclear reactions. There are two possible types of particle induced nuclear reactions, namely 1) the creation of a radioactive species and 2) direct observation of a nuclear reaction.

Creation of a radioactive species involves the conversion, by nuclear reaction, of the isotope of interest to a radioactive species (101-104). Depth profiling is then accomplished by sectioning the specimen and the determing the concentration of radioisotope by the section activity. Because of the similarity to the conventional radiotracer experiments after the sample has been irradiated, no further discussion of induced radioactivity will be included.

The direct observation of nuclear reactions involves bombarding a sample containing the isotope of interest with a monoenergetic

crystal containing 6×10^{25} As-m^{-3}. The solid circles are for a random direction, the triangles are for a crystal alined in the <110> direction, and the open circles are for an alined sample in the <110> direction after a random bombardment of 6.5 $\mu C\text{-}mm^{-2}$ of 1.8 MeV alpha particles.

Recently, channeling and blocking have been combined to locate surface atoms with a precision of 2 pm to study surface relaxation (98-100).

A.5 Particle Induced Nuclear Reactions

Introduction. When it is desirable to obtain concentration versus depth profiles of a specific isotope it is often possible to use particle induced nuclear reactions. There are two possible types of particle induced nuclear reactions, namely 1) the creation of a radioactive species and 2) the direct observation of a nuclear reaction.

Creation of a radioactive species involves the conversion, by nuclear reaction, of the isotope of interest to a radioactive species (101-104). Depth profiling is then accomplished by sectioning the specimen and the determining the concentration of radioisotope by the section activity. Because of the similarity to the conventional radiotracer experiments after the sample has been irradiated, no further discussion of induced radioactivity will be included.

The direct observation of nuclear reactions involves bombarding a sample containing the isotope of interest with a monoenergetic

beam of charged particles and observing the instantaneously emitted energetic particles (2,38,105-143). The remainder of this section will be devoted to this technique.

General. In general the direct observation of nuclear reactions has the following properties (105);

(a) The technique is restricted to the first 10 μm of the sample.

(b) With most reactions there is no natural background.

(c) Most of the reactions have a high Q value (Q is the energy equivalent to the mass difference between the reactant and product nuclei) which allows the use of low energy particles, thus reducing local heating of the target and avoiding competing reactions.

(d) Coulomb barriers prevent the reaction of most nuclei larger than chlorine with the low energy particles employed, thus allowing the determination of light elements in heavy matrices.

(e) The nuclear reactions employed are very specific, in that two isotopes, even of the same element, will react quite differently.

(f) The results obtained are independent of the matrix in which the isotope is embedded, since the physical or chemical state of the atom does not effect the nuclear reaction.

(g) The results are quantitative.

(h) The sensitivity is high, in that as little as 10^{-13} kg-m^{-2} can be determined.

(i) It is possible to measure concentration versus depth profiles.

A partial list of isotopes which can be used for the direct observation of nuclear reactions is given in Table A.2 along with the Q value of the reaction.

Theory. When a monenergetic beam of charged particles of energy $E_i(0)$ is incident on a sample the particles will lose energy almost linearly as they traverse the sample and will have energy $E_i(x)$ at any position within the sample, see Figure A.9. At some depth, say x_1, beneath the surface the particle will react with a nucleus of the isotope of interest and will emit a particle of energy $E_e(x_1,x_1)$. The energy of the emitted particle can be calculated from the following equation (145)

$$E_e(x,x) = \left[\frac{(m_i m_e E_i(x))^{\frac{1}{2}}}{m_e + m_r} \cos\theta \pm \left\{ \frac{m_i m_e E_i(x)}{(m_e + m_r)^2} \cos^2\theta \right.\right.$$

$$\left.\left. + \frac{m_r Q + E_i(x)(m_r - m_i)}{m_e + m_r} \right\}^{\frac{1}{2}}\right]^2 \qquad (A.4)$$

Where m_i, m_e, and m_r are the masses of the incident particle, the emitted particle, and the residual nucleus respectively. The emitted particle will also lose energy almost linearly as it traverses the

TABLE A.1

Q Values for Some Nuclear Reactions Induced by Charged Particles.

Isotope	Qo (MeV)	Isotope	Qo (MeV)	Isotope	Qo (MeV)
		(p,α) *reactions:*			
^{7}Li	17.347	^{6}Li	4.02	^{9}Be	2.125
^{11}B	8.582	^{18}O	3.970	^{31}P	1.917
^{19}F	8.119	^{37}Cl	3.030	^{27}Al	1.594
^{15}N	4.964	^{23}Na	2.379	^{17}O	1.197
				^{10}B	1.147
		(d,α) *reactions:*			
^{20}B	17.819	^{11}B	8.022	^{32}S	4.890
^{6}Li	22.36	^{15}N	7.693	^{18}O	4.237
^{7}Li	14.163	^{9}Be	7.152	^{30}Si	3.121
^{14}N(α_0)	13.579	^{25}Mg	7.047	^{16}O	3.116
^{19}F	10.038	^{23}Na	6.909	^{26}Mg	2.909
^{17}O	9.812	^{27}Al	6.701	^{24}Mg	1.964
^{14}N(α_1)	9.146	^{29}Si	6.012	^{28}Si	1.421
^{31}P	8.170	^{13}C	5.167	^{12}C	<0
		(d,p) *reactions:*			
^{10}B	9.237	^{17}O	5.842	^{26}Mg	4.212
^{25}Mg	8.873	^{27}Al	5.499	^{12}C	2.719
^{14}N(p_0)	8.615	^{24}Mg	5.106	^{16}O	1.919
^{29}Si	8.390	^{6}Li	5.027	^{18}O	1.731
^{32}S	6.418	^{23}Na	4.734	^{14}N(p_5)	1.305
^{28}Si	6.253	^{9}Be	4.585	^{11}B	1.138
^{13}C	5.947	^{19}F	4.379	^{15}N	0.267
^{31}P	5.712	^{30}Si	4.367	^{7}Li	<0

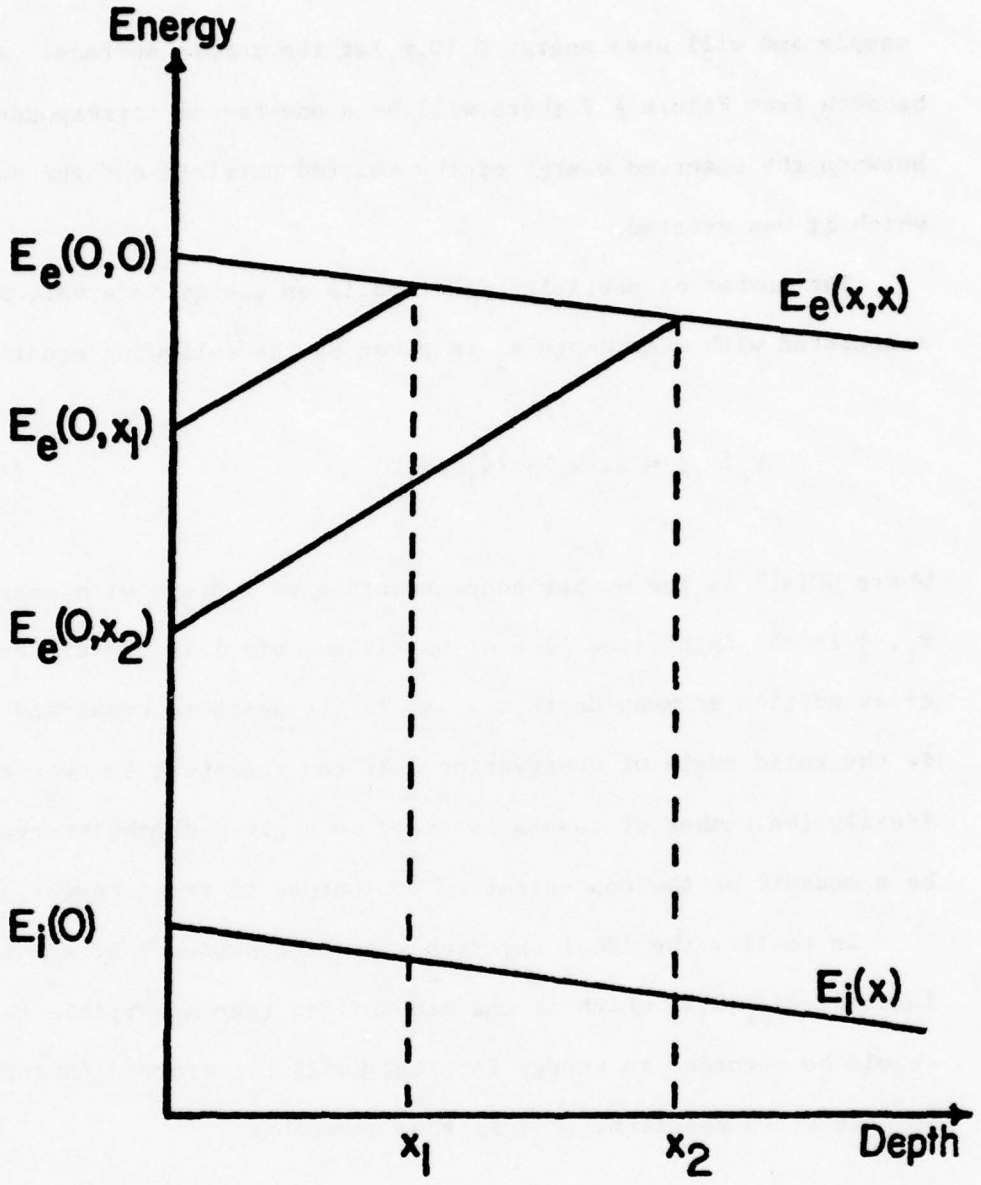

A.9 Depth-energy relationship for the direct obeservation of nuclear reactions.

sample and will have energy $E_e(0,x_1)$ at the sample surface. As can be seen from Figure A.9 there will be a one-to-one correspondence between the observed energy of the emitted particle and the depth at which it was created.

The number of particles detected in an energy interval, $N_o(x_i)$, associated with mean depth x_i is given by the following equation:

$$N_o(x_i) = Nx(x_i)j\sigma(x_i)\Delta x_i \Delta\Omega \qquad (A.5)$$

where $NC(x_i)$ is the number concenteration of isotope with mean depth x_i, j is the integrated flux of particles, $\sigma(x_i)$ is the differential cross section at mean depth x , Δx_i is the depth interval and $\Delta\Omega$ is the solid angle of observation. It can therefore be seen that ideally the number of counts recorded in a given depth interval will be a measure of the concentration of isotope in the interval.

In reality the ideal spectrum will be convoluted by a spreading function $P(E_i,E_j)$, which is the probability that a particle that should be recorded in energy interval i will be recorded in interval j. The distorted spectrum, $[N_o]$ is then given by:

$$[N_{o_i}] = \sum_j N_{o_j} P[E_i,E_j) \qquad (A.6)$$

Experimental. Experimentally a sample is irradiated with a mono-energetic beam of particles and the energetic particle emitted at a

fixed laboratory scattering angle observed using a conventional solid state detector. Because the cross section for Rutherford scattering is greater than ($\sim 10^4$ times) the reaction cross section it is necessary to separate the scattered incident particles from the particle emitted by the reaction to prevent pulse pile-up in the electronics. Two methods exist to separate the scattered particles from the emitted particles, they are: 1) the placing of an absorber in front of the detector, typically mylar (106-108) or nickel (109) and 2) the use of a magnetic spectrometer (33,110) to separate the particles according to their momentum. Figure A.10 (33) shows the advantage of using the magnetic spectrometer over absorbers. Figure A.10.a is a typical spectrum using a mylar absorber, the sample was polycrystalline Al_2O_3 annealed in 21% $^{18}O_2$ for 8.64×10^4 seconds at 1641 K. The reaction induced is the $^{18}O(p,\alpha)^{15}N$ reaction with an incident proton energy of 0.75 MeV. Figure A.10.b is of the same sample only using the magnetic spectrometer, all other parameters are the same. The difference in alpha yield is due to a difference in solid angle.

Figure A.11 shows a typical scattering chamber for the direct observation of nuclear reactions.

Analysis of the experimental data can be performed by either the resonance technique, where the concentration profile is obtained by walking an isolated resonance through a sample as was done in this discertation or by the single spectrum technique where the entire spectrum is deconvoluted to obtain the concentration versus depth profile first used by Robin (2).

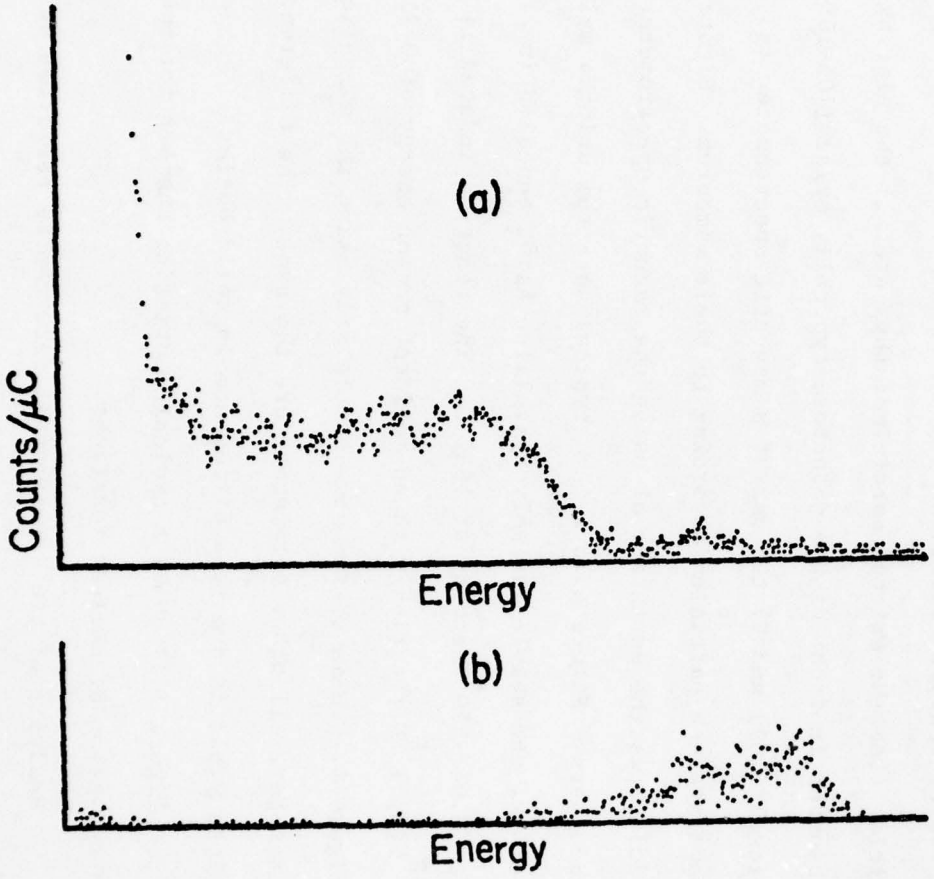

Figure A.10 Comparison of the use of (a) a mylar film and (b) a magnetic spectrometer to separate the backscattered protons from the emitted alpha particles for the $^{18}O(p,\alpha)^{15}N$ reaction (33).

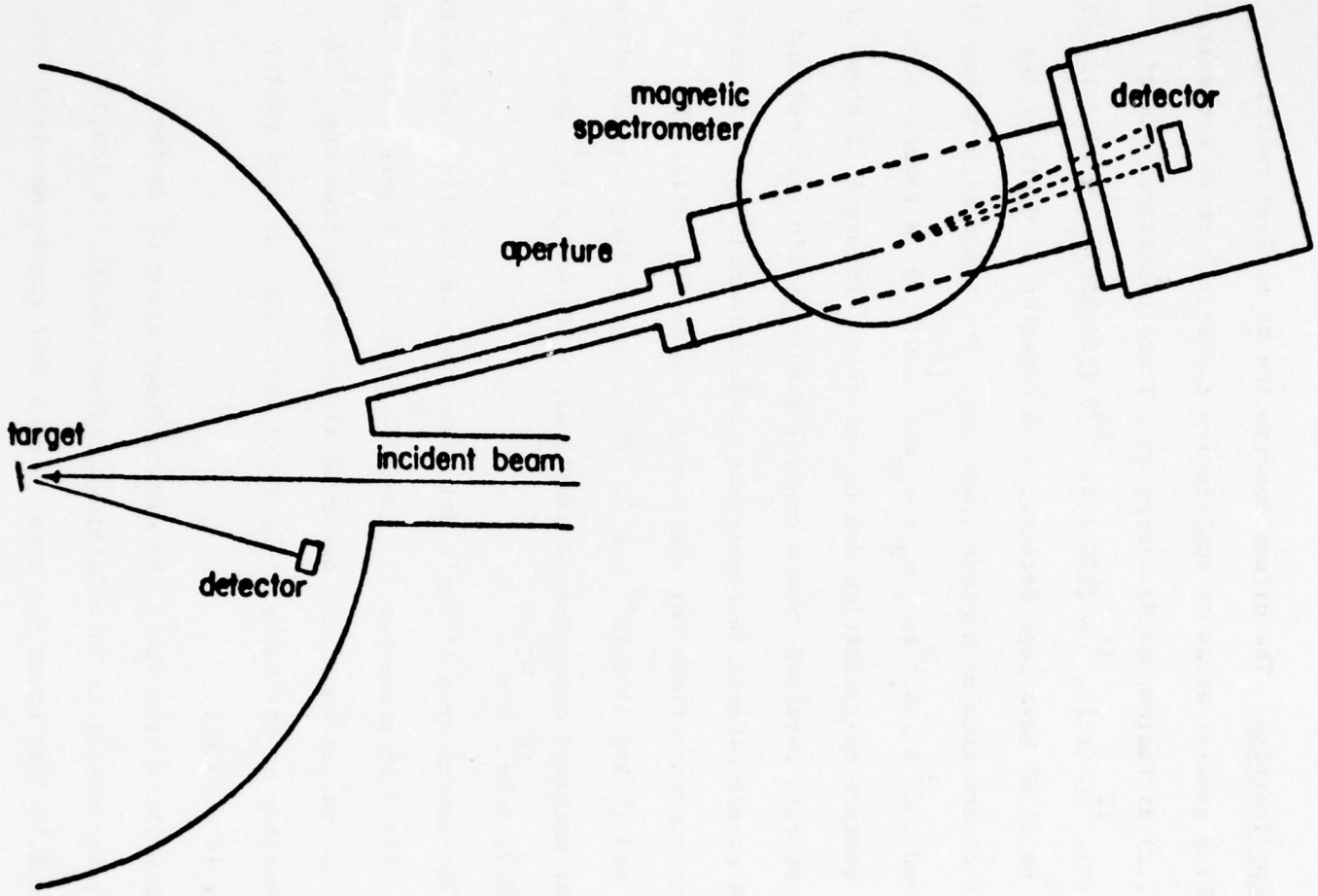

A.11 Typical scattering chamber for the direct observation of nuclear reactions.

Applications. The direct observation of nuclear reactions has three general areas of application namely: 1) trace concentrations, 2) diffusion, and 3) corrosion. Trace concentrations of ^{11}B (120), ^{12}C (121), ^{14}N (122-124), ^{16}O (124-126), ^{18}O (120,127,128), and ^{23}Na (130) have been detected as a function of depth by the direct observation of nuclear reactions. North and Lightowlers (120) utilized the $^{11}B(p,\alpha_1)^{8}Be \rightarrow \alpha_2 + \alpha_3$ and $^{18}O(p,\alpha)^{15}N$ reactions to study surface contamination due to solvents. Figure A.12 shows the alpha spectra obtained from a control sample (solid circles) and from a sample cleaned in electronic grade methanol (open circles). Average concentrations for the control sample are $(2\pm1)\times 10^{15}$ B-m^{-2} and $(1.4\pm0.3) \times 10^{19}$ O-m^{-2}. The corresponding concentrations for the methanol contaminated sample are $(4.0\pm0.4) \times 10^{16}$ B-m^{-2} and $(5.1\pm0.7) \times 10^{19}$ O-m^{-2}.

The second area of application has been in the field of solid state diffusion processes (2, 106-108, 131-137). Figure A.13 (136) shows the variation in the observed alpha spectra from the $^{18}O(p,\alpha)^{15}N$ reaction as the value of Dt is varied. The incident proton energy is 0.75 MeV.

The third area where the direct observation of nuclear reactions has proven useful is in oxidation studies (38,110,114,138,139). Figure A.14 (38) shows the type of data that can be obtained from oxidation studies. The alpha spectrum is from a silicon coupon which was thermally oxidized in $^{16}O_2$ at 1295 K to produce an 0.5 μm

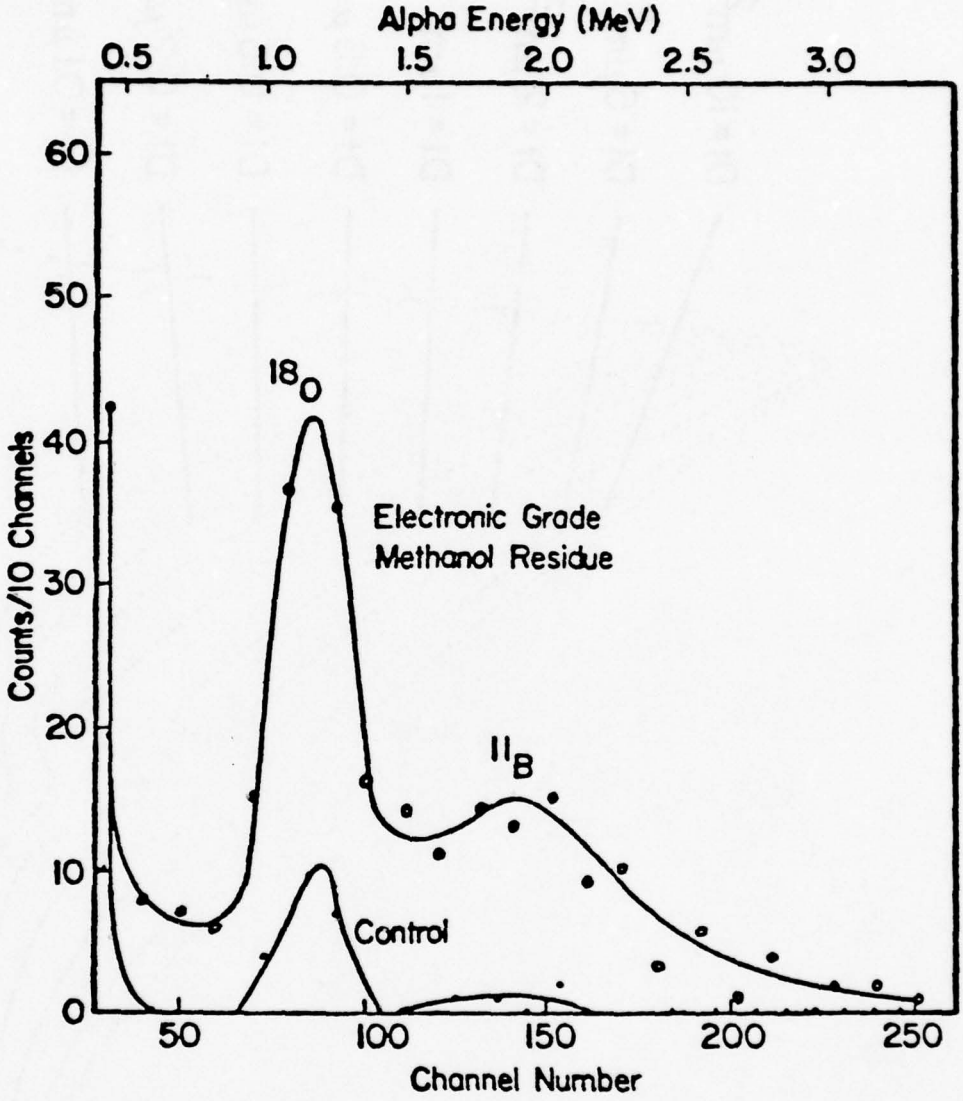

A.12 Alpha spectra showing oxygen and boron contamination due to cleaning in electronic grade methanol (120).

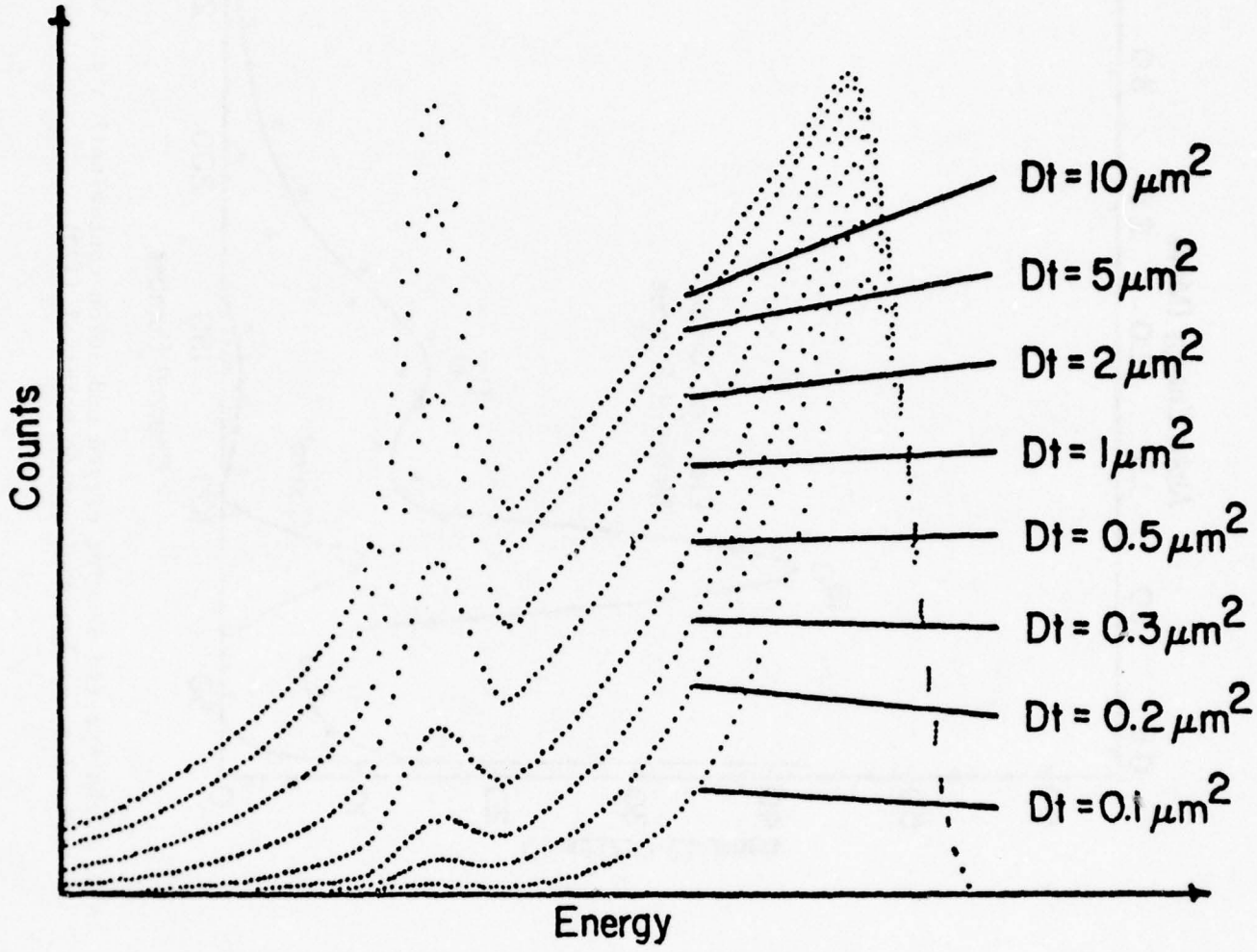

A.13 Alpha spectra as a function of the parameter Dt (136).

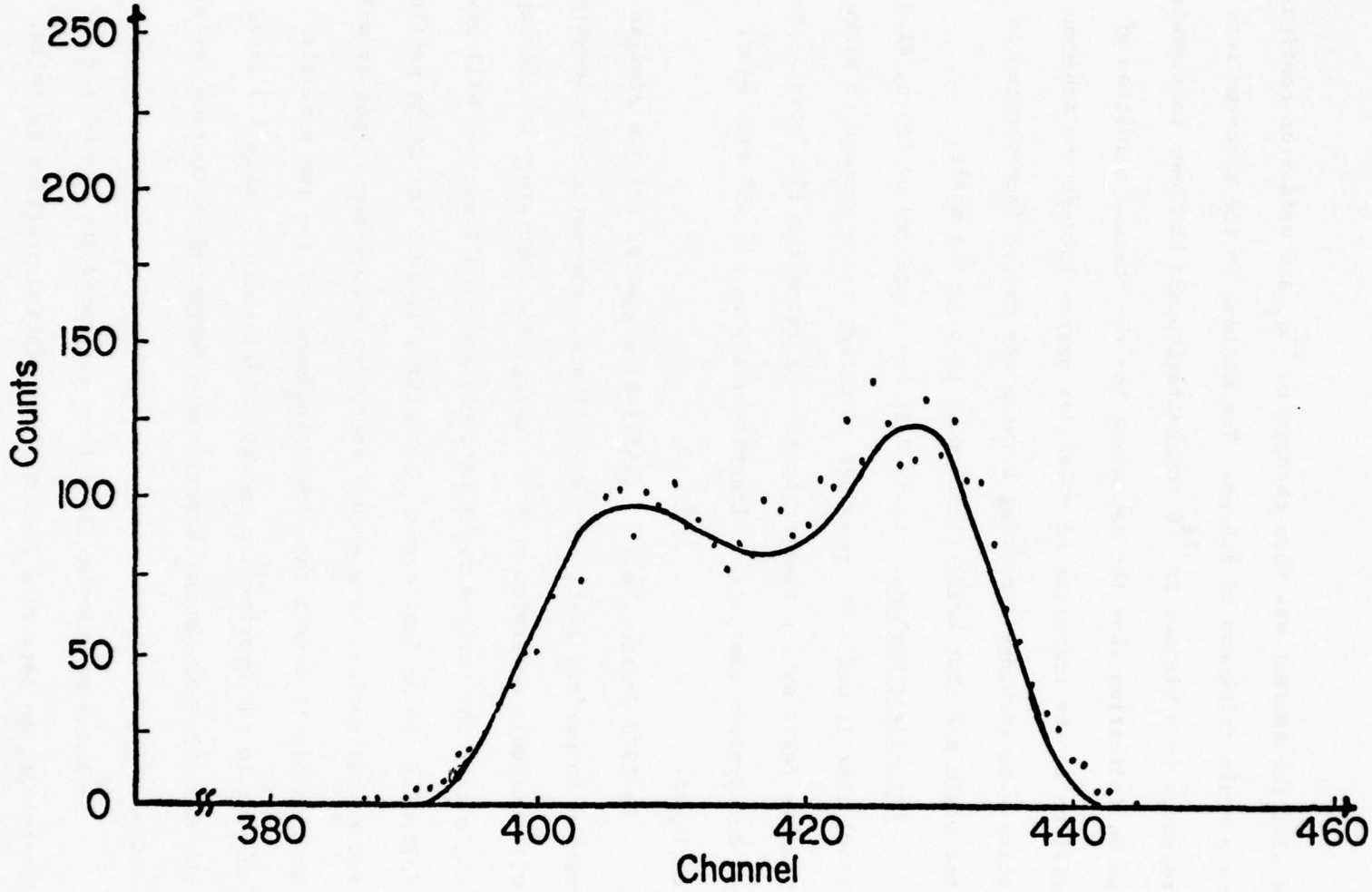

A.14 Alpha spectrum and fit obtained in the study of the thermal oxidation of silicon showing the presence of two processes (38).

scale, the ambient was then changed to $^{18}O_2$ and oxidation continued to a scale thickness of 1.0 μm. The minimum in the spectrum corresponds to a minimum in ^{18}O concentration and has been interpreted as an indication that the mechanism for the thermal oxidation of silicon is the transport of molecular oxygen through the adherent scale with exchange occurring between the oxygen incorporated in the scale and that being transported through the scale.

Coincident Methods. In 1972 it was suggested by Cohen, et.al. (140) that it would be possible to detect trace amounts of hydrogen in thin foils by p-p scattering and observing the time coincidence of the protons emerging at laboratory angles of 45° with equal energies.

In 1975 Coetzee, et.al. (141,142) suggested using a similar method to perform light nuclide analysis. Kinematic relationships will uniquely determine both the energy and laboratory scattering angle that the emitted light particle and recoil nucleus will have following the nuclear event. Therefore, if both the light particle and recoil nucleus have enough energy to escape the target it will be possible to detect the time coincidence of the two particles subject to the appropriate energy relationship. Table A.3 lists the possible coincidence measurements suggested by Coetzee, et.al. (142).

Shaboson and Choyke (143) have suggested the use of $\alpha - \alpha$ scattering to determine helium concentration profiles in foils.

TABLE A.3

Possible Coincidence Measurements

TARGET	REACTION	PRODUCT	Q (MeV)
^{2}H	(d,p)	^{3}H	4.032
^{3}He	(d,p)	^{4}He	18.353
^{6}Li	(p,^{3}He)	^{4}He	4.021
	(d,p)	^{7}Li	5.028
	(d,α)	^{4}He	22.374
	(^{3}He,d)	^{7}Be	0.114
^{7}Li	(p,α)	^{4}He	17.346
	(^{3}He,p)	^{9}Be	11.199
	(^{3}He,α)	^{6}Li	13.325
^{9}Be	(p,α)	^{6}Li	2.125
	(d,p)	^{10}B	4.587
	(d,α)	^{7}Li	7.151
	(^{3}He,p)	^{11}B	10.322
	(^{3}He,d)	^{10}B	1.091
^{10}B	(p,α)	^{7}Be	1.146
	(d,p)	^{11}B	9.231
	(^{3}He,p)	^{12}C	19.694
	(^{3}He,d)	^{11}C	3.197
	(α,p)	^{13}C	4.062
	(α,d)	^{12}C	1.340
^{11}B	(d,p)	^{12}B	1.144
	(d,α)	^{9}Be	8.030
	(^{3}He,p)	^{13}C	13.185
	(^{3}He,d)	^{12}C	10.463
	(^{3}He,α)	^{10}B	9.122
	(α,p)	^{14}C	0.783

A.6 Current Trends

The trends in nuclear microanalysis are to enhance both the depth and lateral resolution for surface analysis. Williams (39) has suggested using low angle incident beams to improve the depth resolution in RBS and particle induced nuclear reactions. By using an incident angle of 5° from the sample surface and using a solid state detector (15 keV FWHM) positioned at 168° it is possible to obtain a depth resolution of 2-3 nm in RBS experiments.

Pierce and Duddleston (145) have reduced the beam size to 25 μm^2 and used a two dimensional scanning technique to map light elements. By combining PIXE, for iron determination, and the direct observation of nuclear reactions, $^{12}C(d,p)^{13}C$, $^{16}O(d,p)^{17}O$, and $^{10}B(d,p)^{11}B$, they were able to map the concentration distributions of iron, carbon, oxygen, and beron across a weld.

A.7 Comparison of Techniques

Recently several authors (146-149) have compared the results obtained by nuclear techniques with those obtained by Auger Electron Spectroscopy (AES), and X-Ray Photoelectron Spectroscopy (XPS). Table A.4 gives a comparison of the various techniques (146,149).

One should bear in mind that none of the techniques are themselves the answer to all surface analysis problems, but with a combination of techniques it is possible to obtain a complete chemical analysis.

TABLE A.4

Comparison of Several Techniques

	PIXE	RBS	Nuc. Rx	AES	XPS
Elements That Can Be Detected	$Z \geq 3$	$Z \geq 1$	Specific Isotopes	$Z \geq 3$	$Z \geq 1$
Elements That Have Been Detected	$Z \geq 4$	$Z \geq 3$	Specific Isotopes	$Z \geq 3$	$Z \geq 3$
Element Identification	Very Good	Good	Excellent	Very Good	Excellent
Sensitivity For Peak/Background = 1 (In Monolayers)	$\sim 10^{-1}$	$10^{-3} - 10^{2}$	$10^{-1} - 10^{0}$	$\sim 10^{-2}$	$\sim 10^{-2}$
Chemical Information	No	No	No	Some	Yes
Depth Sampled (m)	$\sim 10^{-6}$	$10^{-6} - 10^{-5}$	$10^{-6} - 10^{-5}$	$\sim 3 \times 10^{-9}$	$\sim 3 \times 10^{-9}$
Depth Distribution	with Sputtering	Yes	Yes	with Sputtering	with Sputtering
Depth Resolution (m)	$\sim 10^{-7}$	$\sim 2 \times 10^{-8}$	$10^{-8} - 10^{-7}$	$\sim 3 \times 10^{-9}$	$\sim 3 \times 10^{-9}$
Probe Diameter (m)	$\sim 10^{-3}$	$\sim 10^{-3}$	$\sim 10^{-3}$	$\sim 10^{-4}$	$\sim 10^{-2}$
Lateral Resolution (m)	$\sim 5 \times 10^{-4}$	$\sim 5 \times 10^{-4}$	$\sim 5 \times 10^{-4}$	$\sim 5 \times 10^{-5}$	$\sim 10^{-3}$
Results Are	Relative	Absolute	Absolute	Relative	Relative

APPENDIX B

THE $^{15}N(p,\alpha_0)^{12}C$ CROSS SECTION

B.1 Introduction

When nitrogen-15 is bombarded with low energy protons, <2 MeV, it is energetically possible for the following three reactions to occur:

$$^{15}N + p \rightarrow {}^{12}C + \alpha_o$$

$$^{15}N + p \rightarrow {}^{12}C^* + \alpha_1$$

$$^{15}N + p \rightarrow {}^{16}O + \gamma$$

These reactions have been studied by many investigators (150-159) with one of two objectives. The first of these was to gain insight into the nuclear energy levels of the ^{16}O compound nucleus and the second was to study the carbon-nitrogen cycle.

When Bethe (160,161) investigated the carbon-nitrogen cycle as a source of stellar energy, the cross section for these reactions became of interest at stellar energies, near 30 keV. The burning of hydrogen in second generation stars with masses greater than that of the sum in predominantly through the carbon-nitrogen cycle which involves the first two reactions given by (159):

$$^{12}C(p,\gamma)^{13}N(\beta^+\nu)^{13}C(p,\gamma)^{14}N(p,\gamma)^{15}O(\beta^+\nu)^{15}N(p,\alpha)^{12}C$$

This sequence of reactions releases approximately 25 MeV of energy per cycle. The third reaction allows for leakage from the cycle, however, it is returned to the cycle by one of the following sequences (159):

$$^{15}N(p,\gamma)^{16}O(p,\gamma)^{17}F(\beta^{+}\nu)^{17}O(p,\alpha)^{14}N$$

or

$$^{15}N(p,\gamma)^{16}O(p,\gamma)^{17}F(\beta^{+}\nu)^{17}O(p,\gamma)^{18}F(\beta^{+}\nu)^{18}O(p,\alpha)^{15}N$$

It is reported by Rolfs and Rodney (159) that the rate of the $^{15}N(p,\gamma)^{16}O$ reaction will determine the overall abundance of ^{16}O, ^{17}O, and ^{18}O synthesized in the cycle and will therefore play an important role in stellar nucleosynthesis.

This study orginated for two reasons. First, the differential cross section for the $^{15}N(p,\alpha_o)^{12}C$ reaction was not reported for a laboratory scattering angle of 165^{o} and secondly, due to the author's interest in nuclear physics. Realizing that most of the readers are not familiar with nuclear physics a glossary of the symbols used in this Appendix is given in the next section.

B.2 Glossary of Symbols

A ≡ nucleon number

E ≡energy of the incident partcle in appropriate reference frame

$E_o \equiv$ resonant energy in laboratory reference frame (this term is not a constant) defined as

$$E_o = E_\lambda + \Delta_\lambda \tag{B.1}$$

$E_\lambda \equiv$ channel energy in the laboratory reference frame.

$F_\ell(\eta,\rho) \equiv$ regular solution to the radial wave equation (regular coulomb function.

$G_\ell(\eta,\rho) \equiv$ irregular solution to the readial wave equation (irregular coulomb function).

$I, I' \equiv$ intrinsic spin of the target nucleus and recoil nucleus respectively.

$J \equiv$ total angular momentum of the system give by

$$\vec{J} = \vec{s} + \vec{\ell} = \vec{s}' + \vec{\ell}' \tag{B.2}$$

($\vec{s}$ is the channel spin defined below)

$J_o \equiv$ total angular momentum of a particular nuclear energy level.

$N \equiv$ number density.

$N_o \equiv$ number of observed alphas

$P_L(\text{Cos }\theta) \equiv$ Legendre Polynomial given by

$$P_L(\text{Cos }\theta) = \frac{(-)^L}{2^L L!} \quad \frac{d^L}{d(\text{Cos}\theta)^L} \quad (\text{Sin}\theta)^{2L} \tag{B.3}$$

$Q \equiv$ the energy equivalent to the rest mass difference between the reactant and product nuclei.

$S \equiv$ the scattering matrix whose elements are amplitudes of probability flux (S is both unitary and symmetric).

$Z \equiv$ atomic number.

$g_\alpha \equiv$ a real quantity which is related to the partial width of channel α, Γ_α, by :

$$g_\alpha = \pm (\Gamma_\alpha)^{\frac{1}{2}} \tag{B.4}$$

$i,i' \equiv$ the intrinsic spin of the incident and emerging particles respictively.

$j \equiv$ integrated proton flux.

$k \equiv$ wave number.

$m_i \equiv$ atomic mass of species i.

$r \equiv$ interparticle separation.

$r_o \equiv 1.3 \times 10^{-15}$ m.

$r_\alpha \equiv$ the screening radii for the Coulomb field in channel α.

$s,s' \equiv$ the incoming and outgoing channel spins respectively given by :

$$\vec{s} = \vec{i} + \vec{I} \tag{B.5}$$

$$\vec{s} = \vec{I}' + \vec{I}' \tag{B.6}$$

$\ell,\ell' \equiv$ the orbital angular momentum of the incoming and outgoing channels respectively.

$\nu \equiv$ relative velocity of the colliding particles.

$\Gamma \equiv$ the total resonance width in the laboratory reference frame which is a measure of the mean lifetime of the nuclear level.

$\Delta_\lambda \equiv$ the level shift which relates the channel energy, E_λ, and the resonant energy, E_o, by:

$$E_o = E_\lambda + \Delta_\lambda \tag{B.7}$$

$\pi \equiv$ parity which is a measure of symmetry under space inversion.

$\pi_o \equiv$ parity of a particular nuclear energy level.

$\Omega \equiv$ solid angle.

$\alpha, \alpha' \equiv$ channel index for the incoming and outgoing channels respectively, and defines the type and state of the particles.

$\beta \equiv$ the resonant phase shift which is an angular measure of the deviation of the energy from the resonance energy, defined as

$$\beta = \mathrm{Tan}^{-1} \frac{2(E-E_o)}{\Gamma} \tag{B.8}$$

$\eta \equiv$ a term given as

$$\eta = \frac{0.1574\ Z_a Z_x m_a^{\frac{1}{2}}}{E^{\frac{1}{2}}} \tag{B.9}$$

for the incident channel and :

$$\eta = 0.1574\ Z_b Z_y \left(\frac{\mu}{E'}\right)^{\frac{1}{2}} \tag{B.10}$$

for the exit channel

$\theta \equiv$ scattering angle.

$\lambda\!\!\!^{-} \equiv$ deBroglie wavelength (divided by 2π).

μ reduced mass.

$\xi_\ell \equiv$ phaseshift for potential (hard sphere) scattering (quantum mechanical scattering from a hard sphere).

$\rho \equiv$ parameter defined as:

$$\rho = Kr \tag{B.11}$$

$\sigma \equiv$ cross section, a measure of the probability of a reaction occurring.

$\sigma_\ell \equiv$ phaseshift for Coulomb scattering from an inpenetrable sphere.

B.3 Theoretical Treatment of the Reaction Cross Section

The theoretical treatment presented in this section follows that given by Blatt and Biedenharn (162) for the reaction:

$$a + X \rightarrow Y + b \tag{B.12}$$

Here "a" represents the incident particle with intrinsic spin i which collides with the target nucleus X, which has intrinsic spin I. Particle b with intrinsic spin i' emerges at an angle θ to the incident beam in the center-of-mass system and the residual nucleus, Y, recoils in the opposite direction. The intrinsic spin of Y is I'.

It is convenient to describe the system before and after the reaction with three parameters: α(or α'), the channel index, s (or s'), the channel spin, and ℓ(or ℓ'), the orbital angular momentum in the center-of-mass system. The total angular momentum J, of the system is given by vector addition of s and ℓ or s' and ℓ'

$$\vec{s} + \vec{\ell} = \vec{J} = \vec{s}' + \vec{\ell}' \tag{B.13}$$

For the case where the reaction proceeds via a discrete energy level in a compound nucleus, the total angular momentum of the system is equal to the angular momentum of the energy level, J_o:

$$\vec{s} + \vec{\ell} = \vec{J}_o = \vec{s}' + \vec{\ell}' \tag{B.14}$$

The total angular momentum of the system is always conserved (s and ℓ are not conserved quantities).

For strong interactions, which nuclear reactions are, parity, π , is also a conserved quantity. If the parity of the compound nucleus is given by π_o the following condition must be satisfied:

$$(-)^{\ell}\pi_{\alpha} = \pi_o = (-)^{\ell'}\pi_{\alpha'} \tag{B.15}$$

where π_{α} and π_{α} are the channel parities for channel α and α' respectively given by:

$$\pi_{\alpha} = \pi_a \pi_x \tag{B.16}$$

$$\pi_{\alpha'} = \pi_b \pi_y \tag{B.17}$$

In general, one usually introduces a unitary, symmetric matrix, S, known as the scattering matrix whose elements are amplitudes of probability flux for a collision where channel $\alpha s \ell$ goes to channel $\alpha' s' \ell'$ with total angular momentum J (S is a unitary matrix in order to conserve the normaliz tion of the wave function with time and is symmetric in order to conserve time reversal). The cross section is now obtained by averaging over the incident spin directions and summing over the final spin directions, and is given by:

$$d\sigma_{\alpha's';\alpha s} = \lambda\!\!\!^{-}_{\alpha}^{2} (2s+1)^{-1} \sum_{J_1} \sum_{\ell_1} \sum_{\ell_1'} \sum_{J_2} \sum_{\ell_2} \sum_{\ell_2'} i^{-\ell_1+\ell_1'+\ell_2-\ell_2'}$$

$$(\delta_{\alpha'\alpha}\delta_{s's}\delta_{\ell'\ell} - S_{\alpha's'\ell';\alpha s\ell}^{J_1})^{*} \times (\delta_{\alpha'\alpha}\delta_{s's}\delta_{\ell_2'\ell_2} - S_{\alpha's'\ell_2';\alpha s\ell_2}^{J_2})$$

$$\times K(J_1\ell_1'\ell_1;J_2\ell_2\ell_2;s's;\theta)d\Omega \tag{B.18}$$

where $\lambda\!\!\!^{-}$ is the deBroglie wavelength (divided by 2π) and K is purely geometrical in that it is independent of the nature of the channels and the dynamics of the collision and can be written in terms of: $Z(\ell_1 J_1 \ell_2 J_2, sL)$ which are defined as:

$$Z(\ell_1 J_1 \ell_2 J_2, sL) = i^{L-\ell_1+\ell_2}[(2\ell_1+1)(2\ell_2+1)(2J_1+1)$$

$$2(J_2+1)]^{\frac{1}{2}} W(\ell_1 J_1 \ell_2 J_2, sL)(\ell_1 \ell_2 00|\ell_1 \ell_2 L0) \qquad (B.19)$$

$W(\ell_1 J_1 \ell_2 J_2, sL)$ is the Racah coefficient and $(\ell_1 \ell_2 00|\ell_1 \ell_2 L0)$ is the Clebsch-Gordon coefficient (vector addition). The first term, $i^{L-\ell_1+\ell_2}$, is always real, (± 1).

It is now possible to write the differential cross section as a sum of terms in the following manner:

$$d\sigma_{\alpha' s';\alpha s} = \lambda_\alpha^2 (2s+1)^{-1} \sum_{L=0}^{\infty} B_L(\alpha' s';\alpha s) P_L(\cos\theta) d\Omega \qquad (B.20)$$

where:

$$B_L(\alpha' s';\alpha s) = \frac{(-)^{s'-s}}{4} \sum_{J_1} \sum_{J_2} \sum_{\ell_1} \sum_{\ell_2} \sum_{\ell_i'} \sum_{\ell_2'}$$

$$Z(\ell_1 J_1 \ell_2 J_2, sL) Z(\ell_1' J_1 \ell_2' J_2, s'L)$$

$$R.P.[(\delta_{\alpha'\alpha}\delta_{s's}\delta_{\ell_1'\ell_1} - \delta_{\alpha' s'\ell';\alpha s 1}^{J_1})^*$$

$$(\delta_{\alpha'\alpha}\delta_{s's}\delta_{\ell_2'\ell_2} - \delta_{\alpha' s'\ell_2;\alpha s\ell_2}^{J_2})] \qquad (B.21)$$

The notation R.P.[ ] stands for the real part of the term in brackets. The summations in Equation B.21 all run from zero to infinity, however only one of the sums is actually infinite due to the selection rules for nonvanishing Z coefficients. By conservation of time reversal:

$$B_L(\alpha's';\alpha s) = B_L(\alpha s;\alpha's') \tag{B.22}$$

Equation B.21 should be contracted so that each term is counted only once. As written, identical contributions are obtained when the terms are interchanged. The generalized and contracted form of Equation B.21 is given by:

$$B_L(\alpha's';\alpha s) = \frac{(-)^{s'-s}}{4} \sum_{J=0}^{\infty} \sum_{\ell=|J-s|}^{J+s} \sum_{\ell'=|J-s'|}^{J+s'} Z(\ell J \ell J, sL)$$

$$Z(\ell' J \ell' J, s'L) \left| \delta_{\alpha'\alpha} \delta_{s's} \delta_{\ell'\ell} - s_{\alpha's'\ell';\alpha s\ell}^{J} \right|^2$$

$$+ \frac{(-)^{s'-s}}{2} \sum_{J_1=0}^{\infty} \sum_{\ell=|J_1-s|}^{J_1+s} \sum_{\ell_1'=|J_1-s'|}^{J_1+s'} \left\{ \sum_{J_2=J_1+1}^{\infty} \sum_{\ell_2=|J_2-s|}^{J_2+s} \sum_{\ell_2'=|J_2-s'|}^{J_2+s'} \right.$$

$$Z(\ell_1 J_1 \ell_2 J_2, sL) Z(\ell_1' J_1 \ell_2' J_2, s'L) \qquad \text{R.P. [ ]}$$

$$+ \sum_{\ell_2=\ell_1+1}^{J_1+s} \sum_{\ell_2'=|J_1-s'|}^{J_1+s'} Z(\ell_1 J_1 \ell_2 J_1, sL) Z(\ell_1' J_1 \ell_2' J_1, s'L) R.P.[J_2=J_1]$$

$$+ \sum_{\ell_2'=\ell_1'+1}^{J_1+s'} Z(\ell_1 J_1 \ell_1 J_1, sL) Z(\ell_1' J_1 \ell_2' J_1, s'L) RP[J_2=J_1, \ell_2=\ell_1]\} \qquad (B.23)$$

The term R.P.[ ] stands for the corresponding expression in Equation B.21. The additional restriction that:

$$\ell_1 + \ell_2 - L = \text{even}; \quad \ell_1' + \ell_2' - L = \text{even} \qquad (B.24)$$

will also reduce the number of terms in Equation B.23.

In obtaining Equation B.23 no assumptions have been made about the reaction mechanism, with the exception that two particles enter and two particles emerge. For any specific case many simplifications can be made, such as, the case where the reaction proceeds via a definite resonance level of a compound nucleus with angular momentum J_o and parity π_o. Blatt and Biedenharn (162) now find it convenient to introduce a real quantity, $g_{\alpha s \ell}$, which is related to the partial width, $\Gamma_{\alpha s \ell}$, by the following:

$$g_{\alpha s \ell} = \pm(\Gamma_{\alpha s \ell})^{\frac{1}{2}} \qquad (B.25)$$

The ambiguity in sign does not exist in the formula for the cross section, however a study of the angular distribution for the reaction allows the determination of both the magnitude of $T_{\alpha s \ell}$ and the sign of $g_{\alpha s \ell}$.

It is also necessary to introduce the phaseshifts for potential (hard sphere) scattering, ξ_ℓ , which is given by Equation B.26 for charged particles:

$$\exp(2i\xi_\ell) = \exp(2i\sigma_\ell) \frac{G_\ell(\eta,\rho)-iF_\ell(\eta,\rho)}{G_\ell(\eta,\rho)+iF_\ell(\eta,\rho)} \qquad \text{(B.26)}$$

where $F_\ell(\eta,\rho)$ and $G_\ell(\eta,\rho)$ are the regular and irregular solutions to the radial wave equation outside the nuclear surface. For the incident channel the value of η is given by:

$$\eta = \frac{0.1574\ Z_a Z_X m_a^{\frac{1}{2}}}{E^{\frac{1}{2}}} \qquad \text{(B.27)}$$

where Z_a and Z_X are the atomic numbers of the incident particle target nucleus respectively, m_a is the mass of the incident particle in amu and E is the incident particles energy, in MeV, in the laboratory reference frame. For the exit channel η is given by (163):

$$\eta = 0.1574\ Z_b Z_Y \left(\frac{\mu'}{E'}\right)^{\frac{1}{2}} \qquad \text{(B.28)}$$

where Z_b and Z_Y are the atomic numbers of the

emitted particle and recoil nucleus respectively, μ' is the reduced mass given by:

$$\mu' = \frac{m_b m_Y}{m_b + m_Y} \tag{B.29}$$

and E' is the energy available to the reaction given by:

$$E' = \frac{m_X E}{m_a + m_X} + Q \tag{B.30}$$

The parameter ρ is given by:

$$\rho = kr = \frac{\mu v r}{\hbar} \tag{B.31}$$

where μ is the reduced mass, v is the relative velocity of the colliding particles, and r is the interparticle separation. It is also possible to approximate ρ by:

$$\rho \approx \frac{r_o(A_a^{1/3} + A_X^{1/3})}{\lambda} \tag{B.32}$$

where r_o is approximately 1.3×10^{-15} m and A is the nucleon number.

The phaseshift for Coulomb scattering from an impentrable sphere, σ_ℓ, is given by the following formula:

$$\exp(2i\sigma_\ell) = \frac{(\ell+i\eta)(\ell-1+i\eta)\ldots(1+i\eta)}{(\ell-i\eta)(\ell-1-i\eta)\ldots(1-i\eta)} \frac{(i\eta)!}{(-i\eta)!} \tag{B.33}$$

The observed resonant energy, E_o, is not a constant, but is dependent, on the channel energy through a quantity Δ_λ. The resonant energy should be given by:

$$E_o = E_\lambda + \Delta_\lambda \tag{B.34}$$

However in practice E_o can be considered a constant.

The scattering matrix elements vanish unless $J = J_o$ and $\pi = \pi_o$ for the reaction cross section. The scattering matrix can now be written in the form:

$$S_{\alpha's'\ell';\alpha s\ell}^{J_o\pi_o} = \exp[i(\xi_{\alpha\ell} - \eta_\alpha \ln 2k_\alpha r_\alpha)]\exp[i(\xi_{\alpha'\ell'} - \eta_{\alpha'} \ln 2k_{\alpha'} r_{\alpha'})]$$

$$\times [\delta_{\alpha'\alpha}\delta_{s's}\delta_{\ell'\ell} + i \frac{g_{\alpha s\ell} g_{\alpha's'\ell'}}{E_o - E - \frac{1}{2}i\Gamma}] \quad (\text{for } J = J_o,\ \pi = \pi_o) \tag{B.35}$$

Here r_α and $r_{\alpha'}$ are the screening radii for the Coulomb field in channels α and α' respectively. In the final equation the screening radii will drop out. The total width for the level J_o, π_o, E_o is given by:

$$\Gamma = \sum_\alpha \sum_s \sum_\ell \Gamma_{\alpha s\ell} \tag{B.36}$$

and depends on the energy. Equation B.35 assumes that resonances of different J and π are far enough away in energy that their influence can be neglected.

Substituting Equation B.35 into Equation B.21 and allowing:

$$B_L(\alpha's';\alpha s) = R_L(\alpha's';\alpha s) \qquad (B.37)$$

gives:

$$R_L(\alpha's';\alpha s) = \frac{(-)^{s'-s}}{4[(E-E_o)^2+(\tfrac{1}{2}\Gamma)^2]} \sum_{\ell_1=|J_o-s|}^{J_o+s} \sum_{\ell_2=|J_o-s|}^{J_o+s} \sum_{\ell_1'=|J_o-s'|}^{J_o+s'} \sum_{\ell_2'=|J_o-s'|}^{J_o+s'}$$

$$\times Z(\ell_1 J_o \ell_2 J_o, sL) Z(\ell_1' J_o \ell_2' J_o, s'L)\, g_{\alpha s \ell_1}\, g_{\alpha s \ell_2}\, g_{\alpha' s' \ell_1'}\, g_{\alpha' s' \ell_2'}$$

$$\cos[\xi_{\alpha\ell_1} - \xi_{\alpha\ell_2} + \xi_{\alpha'\ell_1'} - \xi_{\alpha'\ell_2'}]$$

$$(\text{for } \alpha,s \neq \alpha',s') \qquad (B.38)$$

The condition of parity conservation, Equation B.15 must also be imposed on Equation B.38. As was the case with Equation B.21 each term in Equation B.38 will occur twice, it therefore should be contracted along the same lines as used to obtain Equation B.23.

The total cross section, σ_ℓ , can be written as:

$$\sigma_o(\alpha's';\alpha s) = \frac{4\pi\lambda_\alpha^2}{2s+1} B_o(\alpha's';\alpha s) =$$

$$\frac{\pi\lambda_\alpha^2}{2s+1} \sum_{J=0}^{\infty} \sum_{\ell=|J-s|}^{J+s} \sum_{\ell'=|J-s'|}^{J+s'} (2J+1) \left| \delta_{\alpha'\alpha}\delta_{s's}\delta_{\ell'\ell} - \delta_{\alpha's'\ell';\alpha s\ell}^{J} \right|^2$$

(B.39)

or substituting

$$\sigma_o(\alpha's',\alpha s) = \pi\lambda_\alpha^2 \frac{2J_o+1}{2s+1} \sum_{\ell} \sum_{\ell'} \frac{\Gamma_{\alpha s\ell}\Gamma_{\alpha's'\ell'}}{(E-E_o)^2 + (\frac{1}{2}\Gamma)^2}$$

(for $\alpha,s \neq \alpha's'$) (B.40)

The sums in Equation B.40 are the same as those in Equation B.38. As can be seen a measurement of the total cross section does not allow a determination of the signs of the g's. However, in principle a measurement of the differential cross section will allow the signs of the g's to be determined.

The selection rules for nonvanishing Z coefficients force B_L to vanish if L violates one of the following:

$$L \leq 2 \cdot J_o \qquad \text{(B.41)}$$

$$L = \text{even} \qquad \text{(B.42)}$$

$$L \leq 2\,\ell_{max} \qquad \text{(B.43)}$$

$$L \leq 2\,\ell'_{max} \tag{B.44}$$

The formulas given to this point have been for reactons which have definite channel spins, however, the channel spins are not measured and the observed cross section is for $\alpha \rightarrow \alpha'$. The differential cross section is given by:

$$d\sigma_{\alpha';\alpha} = \frac{\lambda_\alpha^2}{(2i+1)(2I+1)} \sum_{L=0}^{L_{max}} B_L(\alpha';\alpha) P_L(\cos\theta)\, d\Omega \tag{B.45}$$

where

$$B_L(\alpha';\alpha) = R_L(\alpha';\alpha) = \sum_{s=|I-i|}^{I+i} \sum_{s'=|I'-i'|}^{I'+i'} R_L(\alpha's';\alpha s) \tag{B.46}$$

It should be emphasized again that Equation B.45 applies to reactions only, that is $\alpha \neq \alpha'$, and assumes the resonances of different J and π are far enough away in energy that their influence can be neglected.

In practice the differential cross section at an energy intermediate to two isolated resonances is given by:

$$d\sigma = d\sigma_1 + d\sigma_1 + d\sigma_2 \tag{B.47}$$

where $d\sigma_1$ and $d\sigma_2$ are the cross sections given by Equation B.45 for resonances 1 and 2 respectively and $d\sigma_{12}$ is the interference between the two resonances. The interference term is given by:

$$d\sigma_{12_{\alpha';\alpha}} = \frac{\lambda_\alpha^2}{(2i+1)(2I+1)} \sum_{L=0}^{L_{max}} \{4[(E-E_{o_1})^2 + (\tfrac{1}{2}\Gamma_1)^2]\}^{-\frac{1}{2}} \{4[(E-E_{o_2})^2$$

$$+ (\tfrac{1}{2}\Gamma_2)^2]\}^{-\frac{1}{2}} \; g_{\alpha_1 s\ell_1} \; g_{\alpha_1' s\ell_1'} \; g_{\alpha_2 s\ell_2} \; g_{\alpha_2' s\ell_2'} \quad Z(\ell_1 J_{o_1} \ell_2 J_{o_2}, sL)$$

$$Z(\ell_1' J_{o_1} \ell_2' J_{o_2} s'L) \cos(\xi_{\alpha_1\ell_1} - \xi_{\alpha_2\ell_2} + \xi_{\alpha_1'\ell_1'} - \xi_{\alpha_2'\ell_2'} + \beta_1 - \beta_2)$$

$$P_L(\cos\theta) \qquad \text{(B.48)}$$

The subscripts 1 and 2 in the above equation refer to resonances 1 and 2 respectively and β is an angular parameter which measures the deviation of the energy from the resonance energy. The value of β is given by:

$$\beta = \text{Tan}^{-1} \frac{2(E-E_o)}{\Gamma} \qquad \text{(B.49)}$$

The summation over L in Equation B.48 runs from 0 to L_{max} and includes odd values of L if $\pi_1 \neq \pi_2$.

B.4 Calculation of the $^{15}N(\rho,\alpha_o)^{12}C$ Differential Cross Section

The differential cross section for the $^{15}N(\rho,\alpha_o)^{12}C$ reaction between 0 and 1.5 MeV can be written as:

$$d\sigma_{total} = d\sigma_{338} + d\sigma_{338/1028} + d\sigma_{1028} + d\sigma_{1028/1050} + d\sigma_{1050} +$$

$$d\sigma_{1050/1210} + d\sigma_{1210} \qquad \text{(B.50)}$$

where $d\sigma_i$ is the differential cross section do to the resonance at energy i given by Equation B.45 and $d\sigma_{i/j}$ is the interference term due to resonances at energies i and j given by Equation B.49. Each term was calculated using the resonance parameters given by Ajzenberg-Selove (164). These parameters have been tabulated in Table B.1. The partial width for the α_o channel, Γ_{α_o}, for the 1210 keV resonance was calculated using Equation B.36 and found to be 10.2 keV (22.5-4.1-8.2 = Γ_{α_o}). Ad'yasevich, et al. (157) have reported that the product $\Gamma_p\Gamma_{\alpha_o}$ to be 500 keV^2 for the 1050 keV resonance with the terms Γ_p,Γ_{α_o}, Γ_{lab} equal to either 1,500,501 or 2,250,252 in keV respectively. Calculations were carried out using both sets of parameters.

In order to determine the orbital angular momentum for each channel it is necessary to know the intrinsic spins and parities for each of the particles involved. For the present case $i^\pi = \frac{1}{2}^+$, $I^\pi = \frac{1}{2}^-$, $i'^\pi = 0^+$, and $I'^\pi = 0^+$. Using Equations B.5 and B.6 the channel spins are found to be s = 0 or 1 and s'= 0. If the 1210 keV resoannce is used as an example $J_o^{\pi_o} = 3^-$ and to satisfy the conditions given in Equations B.14 and B.15 we find that for the incoming channel s = 1 and ℓ = 2 or 4 ($s \neq 0$ by parity considerations)

TABLE B.1

Resonance Parameters for the $^{15}N(p,\alpha_o)^{12}C$ Reaction

E_p(keV)	Γ_p(keV)	Γ_{α_o}(keV)	Γ_{lab}(keV)	$J_o^{\pi_o}$
338	1.2	95	96	1^-
1028 ± 10	100	40	140 ± 10	1^-
1050 ± 150	$\Gamma_p\Gamma_{\alpha_o}$ = 500 keV^2			2^+
1210 ± 3	4.1	resonant	22.5 ± 1	3^-

and for the outgoing channel $s' = 0$ and $\ell' = 3$. Penetration considerations indicate that $\ell = 4$ will at most be a small correction to the cross section at these energies and can therefore be ignored.

The Z coefficients used in the calculations were obtained from Biedenharn's tabulation of Racah Coefficients (165).

Figures B.1 - B.7 show the contributions of each of the terms in Equation B.50 at a laboratory scattering angle of 165°. It should be noted that because the signs of the g's ($\pm(\Gamma)^{\frac{1}{2}}$) are not known and the interference terms may add as the reciprical of the values given. After each of the individual terms were obtained they were combined according to Equation B.50. The possible total differential cross sections at a laboratory scattering angle of 165° are shown in Figures B.8-B.15. The curves shown in parts a and b are for Γ_{1ab} of the 1050 keV resonance equal to 252 keV and 501 keV respectively. The plus sign indicates that the term added as shown in Figures B.1-B.7.

B.5 Measurement of the $^{15}N(p,\alpha_o)^{12}C$ Differential Cross Section

In order to experimentally measure the $^{15}N(p,\alpha_o)^{12}C$ differential cross section at a laboratory angle of 165° three $Si_3{}^{15}N_4$ targets were prepared by C. J. Mogab (Bell Laboratories, Murray Hill, New Jersey). The target thicknesses were 0.33 keV(6.5 nm), 1.30 keV (26.0 nm), and 1.95 keV (39.0 nm) to 1.0 MeV protons and the nitrogen-15 density was 5.5×10^{28} atoms-m^{-3}.

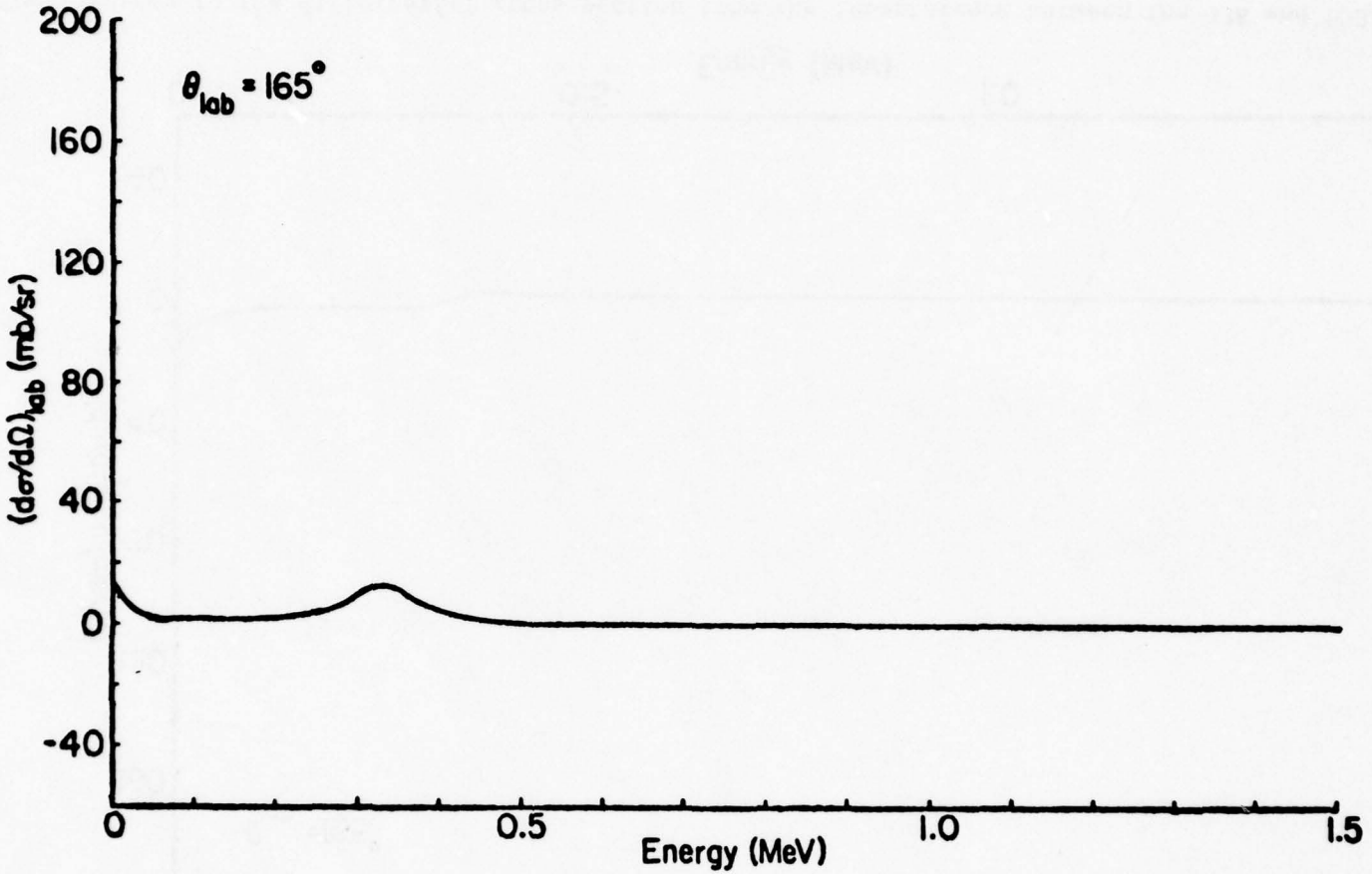

B.1 Contribution to the differential cross section from the 338 keV resonance ($d\sigma(338)$).

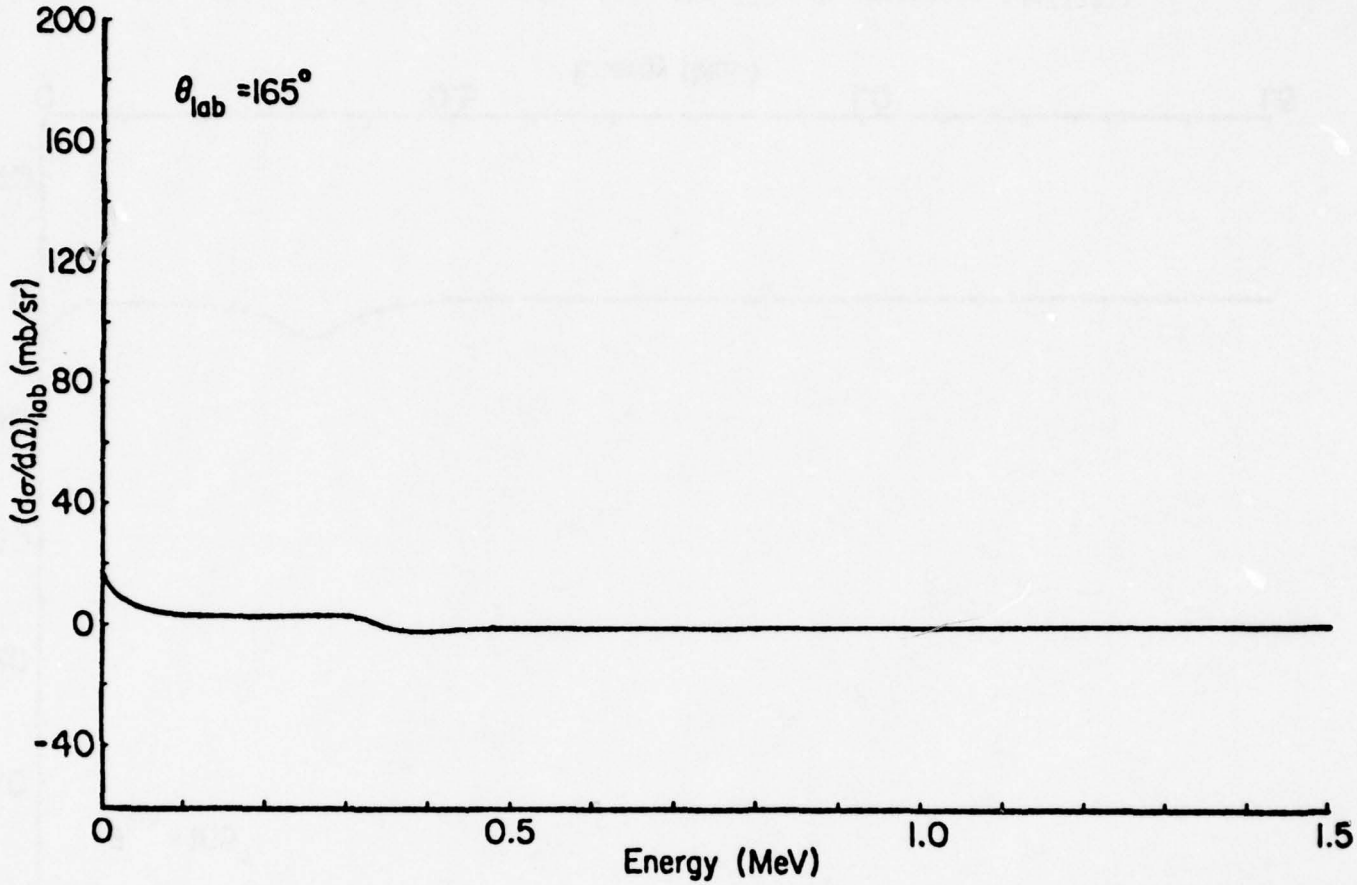

B.2 Contribution to the differential cross section from the interference between the 338 and 1028 keV resonances ($d\sigma(338/1028)$).

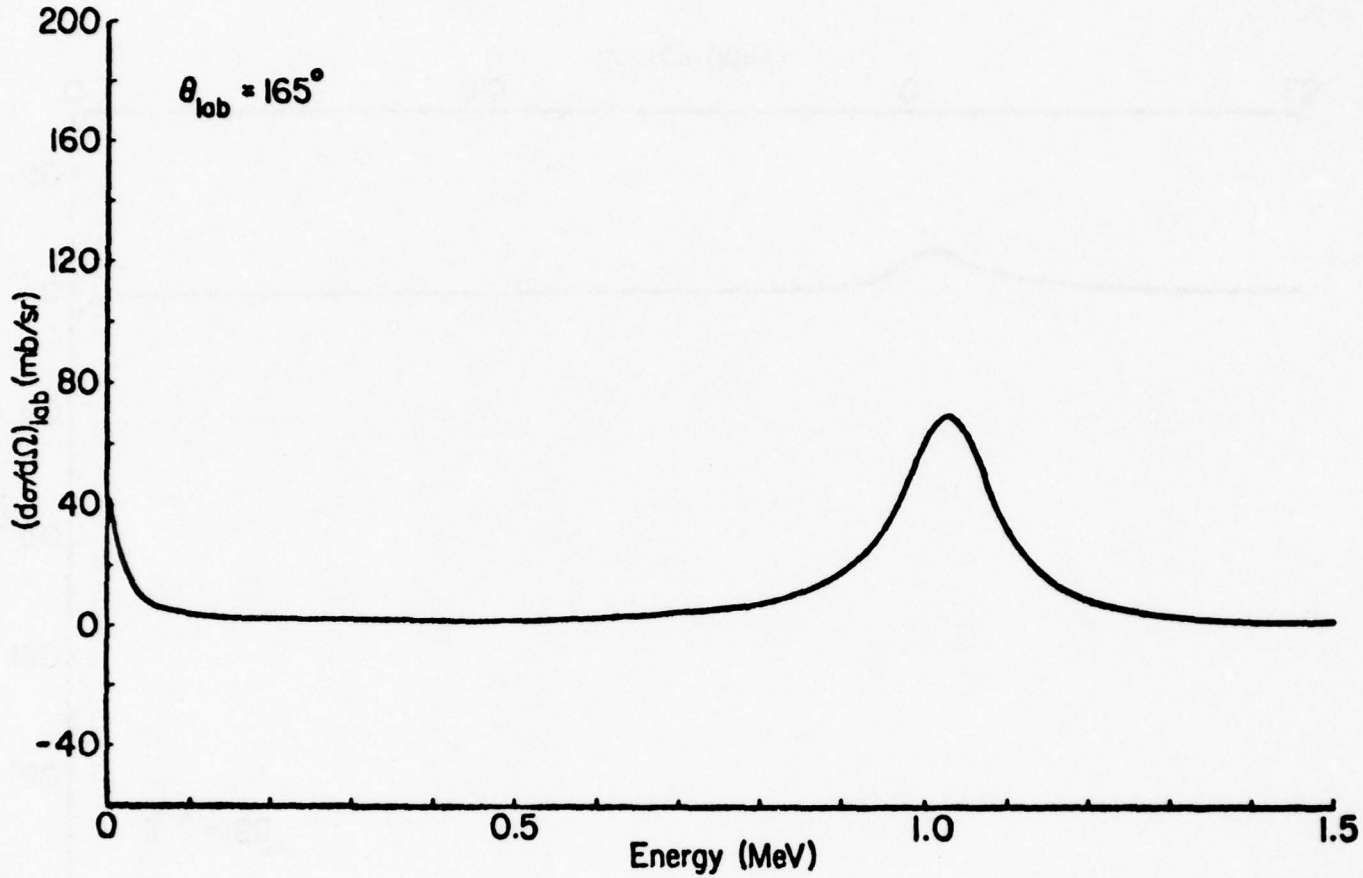

B.3 Contribution to the differential cross section from the 1028 keV resonance ($d\sigma(1028)$).

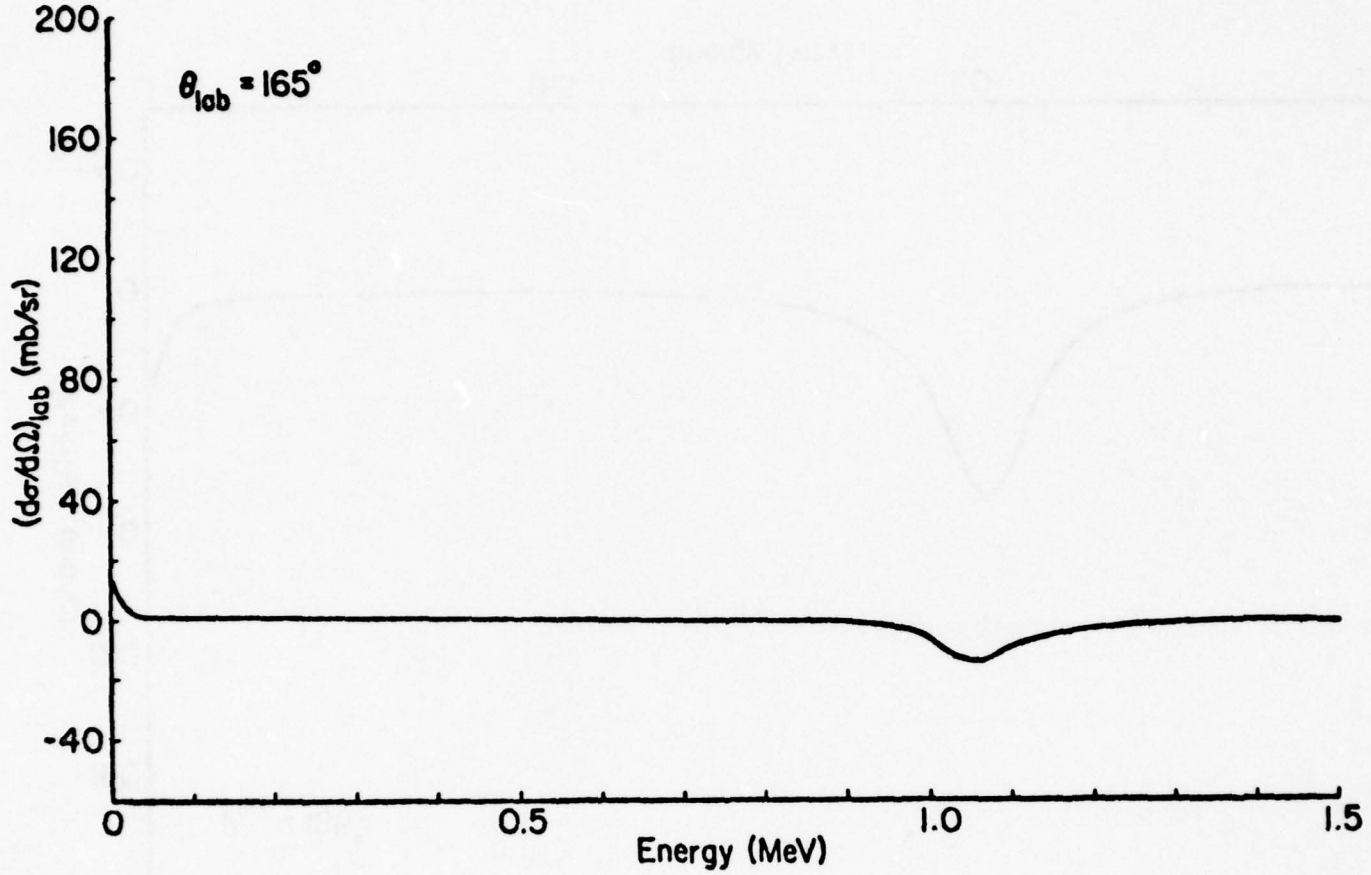

B.4a Contribution to the differential cross section from the interference between the 1028 and 1050 (Γ= 252) keV resonances (d (1028/1050a)).

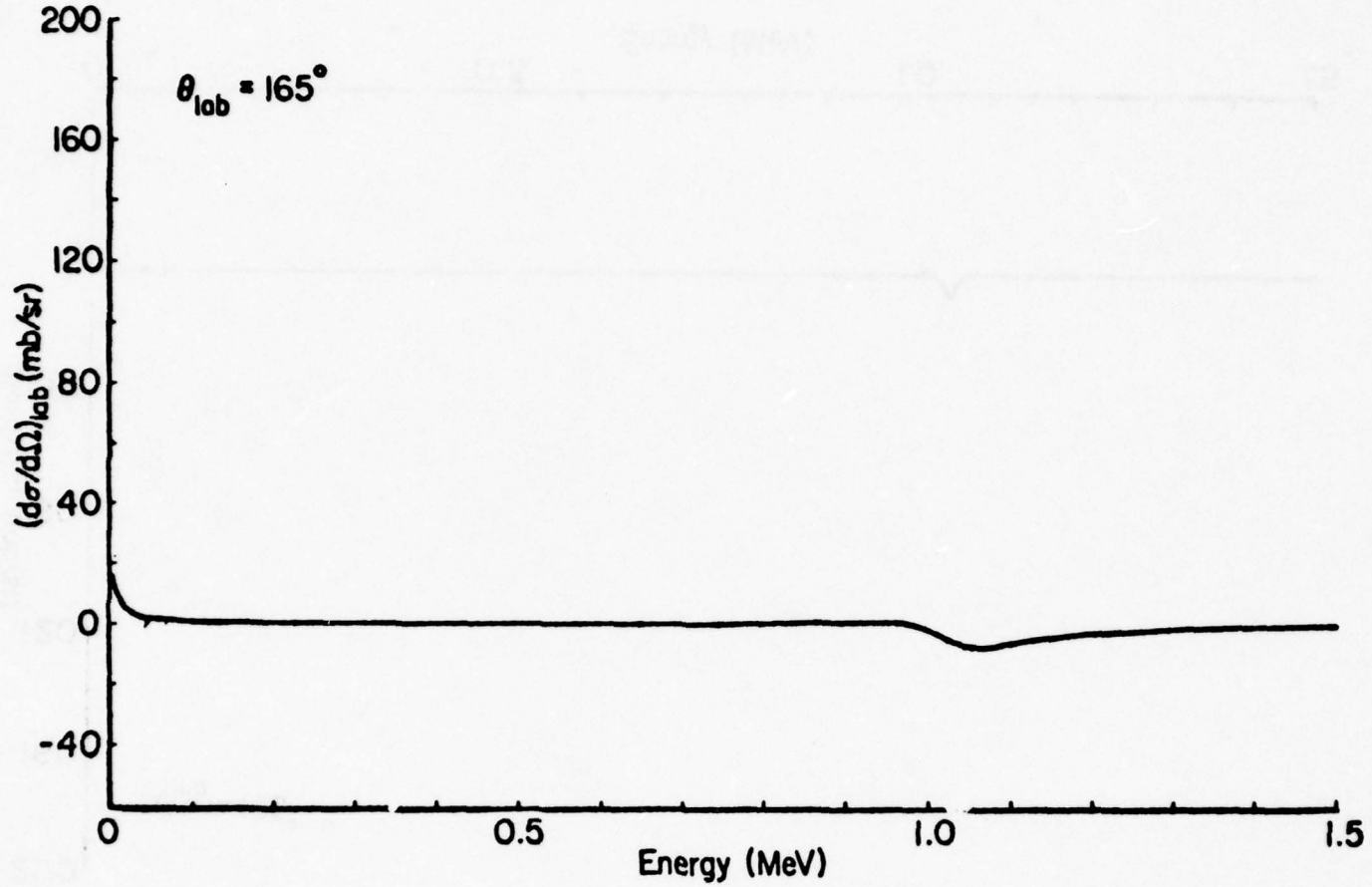

B.4b Contribution to the differential cross section from the interference between the 1028 and 1050 (Γ = 501) keV resonances ($d\sigma$(1028/1050b)).

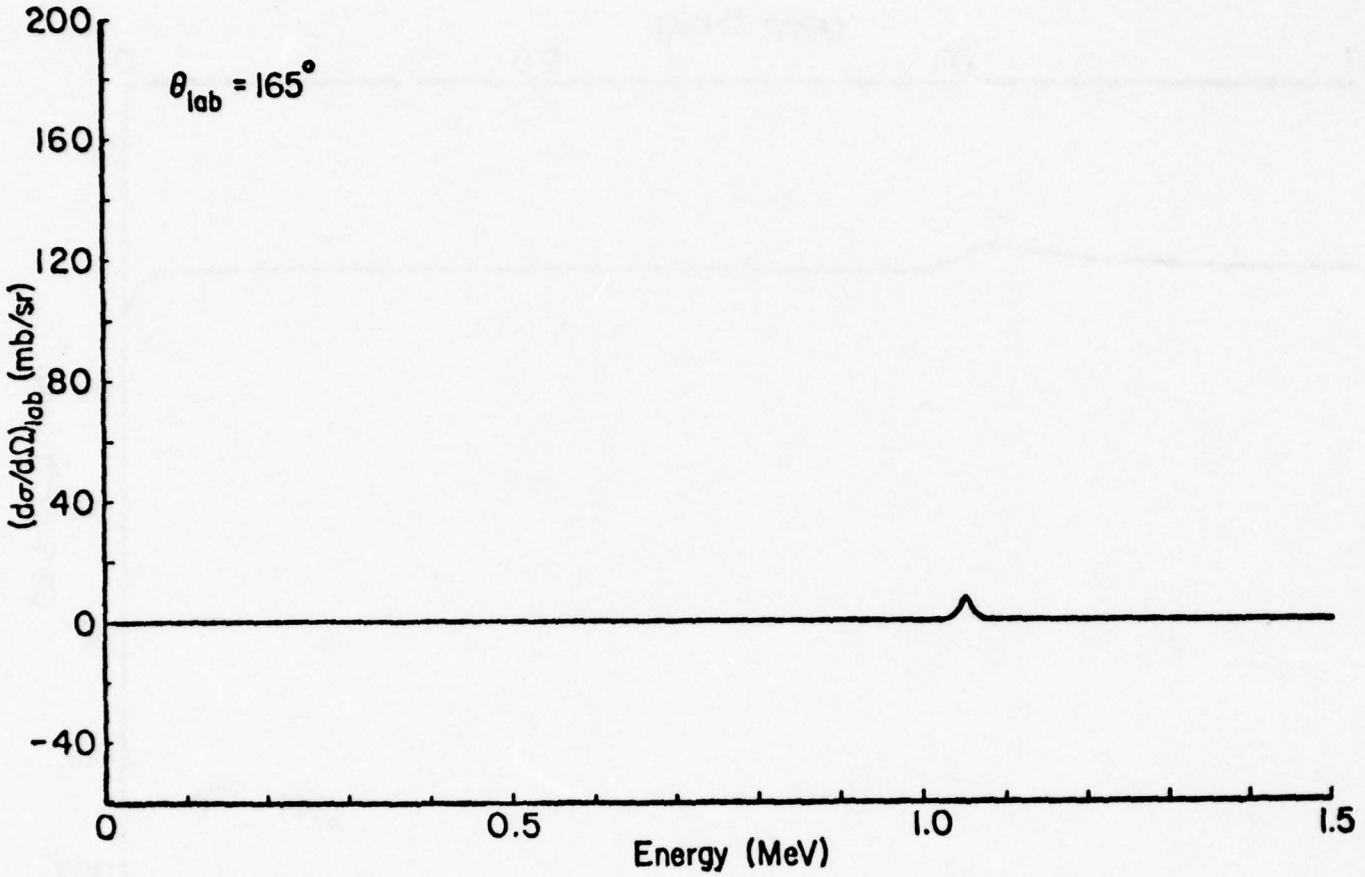

B.5a Contribution to the differential cross section from the 1050 (Γ = 252)keV resonance ($d\sigma$(1050a)).

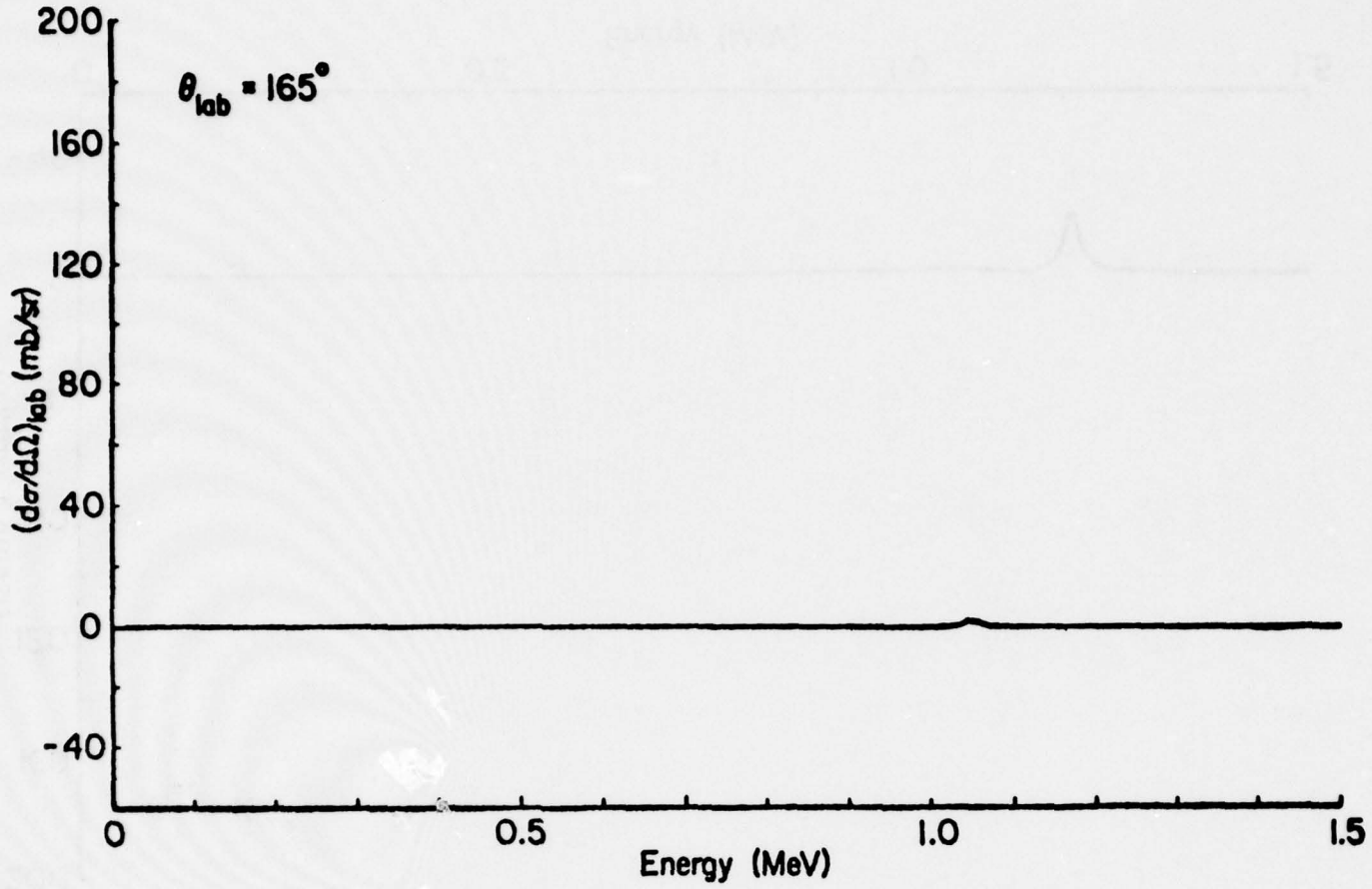

B.5b Contribution to the differential cross section from the 1050 (Γ = 501)keV resonance ($d\sigma$(1050b)).

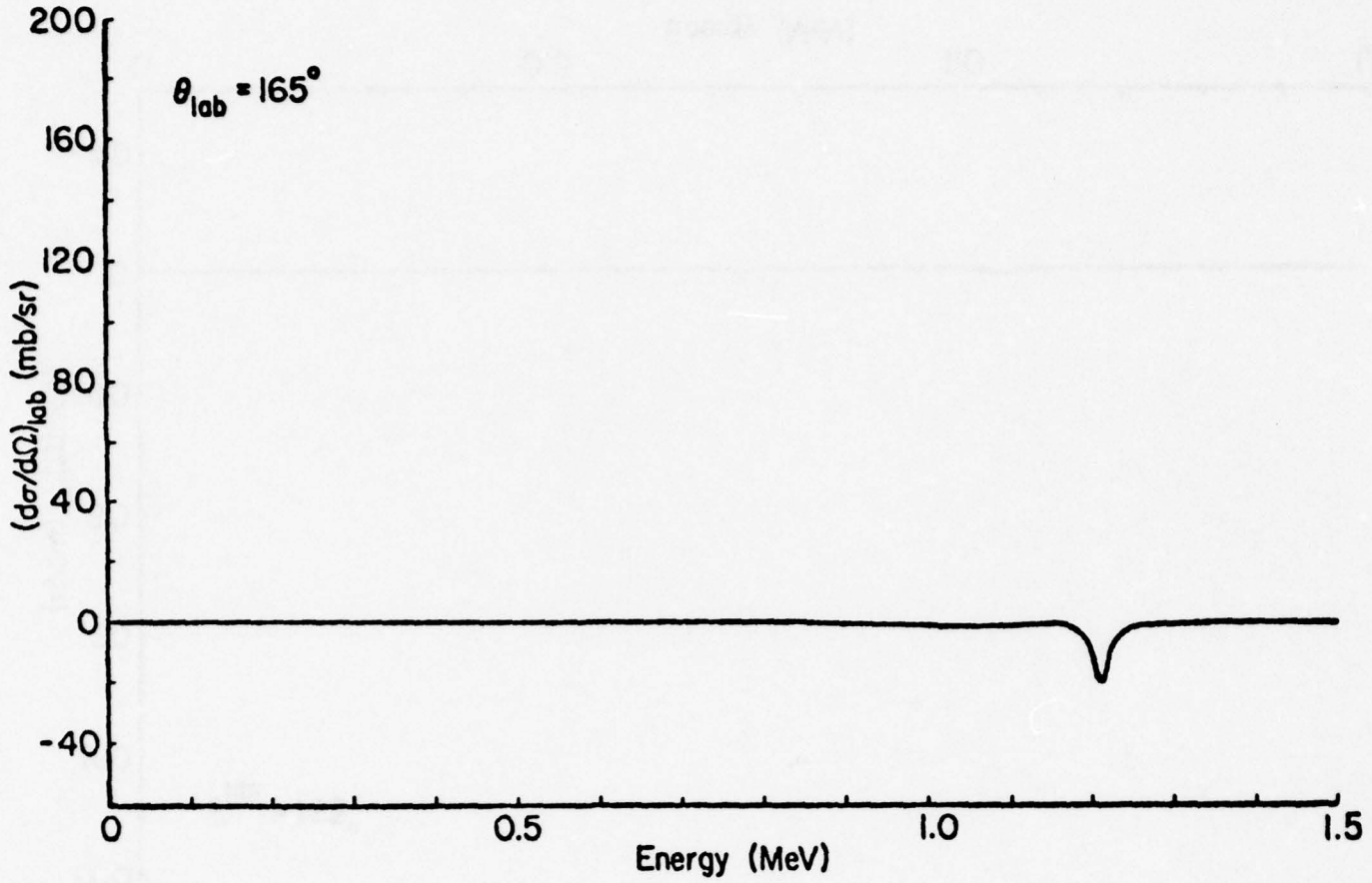

B.6a Contribution to the differential cross section from the interference between the 1050 (Γ = 252) and 1210 keV resonances ($d\sigma$(1050a/1210)).

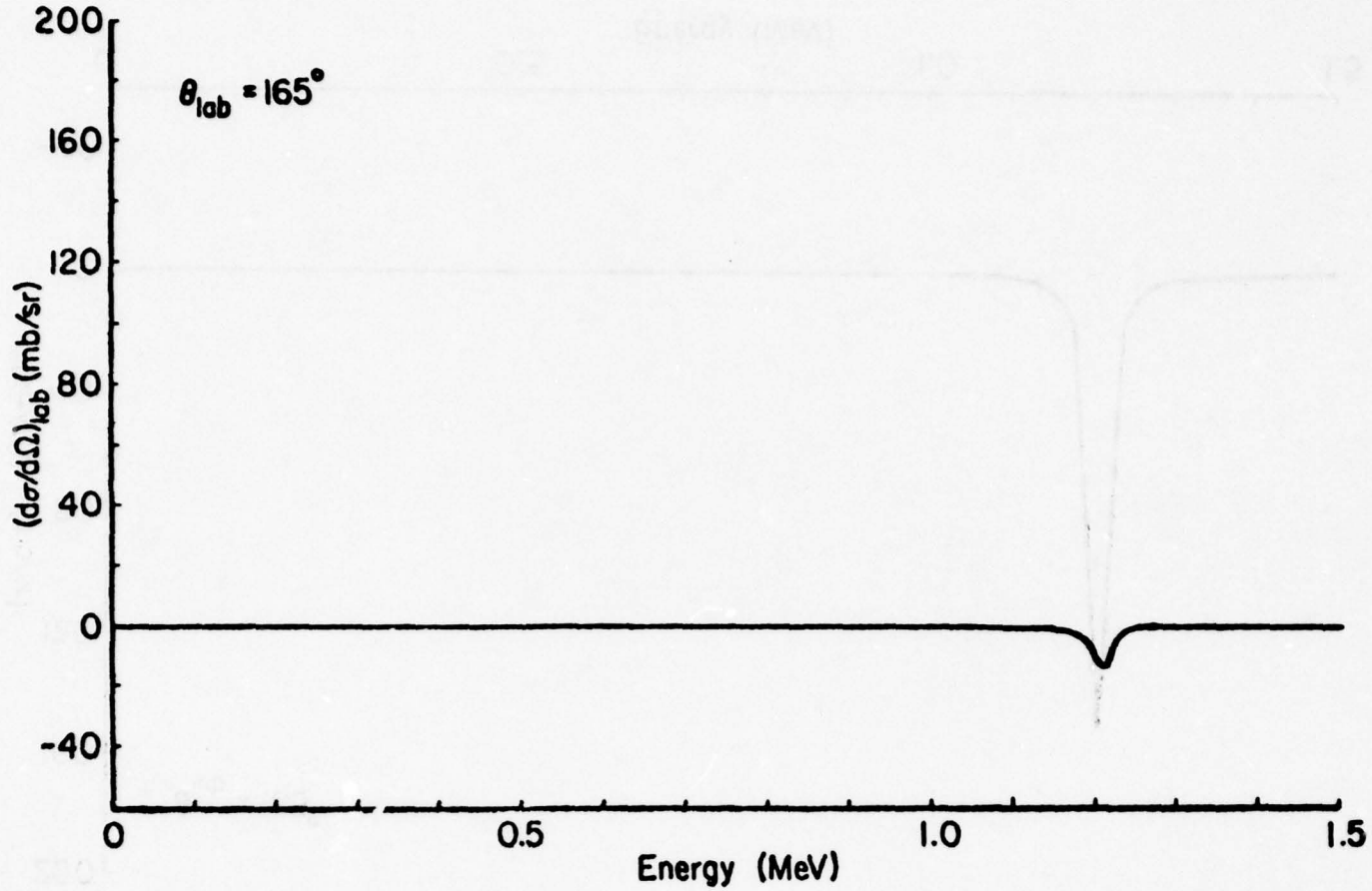

B.6b Contribution to the differential cross section from the interference between the 1050 (Γ = 501) and 1210 keV resonances ($d\sigma$(1050b/1210)).

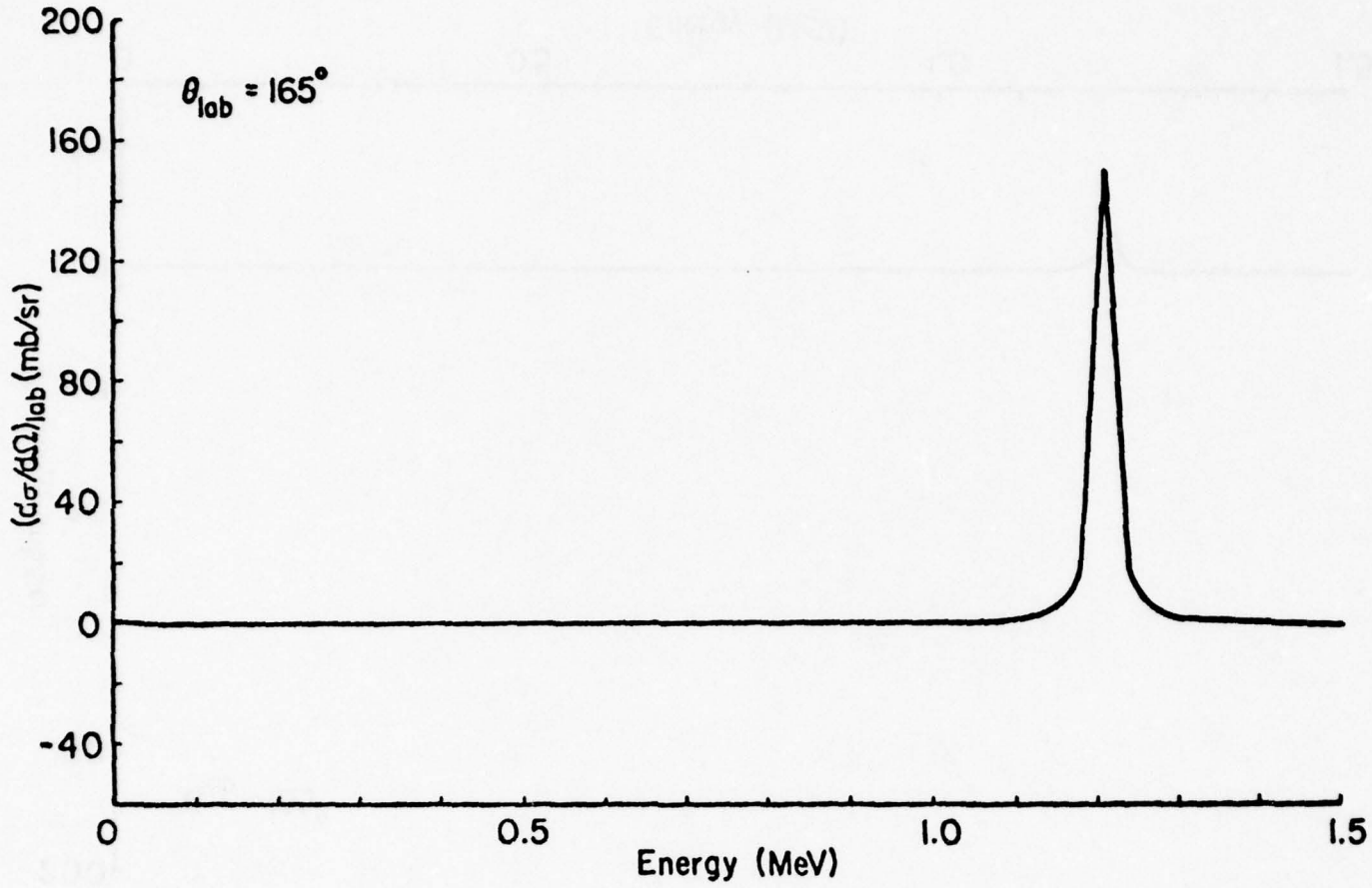

B7 Contribution to the differential cross section from the 1210 keV resonance ($d\sigma(1210)$).

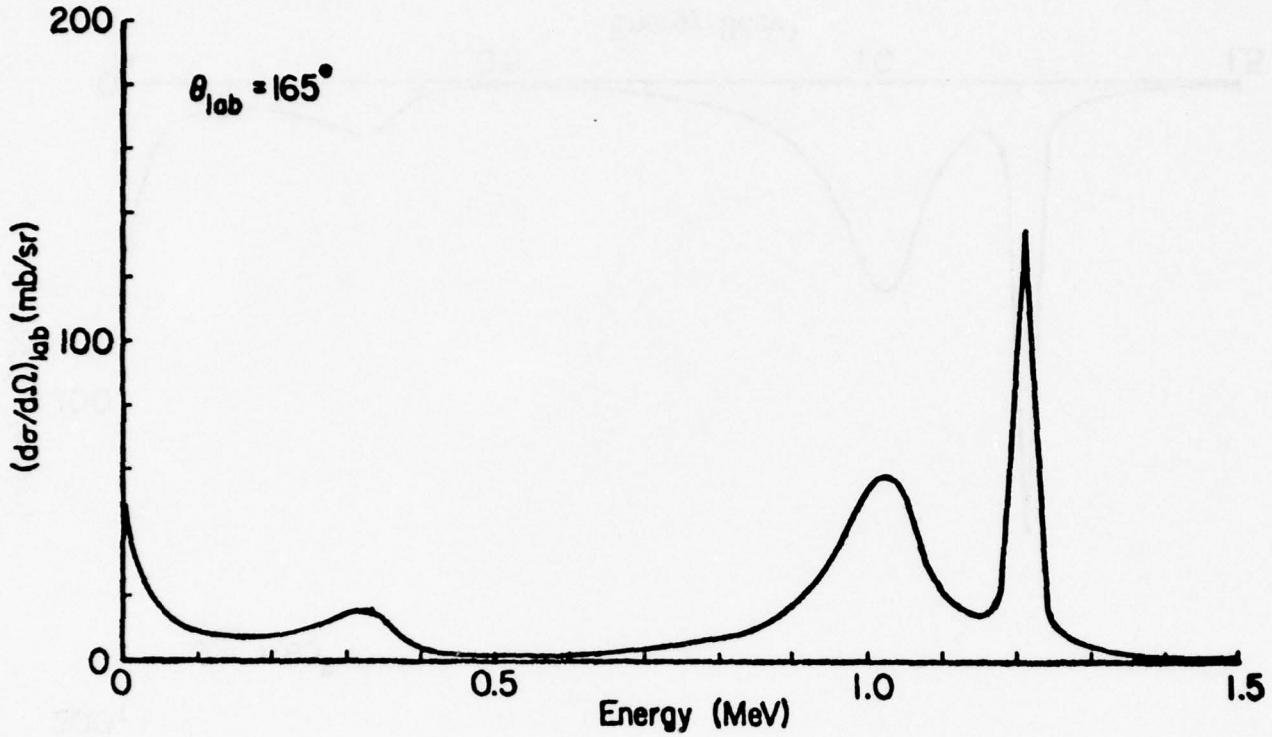

B.8a Possible differential cross section given by $d\sigma(338) + d\sigma(338/1028) + d\sigma(1028) + d\sigma(1028/1050a) + d\sigma(1050a) + d\sigma(1050a/1210) + d\sigma(1210)$.

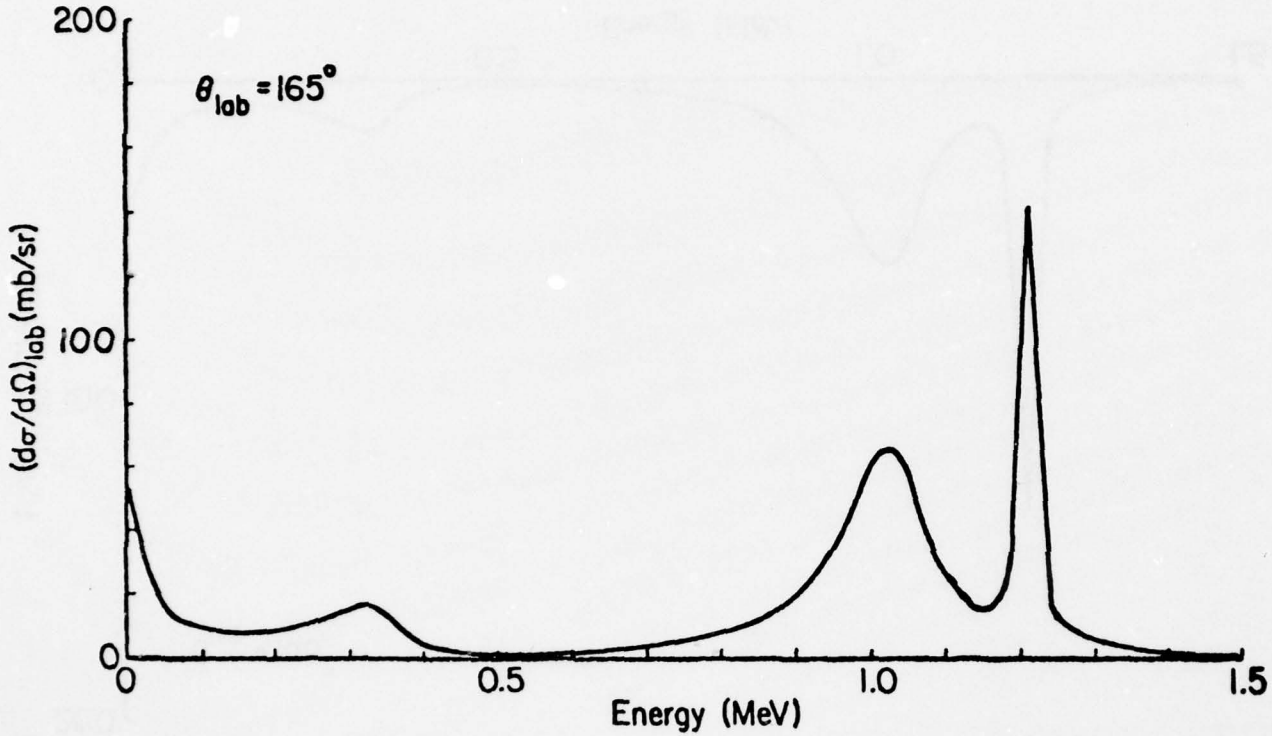

B.8b Possible differential cross section given by $d\sigma(338) + d\sigma(338/1028) + d\sigma(1028) + d\sigma(1028/1050b) + d\sigma(1050b) + d\sigma(1050b/1210) + d\sigma(1210)$.

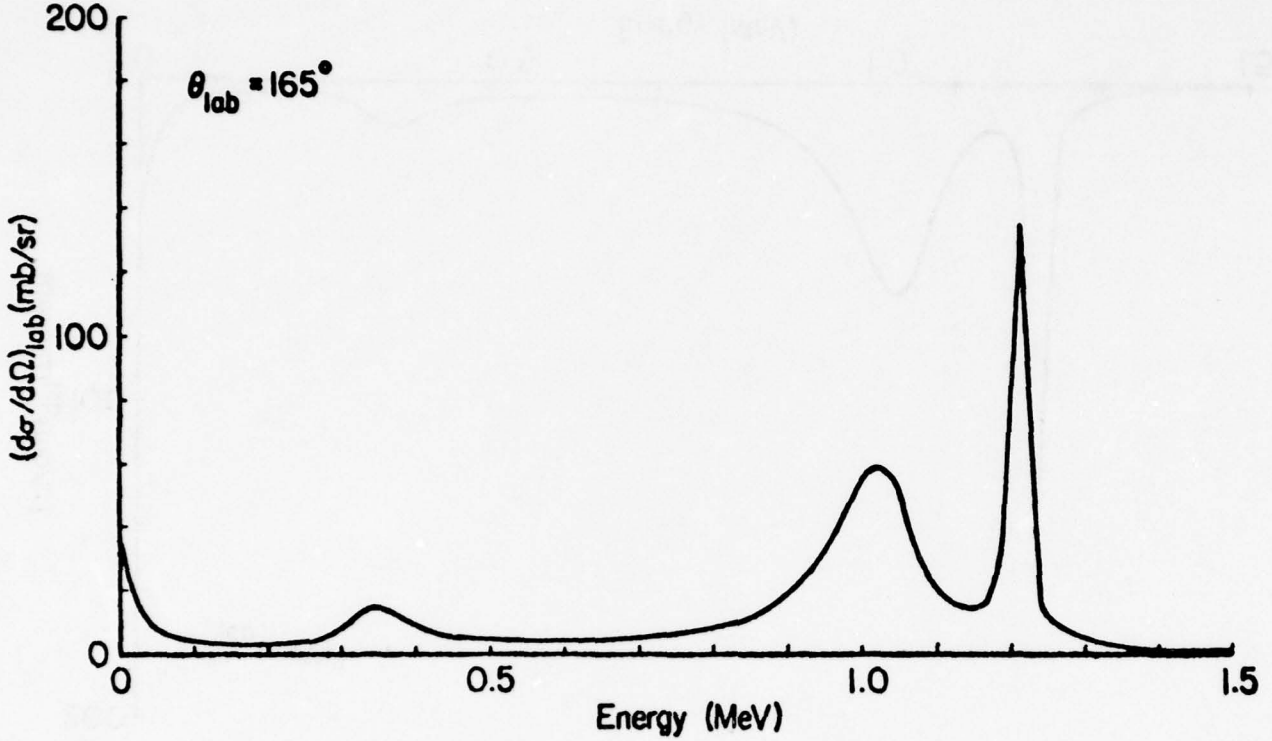

B.9a Possible differential cross section given by $d\sigma(338) - d\sigma(338/1028) + d\sigma(1028) + d\sigma(1028/1050a) + d\sigma(1050a) + d\sigma(1050a/1210) + d\sigma(1210)$.

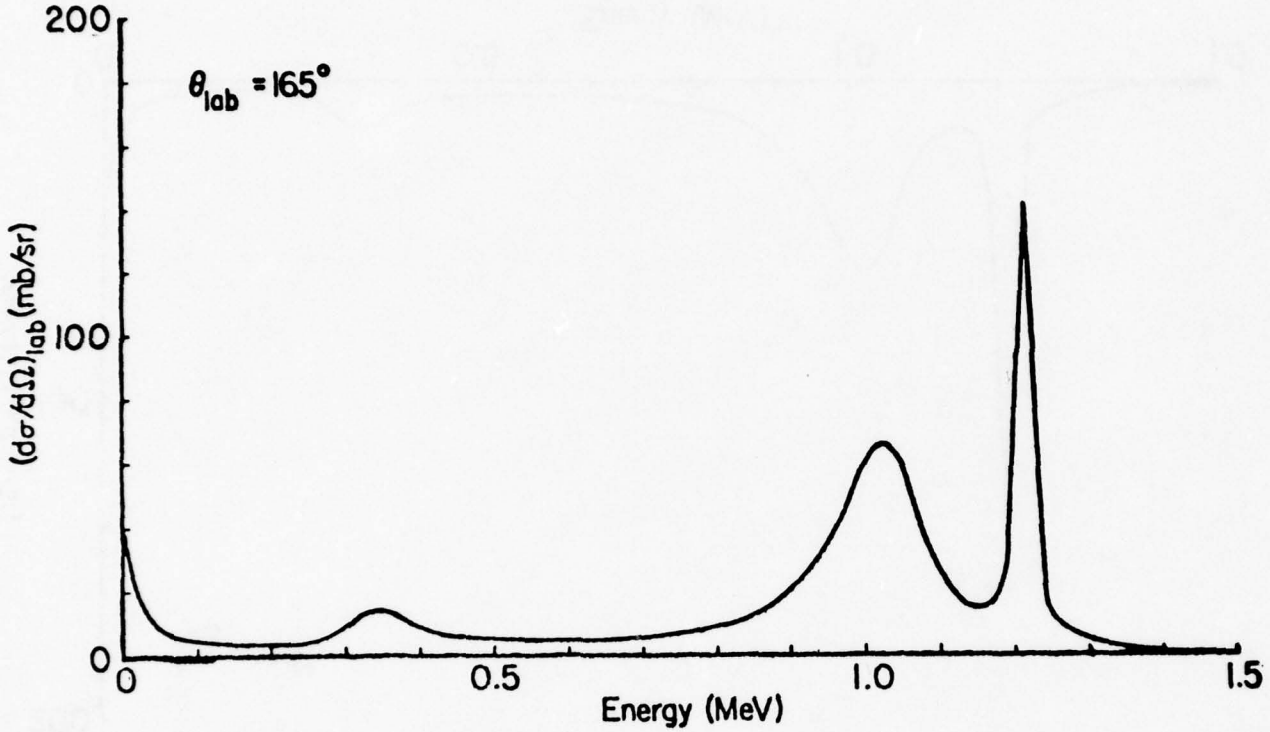

B.9b Possible differential cross section given by dσ(338) - dσ(338/1028) + dσ(1028) + dσ(1028/1050b) + dσ(1050b) + dσ(1050b/1210) + dσ(1210).

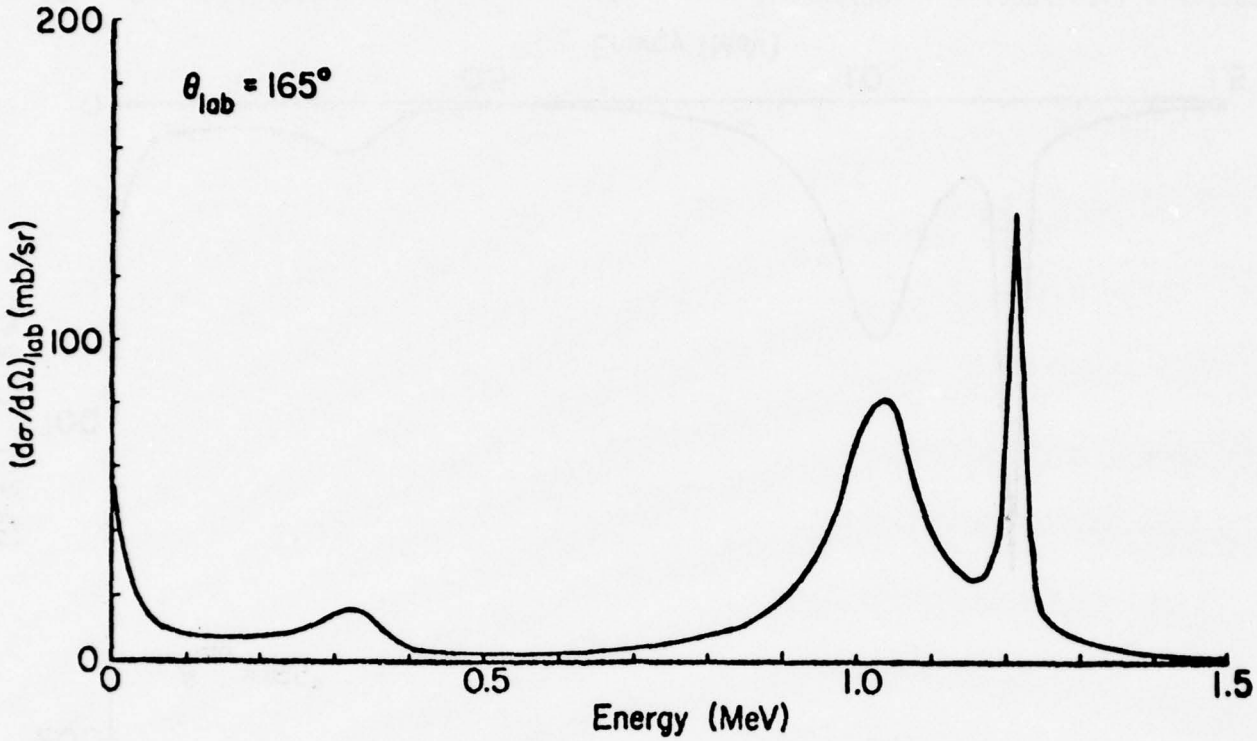

B.10a Possible differential cross section given by dσ(338) + dσ(338/1028) + dσ(1028) - dσ(1028/1050a) + dσ(1050a) + dσ(1050a/1210) + dσ(1210).

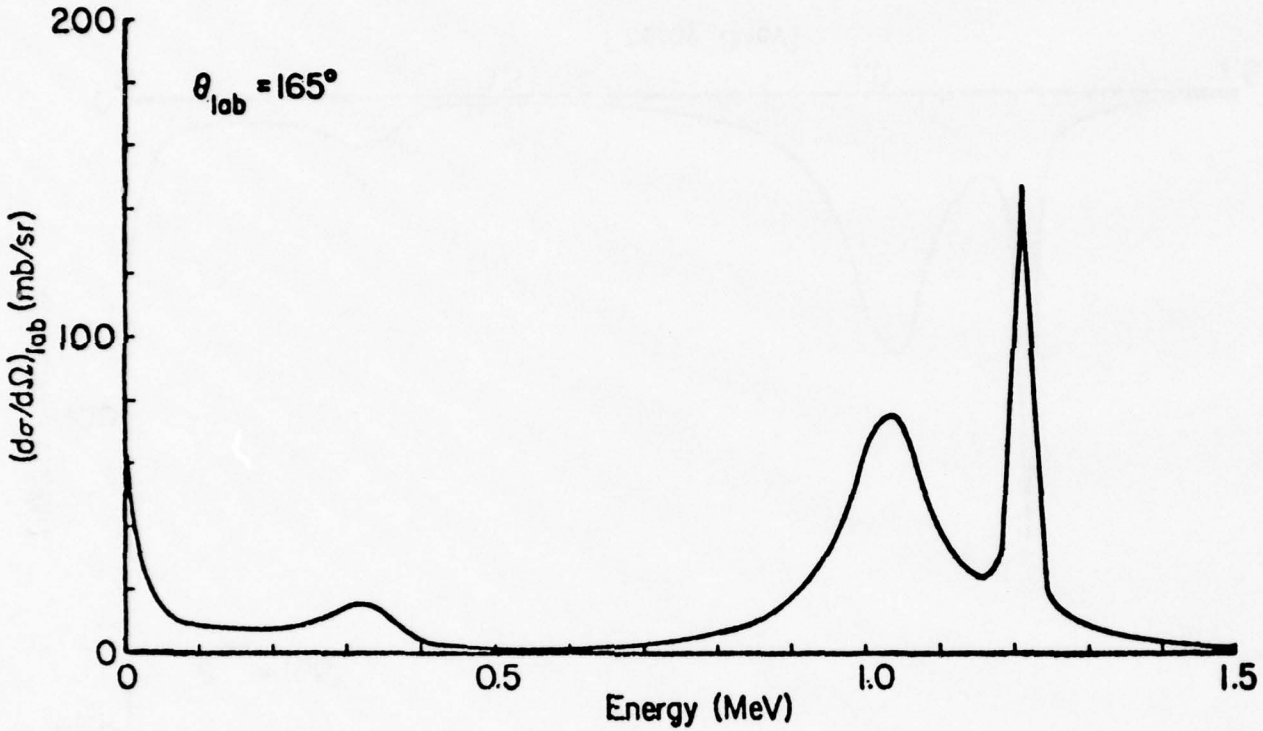

B.10b Possible differential cross section given by $d\sigma(338) + d\sigma(338/1028) + d\sigma(1028) - d\sigma(1028/1050b) + d\sigma(1050b) + d\sigma(1050b/1210) + d\sigma(1210)$.

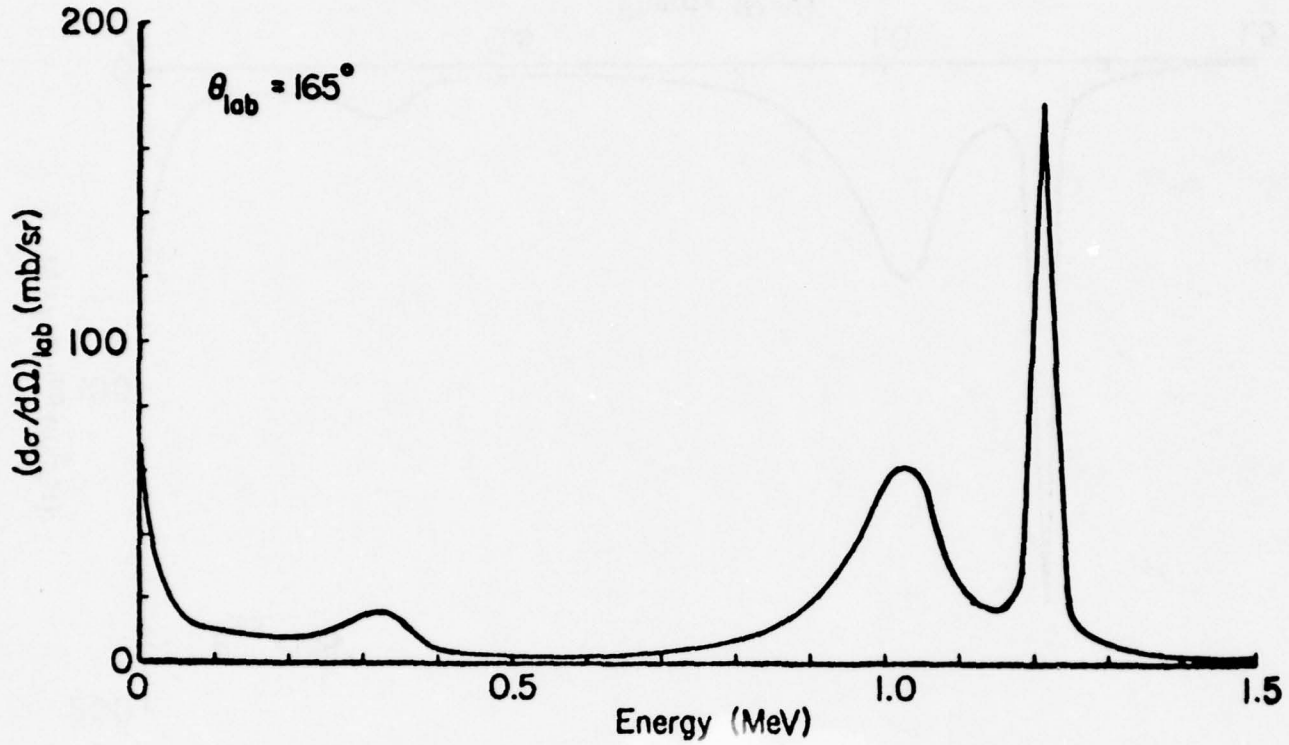

B.11a Possible differential cross section given by $d\sigma(338) + d\sigma(338/1028) + d\sigma(1028) + d\sigma(1028/1050a) + d\sigma(1050a) - d\sigma(1050a/1210) + d\sigma(1210)$.

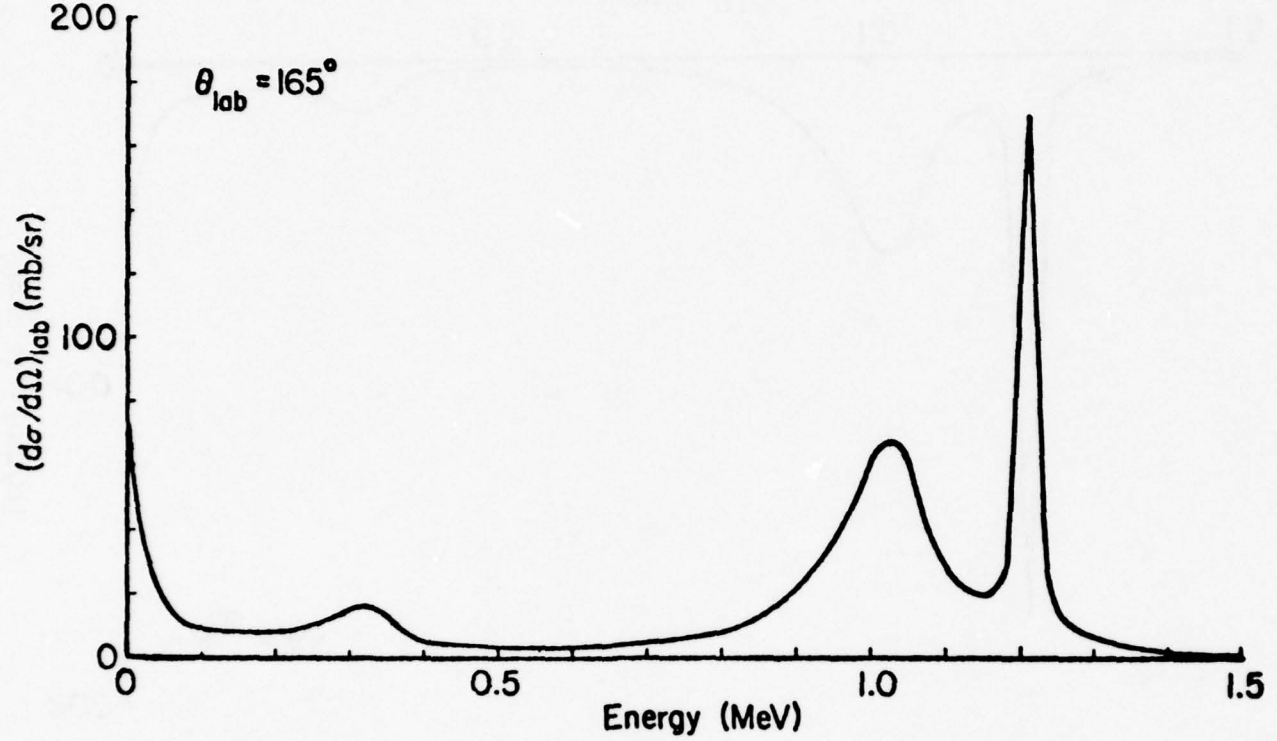

B.11b Possible differential cross section given by dσ(338) + dσ(338/1028) + dσ(1028) + dσ(1028/1050b) + dσ(1050b) - dσ(1050b/1210) + dσ(1210).

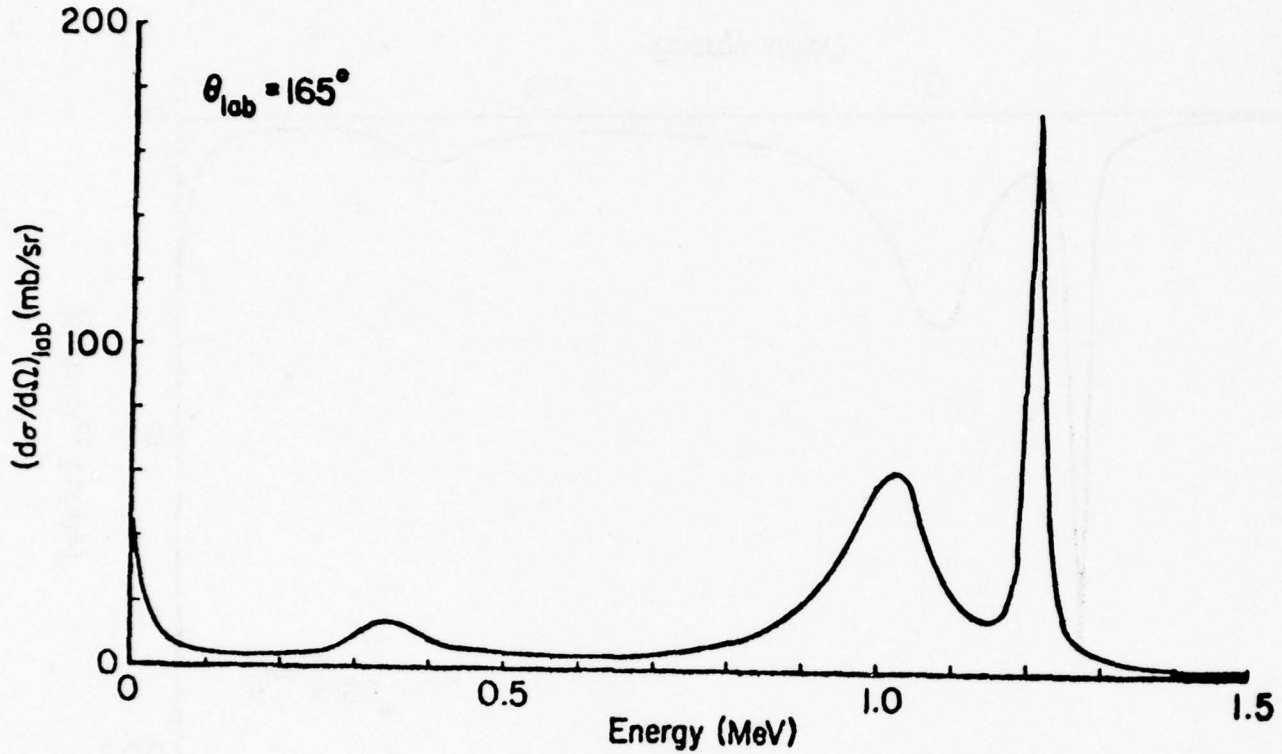

B.12a Possible differential cross section given by dσ(338) - dσ(338/1028) + dσ(1028) + dσ(1028/1050a) + dσ(1050a) - dσ(1050a/1210) + dσ(1210).

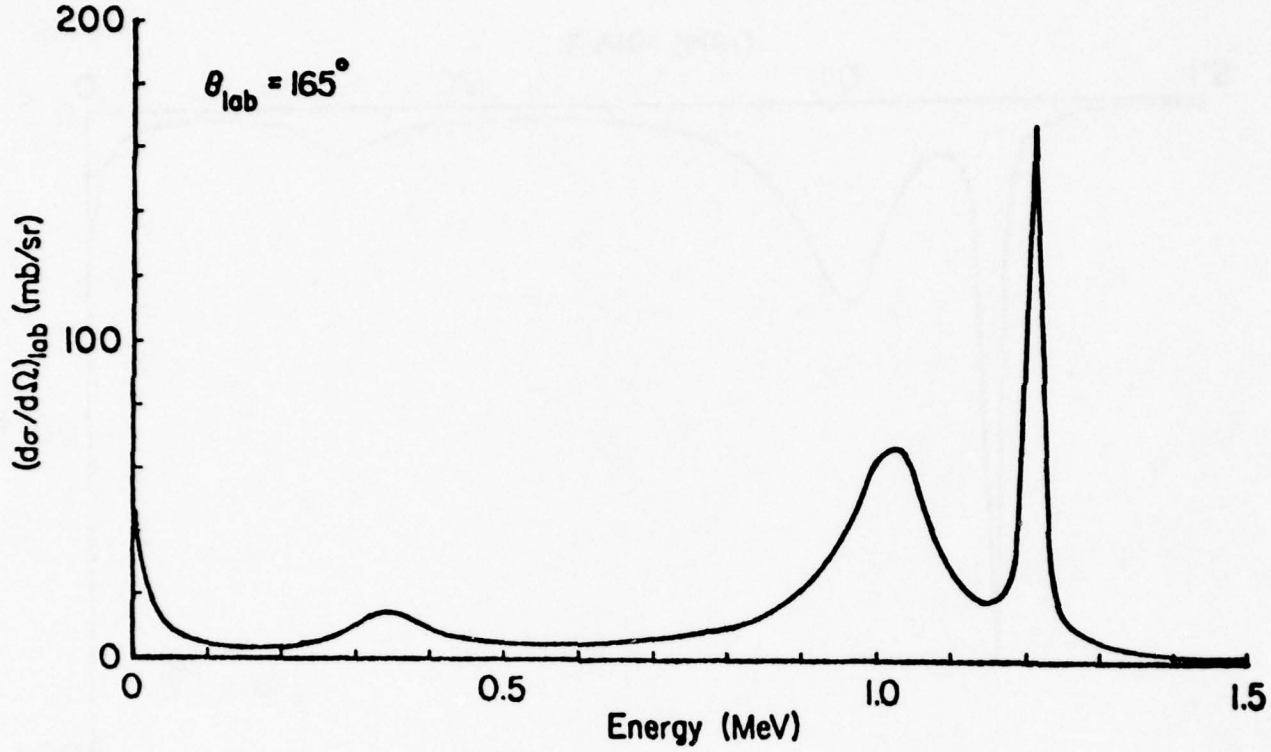

B.12b Possible differential cross section given by $d\sigma(338) - d\sigma(338/1028) + d\sigma(1028) + d\sigma(1028/1050b) + d\sigma(1050b) - d\sigma(1050b/1210) + d\sigma(1210)$.

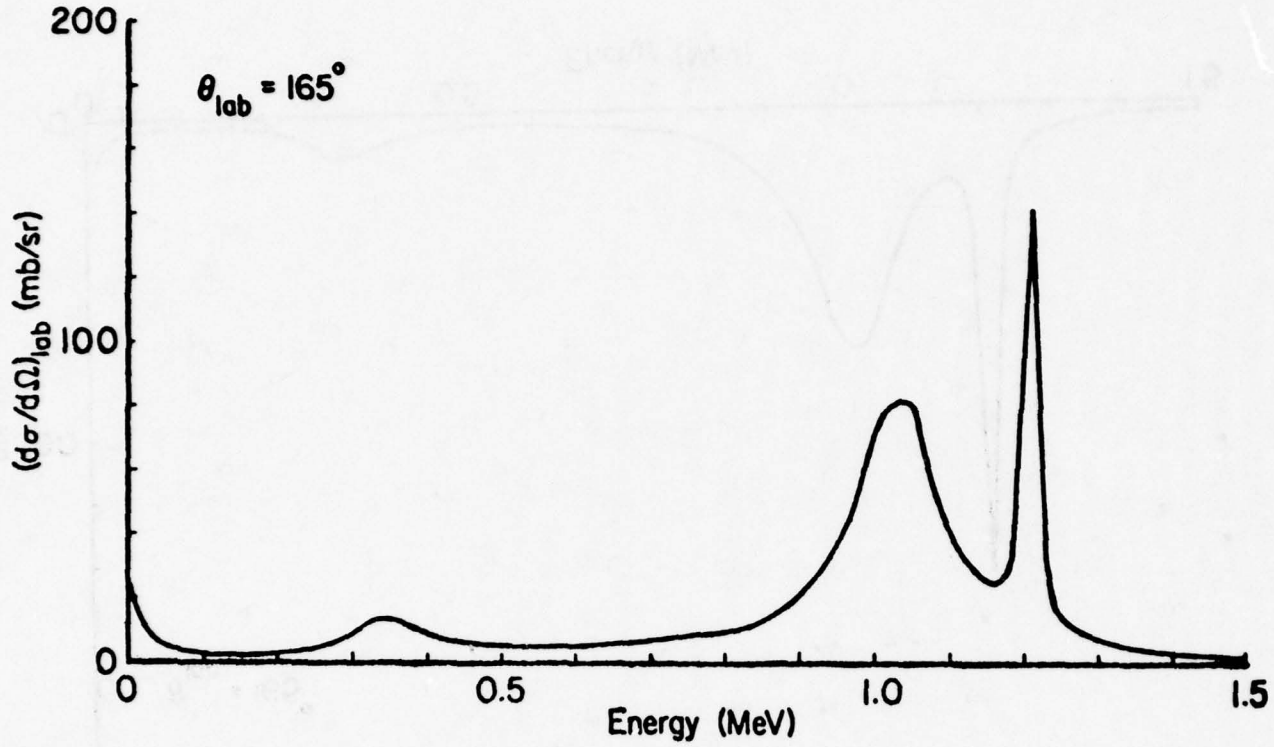

B.13a Possible differential cross section given by $d\sigma(338) - d\sigma(338/1028) + d\sigma(1028) - d\sigma(1028/1050a) + d\sigma(1050a) + d\sigma(1050a/1210) + d\sigma(1210)$.

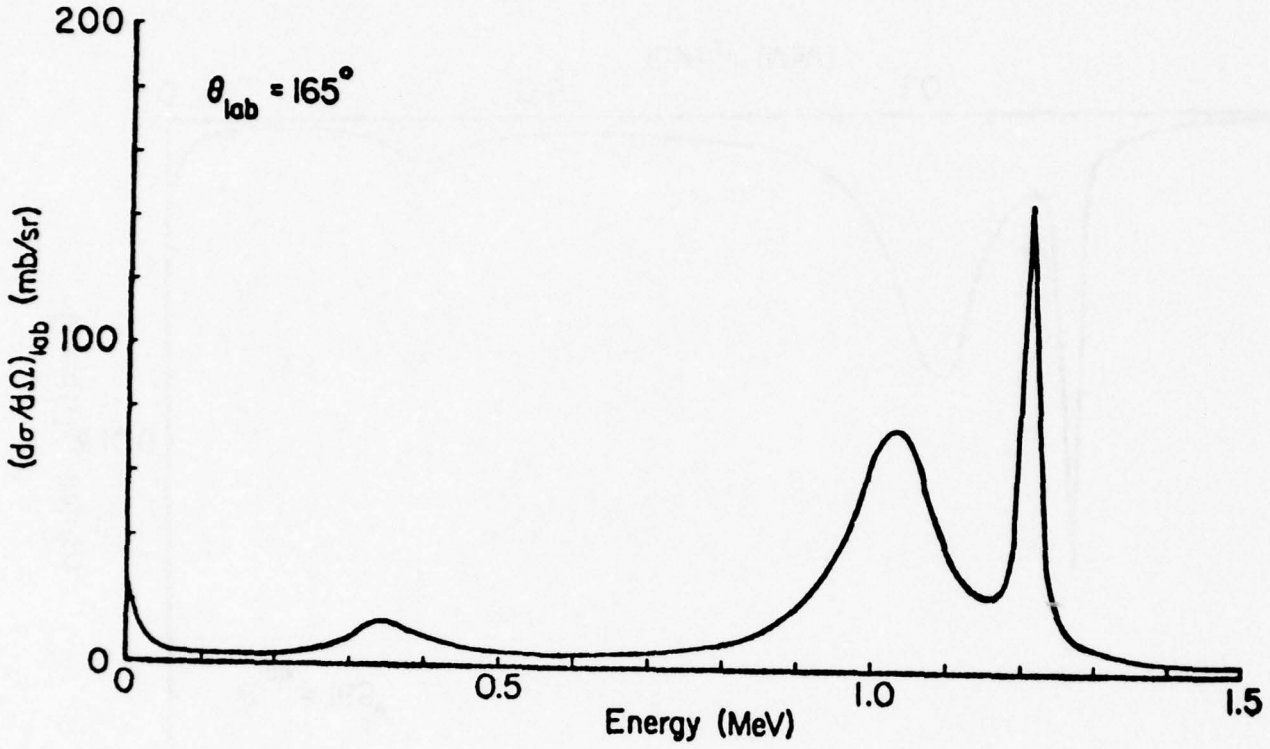

B.13b Possible differential cross section given by $d\sigma(338) - d\sigma(338/1028) + d\sigma(1028) - d\sigma(1028/1050b) + d\sigma(1050b) + d\sigma(1050b/1210) + d\sigma(1210)$.

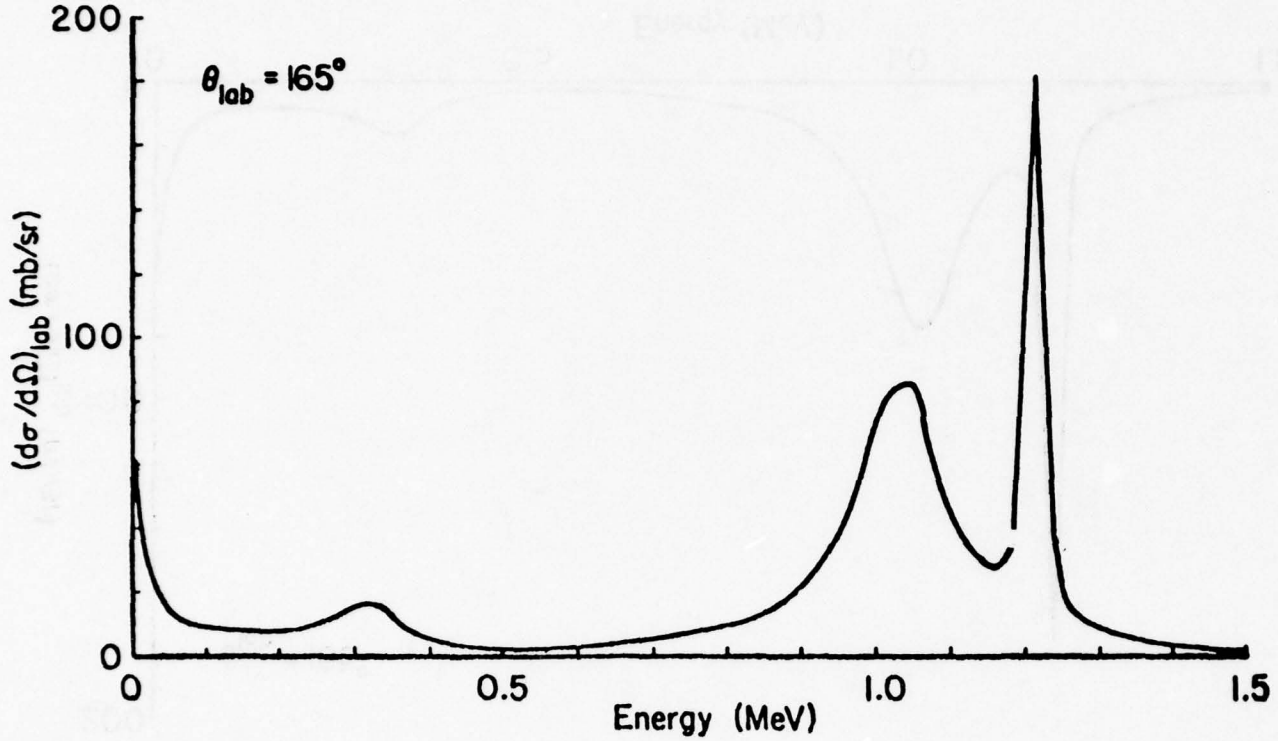

B.14a Possible differential cross section given by $d\sigma(338) + d\sigma(338/1028) + d\sigma(1028) - d\sigma(1028/1050a) + d\sigma(1050a) - d\sigma(1050a/1210) + d\sigma(1210)$.

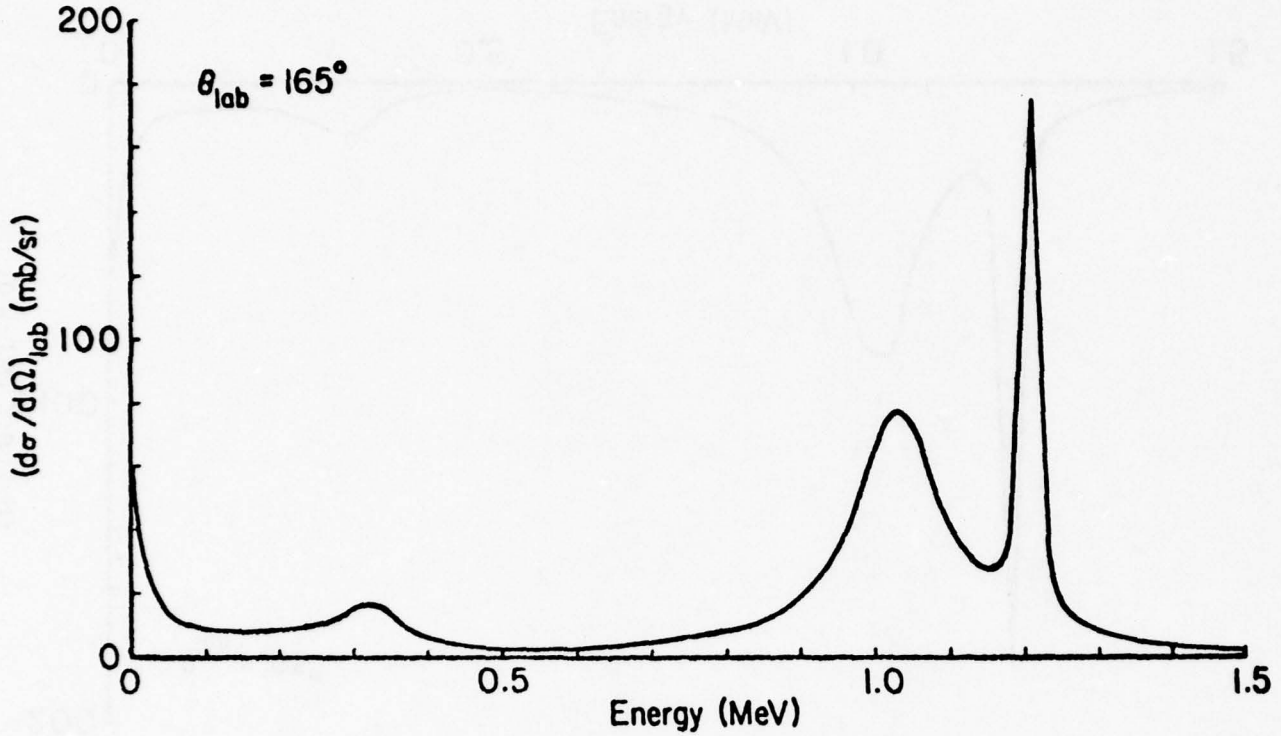

B.14b Possible differential cross section given by $d\sigma(338) + d\sigma(338/1028) + d\sigma(1028) - d\sigma(1028/1050b) + d\sigma(1050b) - d\sigma(1050b/1210) + d\sigma(1210)$.

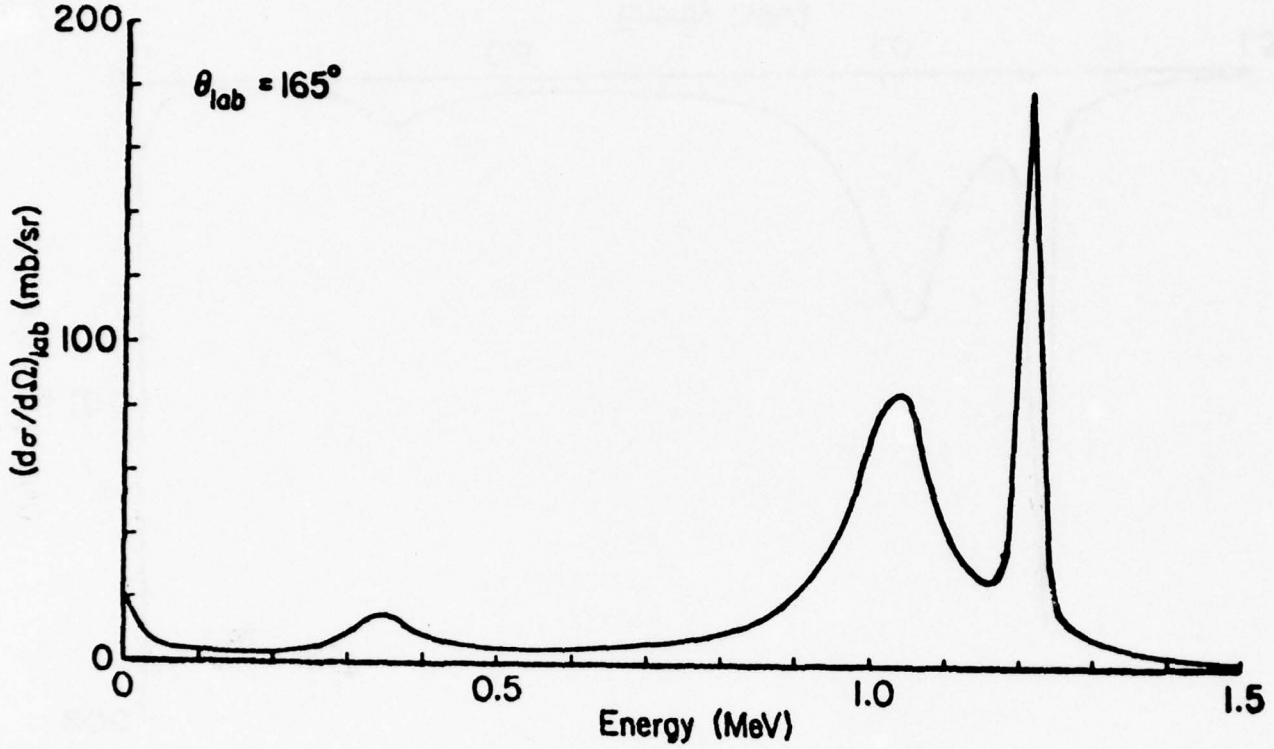

B.15a Possible differential cross section given by dσ(338) - dσ(338/1028) + dσ(1028) - dσ(1028/1050a) + dσ(1050a) - dσ(1050a/1210) + dσ(1210).

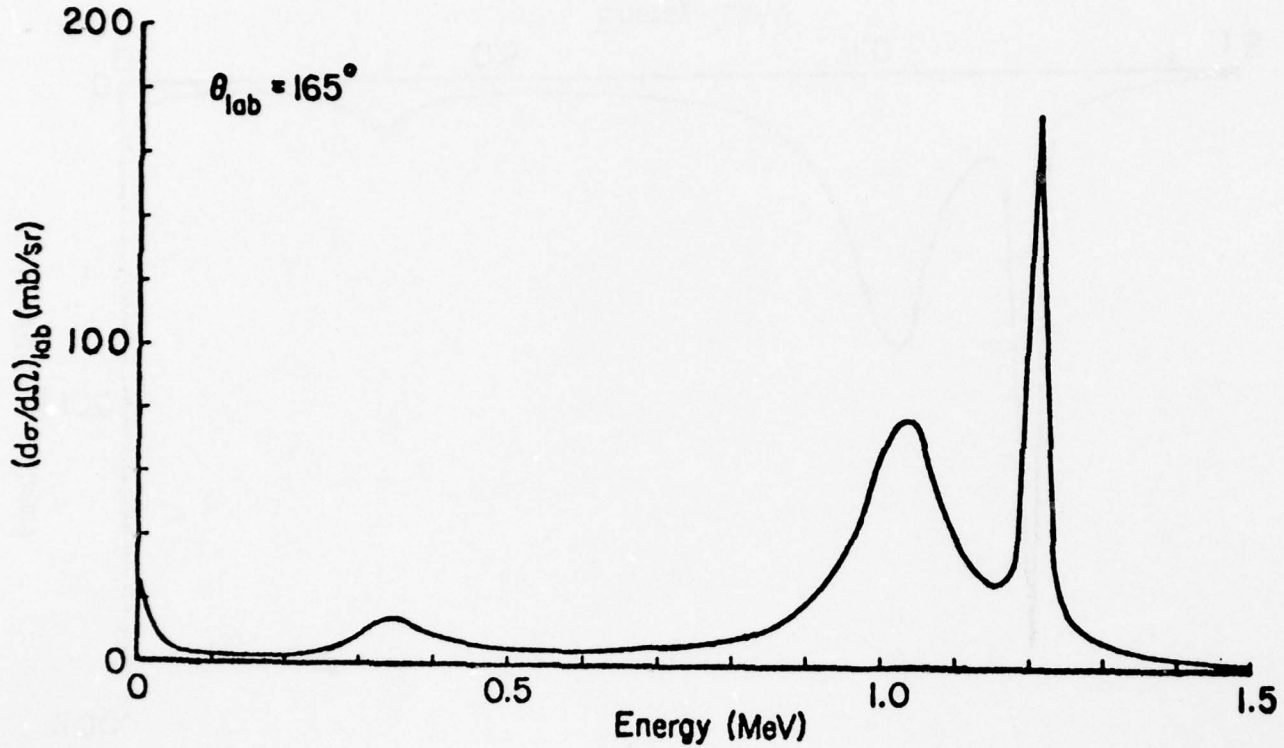

B.15b Possible differential cross section given by $d\sigma(338) - d\sigma(1338/1028) + d\sigma(1028) - d\sigma(1028/1050b) + d\sigma(1050b) - d\sigma(1050b/1210) + d\sigma(1210)$.

Monoenergetic proton beams (±1 keV), between 0.7 MeV and 1.5 MeV supplied by a 3.0 MeV Van de Graaff accelerator were used to obtain yield curves for each of the three samples. The typical beam current was 0.4 μA and the beam profile was elliptical with a major axis of 3 mm and a minor axis of 1 mm. The energetic alpha particles were detected at a laboratory scattering angle of 165^{o} with a partially depleted surface barrier detector (25 keV α resolution, 450 mm active area, and 100 μm depleted depth) which subtended a solid angle of 7.24×10^{-5} sr.

The yield curves were used to calculate the differential cross section using the following relationship:

$$N_o = N\, j \times \Delta\Omega \left(\frac{d\sigma(\theta)}{d\Omega}\right)_{lab} \qquad (B.51)$$

where N_o is the alpha yield, N is the nitrogen-15 density, j is the integrated proton flux, x is the sample thickness, and $\Delta\Omega$ is the solid angle of observation. No correction was included in the calculations for target thickness since the thickest target was only 8.7% of the narrowest resonance width.

Figures B.16-B.18 show the experimental differential cross sections for each of the three samples. The experimental uncertainities in each of the experimental points is due to counting statistics and the energy stability of the machine. Counting statistics lead to errors as large as ±50% at low values of the cross section and to ±2% at large values of the cross section. The uncertainities due

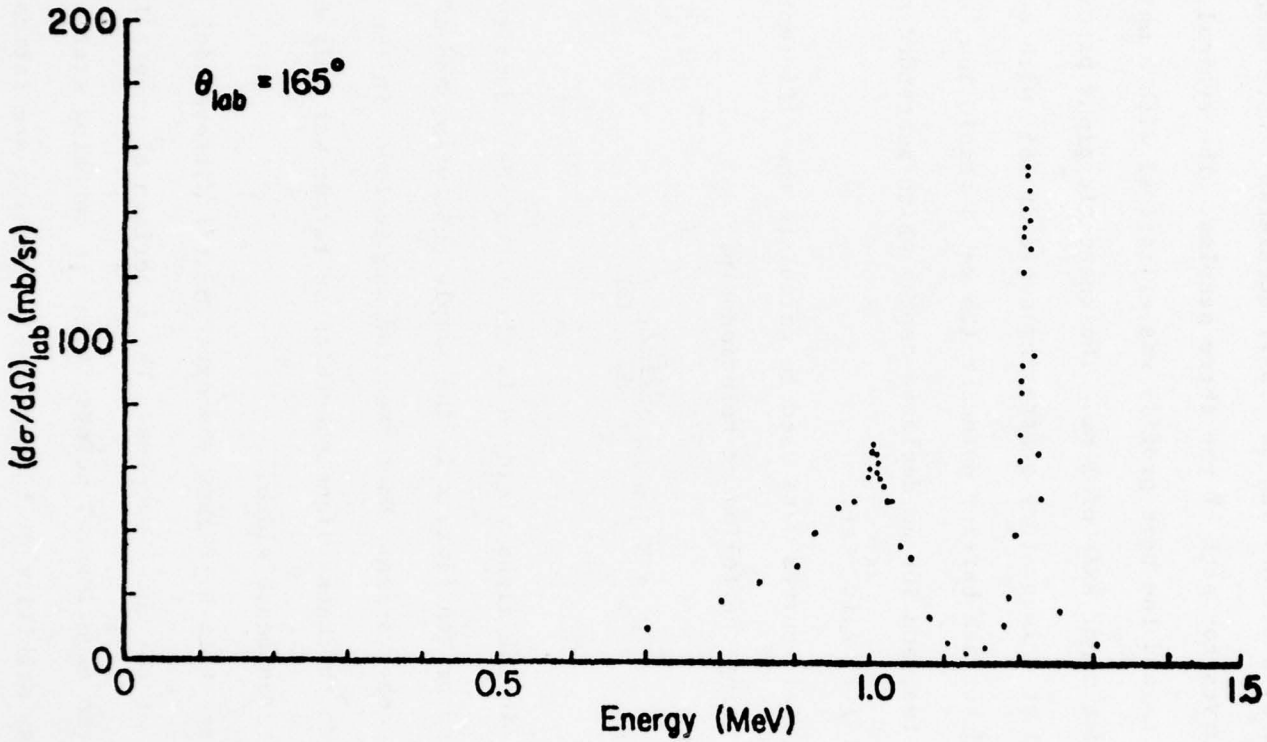

B.16 Experimental differential cross section using a 0.33 keV thick target.

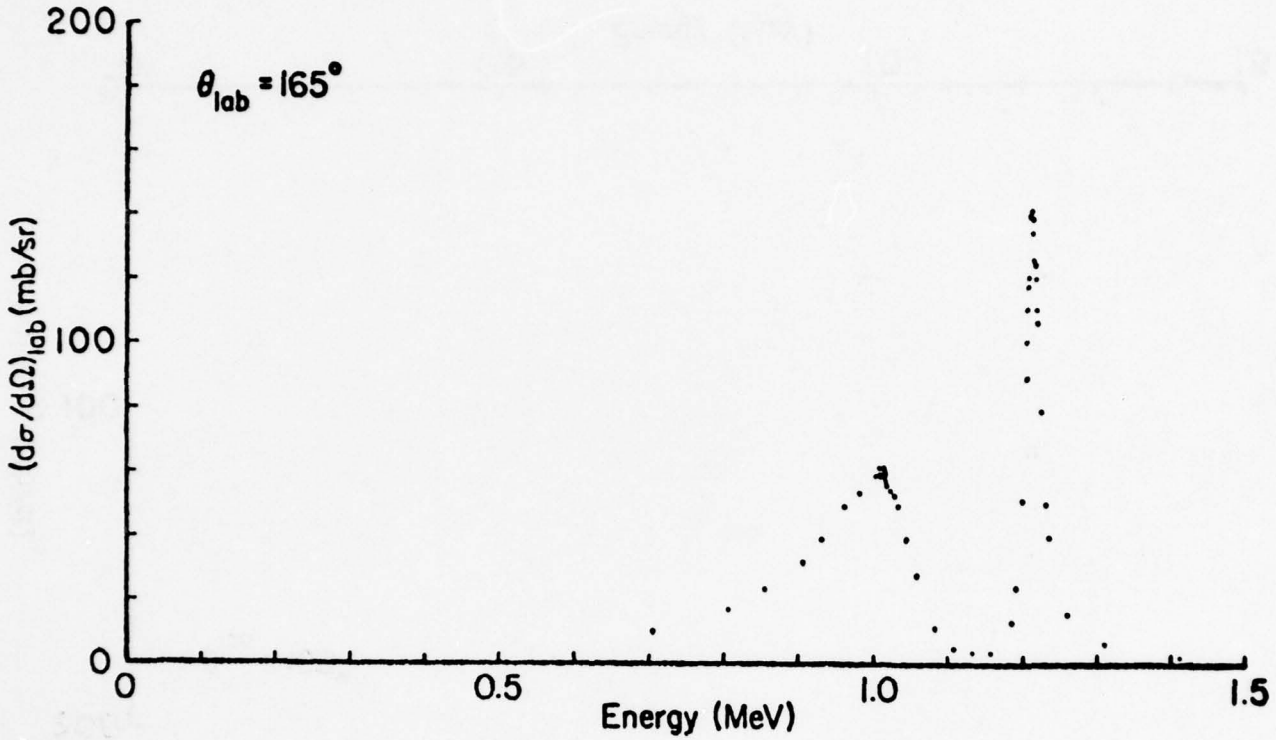

B.17 Experimental differential cross section using an 1.30 keV thick target.

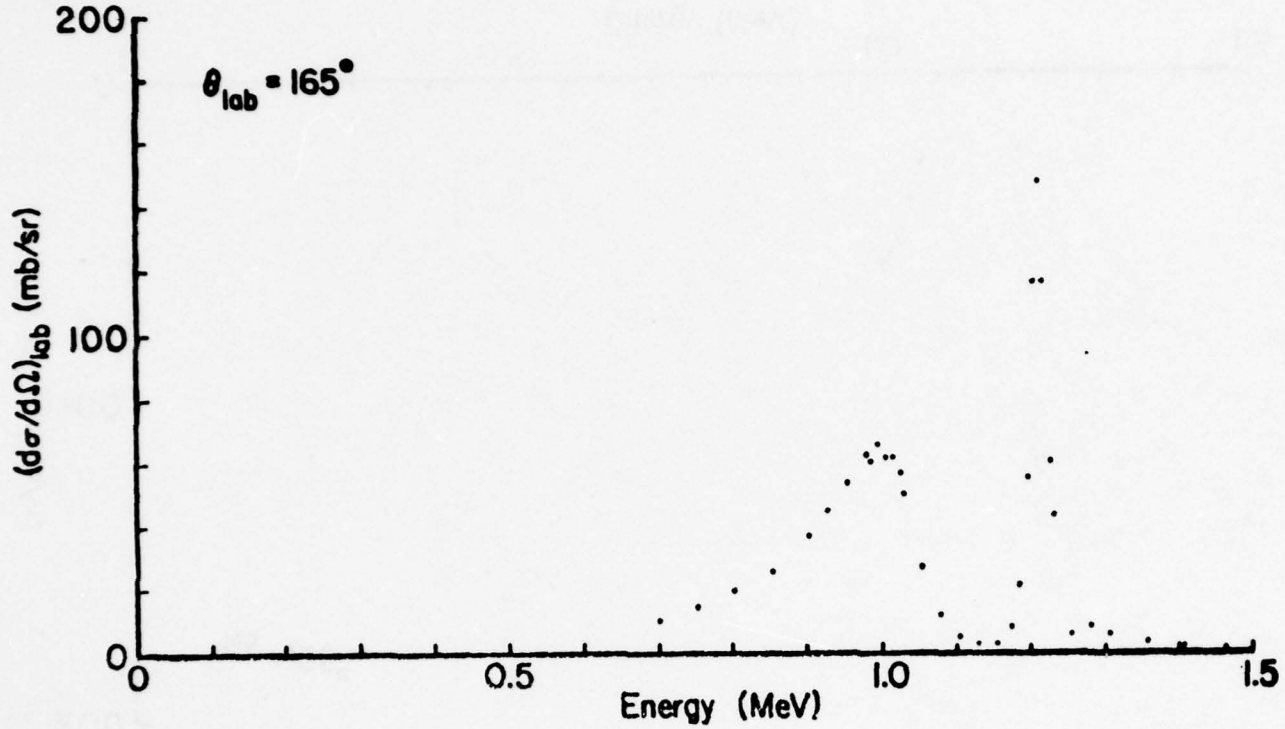

B.18 Experimental differential cross section using an 1.95 keV thick target.

to the energy stability of the Van de Graaff are equal to the derivative of the cross section with respect to energy at any point. Considering the experimental errors good agreement was found between the calculated cross sections from the three samples.

B.6 Comparison of Experimental and Theoretical Differential Cross Sections

Due to the large uncertainities in the experimentally measured cross section it is impossible to determine which of the theoretical curves, Figures B.8-B.15, best fits the experimental data. However, it is possible to estimate the resonance energies and resonance widths from the experimental data and compare them with the values given by Ajzenberg-Selove (164). These results are tabulated in Table B.2.

TABLE B.2

Comparison of Experimental Resonance Parameters

Target	E_{o_1} (keV)	Γ_{lab_1} (keV)	E_{o_2} (keV)	Γ_{lab_2} (keV)
0.33 keV	1004 ± 3	136 ± 15	1211 ± 1	21 ± 2
1.30 keV	1010 ± 5	156 ± 10	1213 ± 1	24 ± 1
1.95 keV	999 ± 15	161 ± 7	1210 ± 1	26 ± 1
Literature Value (164)	1028 ± 10	140 ± 10	1210 ± 3	22.5 ± 1

REFERENCES

1. Ceramics for High Performance Application; edited by Burke, J. J.; Gorum, A. E. and Katz, R. N.; Brook Hill, New York (1974).

2. Robin, R. C.; Ph.D. Dissertation, Case Western Reserve University (1971).

3. Fisher, J. C.; Journal of Applied Physics, 22, 74 (1951).

4. Whipple, R. T. P.; The Philosophical Magazine, 45, 1225 (1954).

5. Suzuoka, T.; Transactions of the Japanese Institute of Metals, 2, 25 (1961).

6. LeClaire, A. D.; British Journal of Applied Physics, 14, 351 (1963).

7. Levine, H. S. and MacCallum, C. J.; Journal of Applied Physics, 31, 595 (1960).

8. Borisov, V. G. and Lyubov, B. Y.; Fiz Metallev I Metallevedenie, 1, 298 (1958).

9. Lundy, T. S. and Federer, J. I.; Transactions of the Metallurgical Society of AIME, 224, 1285 (1962).

10. Smeltzer, W. W. and Desmaison, J. C.; Invited Review, NATO ASI-Nitrogen Ceramics, Canterbury, England (August 1976).

11. Wagner, Jr., J. B.; Mass Transport in Oxides; edited by Watchman, Jr., J. B. and Franklin, A. D. - National Bureau of Standards Special Publication 296, Washington.

12. Kofstad, P.; Nonstoichiometry, Diffusion, and Electrical Conductivity in Binary Metal Oxides; John Wiley and Sons, New York (1972).

13. Kingery, W. D.; Introduction to Ceramics; John Wiley and Sons, New York (1960) p.376.

14. Coble, R. L.; Journal of Applied Physics, 41, 4798 (1970).

15. Condit, R. H.; Holt, J. B. and Himmel, L.; Journal of The Electrochemical Society, 114, 1100 (1967).

16. Holt, J. B. and Almassy, M. Y.; Journal of the American Ceramic Society, 52, 631 (1969).

17. Kijima, K. and Shirasaki, S.; Journal of Chemical Physics, 65, 2668 (1976).

18. Samsonov, G. B.; Nonmetallic Nitrides (Metallurgia Moscow 1969).

19. Atkinson, A.; Leatt, P. J. and Moulson, A. J.; Proceedings of the British Ceramic Society, 22, 253 (1973).

20. Inomata, Y. and Vemura, Y; Yogyo-Kyokai-Shi, 85, 244 (1975).

21. Batha, D. and Whitney, E. D.; Journal of the American Ceramic Society, 56, 365 (1973).

22. Blakely, J. M.; Introduction to the Properties of Crystal Surfaces; Pergamon Press, New York (1973).

23. Wuensch, B. J. and Vasiles, T.; N00014-73-C-0212 (December 1975).

24. Brook, R. J.; Carruthers, T. G.; Bowen, L. J. and Weston, R. J.; NATO ASI-Nitrogen Ceramics, Canterbury, England (August 1976).

25. Oishi, Y.; Terai, R. and Veda, H.; Mass Transport Phenomena in Ceramics; edited by Cooper, A. R. and Heuer, A. H.; Plenum Press, New York (1975) p. 297-310.

26. Lou, V.; Private Communication.

27. Kossowsky, R.; Journal of *Materials Science*, 8, 1603 (1973).

28. Hofman, S. and Gauckler, L. J.; Powder Metallurgy International, 6, 90 (1974).

29. Powell, B. D. and Drew, P.; Journal of Materials Science, 9, 1987 (1974).

30. Lou, V.; Mitchell, T. E. and Heuer, A. H.; Bulletin of the American Ceramic Society (to be published).

31. Bart, R.; Private Communication.

32. Jack, K. H.; Journal of Materials Science, 11, 1134 (1976).

33. JANAF Thermochemical Tables; 2nd Edition; NSRDS-NBS 37 (June 1971).

34. Lindstrom, W. W. and Heuer, A. H.; Nuclear Instruments and Methods, 115, 1 (1974).

35. Williamson, C. F.; Boujot, J. P. and Picard, J.; CEA-R 3042 (1966).

36. Bevington, P. R.; Data Reduction and Error Analysis for the Physical Sciences; McGraw Hill, New York (1969) p. 54-65, 92-118.

37. Crank, J.; The Mathematics of Diffusion; Oxford (1970) p. 326.

38. Gauckler, L. J.; Lukas, H. L. and Tien, T. Y.; Materials Research Bulletin, 11, 503 (1976).

39. Major, Jr., L. D.; M. S. Thesis, Case Western Reserve University (1975) unpublished.

40. Williams, J. S.; Nuclear Instruments and Methods, 126, 205 (1975).

41. Harvey, B. G.; Introduction to Nuclear Physics and Chemistry; 2nd Edition; Prentice-Hall, New Jersey (1969) p. 236.

42. Moseley, H. G. J.; Philosophical Magazine, 26, 1024 (1963).

43. Johansson, T. B.; Akelsson, R. and Johansson, S. A. E.; Nuclear Instruments and Methods, 84, 141 (1970).

44. Valkovic, V.; Contemporary Physics, 14, 415 (1973).

45. Johansson, S. A. E. and Johansson, T. B.; Nuclear Instruments and Methods, 137, 473 (1976).

46. Mittler, A.; Barnes, B. K.; Litman, R.; Holton, F. and Barry, E. F.; Analytical Chemistry, 49, 432 (1977).

47. Patnaik, B. K. and Dhere, N. G.; Nuclear Instruments and Methods, 131, 503 (1975).

48. Seaman, G. G. and Shane, K. C.; Nuclear Instruments and Methods, 126, 473 (1975).

49. Katsanos, A.; Xenoulis, A.; Jadjiantoniou, A. and Fink, R. W.; Nuclear Instruments and Methods, 137, 119 (1976).

50. Rickards, J. and Ziegler, J. F.; Applied Physics Letters, 27, 707 (1975).

51. Sioshansi, P.; Lodhi, A. S. and Payrouan, H.; Nuclear Instruments and Methods, 142, 285 (1977).

52. Birks, L. S.; Analytical Chemistry, 49, 1505 (1977).

53. Shiokawa, T.; Chu, T. C.; Navarrette, V. R.; Kaji, H.; Izawa, G.; Ishii, K.; Morita, S. and Tawara, H.; Nuclear Instruments and Methods, 142, 199 (1977).

54. Chu, T. C.; Navarrette, V. R.; Kaji, H.; Izawa, G.; Shiokawa, T.; Ishii, K.; Morita, S. and Tawara, H.; Journal of Radioanalytical Chemistry, 36, 195 (1977).

55. Kemp, K. and Jensen, F. P.; Nuclear Instruments and Methods, 142, 101 (1977).

56. Walter, R. L.; Willis, R. D.; Gutnecht, W. F. and Shaw, Jr., R. W.; Nuclear Instruments and Methods, 142, 181 (1977).

57. Mangelson, N. F.; Hill, M. W.; Nielson, K. K. and Ryder, J. F.; Nuclear Instruments and Methods, 142, 133 (1977).

58. Deconninck, G.; Nuclear Instruments and Methods, 142, 275 (1977).

59. Hasselmann, I.; Koenig, W.; Richter, F. W.; Steiner, V.; Watjen, V.; Bode, J. C. and Ohta, W.; Nuclear Instruments and Methods, 142, 163 (1977).

60. Vis, R. D.; VanderKam, P.M.A. and Verheul, H.; Nuclear Instruments and Methods, 142, 159 (1977).

61. Persigehl, M.; Schicha, H.; Kasperek, K. and Feinendegen, L. E.; Journal of Radioanalytical Chemistry, 37, 611 (1977).

62. Van Rinsvelt, H. A.; Lear, R. D. and Adams, W. R.; Nuclear Instruments and Methods, 142, 171 (1977).

63. Valkovic, V.; Nuclear Instruments and Methods, 142, 151 (1977).

64. Ahlberg, M.; Nuclear Instruments and Methods, 131, 381 (1975).

65. Kropf, A.; Nuclear Instruments and Methods, 142, 79 (1977).

66. Benka, O.; Geretschlager, M. and Paul, H.; Nuclear Instruments and Methods, 142, 83 (1977).

67. Greiger, H. and Marsden, E.; Proceedings of the Royal Society, 82, 495 (1909).

68. Rutherford, E.; The Philosophical Magazine, 21, 669 (1911).

69. Turkevich, A.; Knelle, K.; Emmert, R. A.; Anderson, W. A.; Patterson, J. H. and Franzgate, E.; Review of Scientific Instruments, 37, 1681 (1966).

70. Turkevich, A.; Franzgrate, E. and Patterson, J. H.; Science, 158, 635 (1967).

71. Chu, W. K.; New Uses of Ion Accelerators; edited by Ziegler, J. F.; Plenum, New York (1975) p. 135-158.

72. Mayer, J. W. and Ullrich, B. M.; New Uses of Ion Accelerators; edited by Ziegler, J. F.; Plenum, New York (1975) p. 105-134.

73. Pieraux, S. T. and Vook, F. L.; Applied Physics Letters, 18, 191 (1971).

74. Mayer, J. W. and Tu, K. N.; Journal of Vacuum Science and Technology, 11, 86 (1974).

75. Ziegler, J. F. and Baglin, J. E. E.; Journal of Applied Physics, 42, 2031 (1971).

76. Morgan, D. V.; Journal of Physics D: Applied Physics, 7, 653 (1974).

77. Morgan, D. V. and Gittins, R. P.; Physica Status Solidi (a), 13, 517 (1972).

78. Wenz, R. P. and Hoffman, R. W.; Proceedings 7th International Vacuum Congress and 3rd International Conference on Solid Surfaces, Vienna (1977).

79. Wenz, R. P.; Ph.D. Dissertation, Case Western Reserve University (1977).

80. Chou, S.; Davidson, L. A. and Gibbons, J. F.; Applied Physics Letter, 17, 23 (1970).

81. Mackintosh, W. D.; Journal of Radioanalytical Chemistry, 17, 45 (1973).

82. Brown, F. and Mackintosh, W. D.; Journal of the Electrochemical Society, 120, 1096 (1973).

83. Silverman, P. J. and Schwartz, N.; Journal of the Electrochemical Society, 121, 550 (1974).

84. Hirvonen, J.; Revesz, A. G. and Kiskendale, T. D.; Thin Solid Films, 33, 315 (1976).

85. Mackintosh, W. D. and Plattner, H. H.; Journal of the Electrochemical Society, 124, 396 (1977).

86. Christodoulides, C. E.; Grant, W. A. and Williams, J. S.; Journal of the Electrochemical Society, 124, 1651 (1977).

87. Krautle, H.; Nuclear Instruments and Methods, 137, 553 (1976).

88. Schmid, K. and Ryssel, H.; Nuclear Instruments and Methods, 119, 287 (1974).

89. Mackenzie, C. D. and Armitage, B. H.; Nuclear Instruments and Methods, 133, 489 (1976).

90. Stark, J. and Wendt G.; Annal de Physique, 38, 921 (1912).

91. Picrauz, S. T.; New Uses of Ion Accelerators; edited by Ziegler, J. F.; Plenum, New York (1975) p. 229-281.

92. Mitchell, I. V.; Kamoshida, M. and Mayer, J. W.; Journal of Applied Physics, 42, 4378 (1971).

93. Rimini, E.; Haskell, J. and Meyer, J. W.; Applied Physics Letters, 20, 237 (1972).

94. Feldman, L. C. and Appleton, B. R.; Applied Physics Letters, 15, 305 (1969).

95. Quere, Y.; Journal of Nuclear Materials, 53, 262 (1974).

96. Finger, U.; Gartner, K.; Koch, H. D. and Trippensee, W.; Journal of Radioanalytical Chemistry, 28, 49 (1975).

97. Quere, Y.; Radiation Effects, 28, 253 (1976).

98. Turkenburg, W. C.; Soszka, W.; Saris, F. W.; Kersten, H. H. and Colenbrander, B. G.; Nuclear Instruments and Methods, 132, 587 (1976).

99. Jackson, D. P.; Nuclear Instruments and Methods, 132, 603 (1976).

100. Davis, J. A.; Jackson, D. P.; Mitchell, J. B.; Norton, P. R. and Tapping, R. L.; Nuclear Instruments and Methods, 132, 609 (1976).

101. Anderson, R. L.; D. Sc. Dissertation, Massachusetts Institute of Technology (1967).

102. Kuin, P. N. and Reynders, J. P.; Journal of Radioanalytical Chemistry, 16, 403 (1973).

103. Kirvan, V.; Swindle, D. L. and Schweikert, E. A.; Analytical Chemistry, 46, 1626 (1974).

104. Sellschop, J. P. F.; Reddy, R. J.; Mingay, D. W.; Renan, M. J. and Schuster, D. G.; International Journal of Applied Radiation and Isotopes, 26, 640 (1975).

105. Amsel, G.; Nadai, J. P.; D'Artemure, E.; David, D.; Girard, E. and Moulin, J.; Nuclear Instruments and Methods, 92, 481 (1971).

106. Choudhury, A.; Palmer, D. W.; Amsel, G.; Gurien, H. and Baruch, P.; Solid State Communications, 3, 119 (1965).

107. Palmer, D. W.; Nuclear Instruments and Methods, 38, 187 (1965).

108. Robin, R.; Cooper, A. R. and Heuer, A. H.; Journal of Applied Physics, 44, 3770 (1973).

109. Gass, J. E.; Muller, H. H.; Schmied, H.; Jorissen, L. and Ziffermayer, G.; Nuclear Instruments and Methods, 106, 109 (1973).

110. Ollerhead, R. W.; Almquist, E. and Kuehner, J. A.; Journal of Applied Physics, 37, 2440 (1966).

111. Mansour, N. A.; Saad, H. R.; Saleh, Z. A.; Sayed, E. M.; Zaloubvsky, I. I. and Gontcher, V. I.; Nuclear Physics, 65, 433 (1965).

112. Din, G. U.; AEC AT(11-1)-1120 (1966).

113. Amsel, G. and Samuel, D.; Analytical Chemistry, 39, 1689 (1967).

114. Croset, M.; Petreanu, E.; Samuel, D.; Amsel, G. and Nadai, J. P.; Journal of the Electrochemical Society, 118, 717 (1971).

115. Wise, P. J.; Barnes, D. G. and Neild, D. J.; Journal of Physics D: Applied Physics, 7, 1475 (1974).

116. Gass, J. and Muller, H. H.; Nuclear Instruments and Methods, 136, 559 (1976).

117. Shaudhri, M. A.; Burns, G.; Reen, E.; Rouse, J. L. and Spicer, B. M.; Journal of Radioanalytical Chemistry, 37, 243 (1977).

118. Moller, W.; Hufschmidt, H. and Kamke, D.; Nuclear Instruments and Methods, 140, 157 (1977).

119. Kregar, M.; Muller, J.; Rupnik, P. and Spiler, F.; Nuclear Instruments and Methods, 142, 495 (1977).

120. North, J. C. and Lightowlers, E. C.; Journal of the Electrochemical Society, 121, 593 (1974).

121. Schulte, R. L.; Nuclear Instruments and Methods, 137, 251 (1976).

122. Olivier, C.; Peisach, M. and Pierce, T. B.; Journal of Radioanalytical Chemistry, 32, 71 (1976).

123. Sundquist, B.; Gonzi, L.; Koersner, I.; Bergman, R. and Lindhj, U.; International Journal of Applied Radiation and Isotopes, 27, 273 (1976).

124. Yatsurugi, Y.; Akiyama, N.; Endo, Y. and Nozaki, T.; Journal of the Electrochemical Society, 120, 975 (1973).

125. Turos, A.; Wielunski, L. and Barez, A.; Nuclear Instruments and Methods, 111, 605 (1973).

126. Turos, A.; Wielunski, L. and Olenski, J.; Physica Status Solidi (a), 16, 211 (1973).

127. Neild, D. J.; Wise, P. J. and Barnes, D. G.; Journal of Physics D: Applied Physics, 5, 2292 (1972).

128. Turos, A.; Wielunski, L. and Jelinska, J.; Acta Physica Polonica, A43, 657 (1973).

129. Lightowlers, E. C.; North, J. C.; Jordan, A. S.; Derick, L. and Merz, J. L.; Journal of Applied Physics, 44, 4758 (1973).

130. Carnera, A.; Della Mea, G.; Drigo, A. V.; LoRusso, S. and Mazzoldi, P.; Journal of Noncrystalline Solids, 23, 123 (1977).

131. Amsel, G.; Beranger, G.; de Gelas, B. and Lacombe, P.; Journal of Applied Physics, 39, 2246 (1968).

132. Davis, D.; Amsel, G.; Boiset, P. and Beranger, G.; Journal of the Electrochemical Society, 122, 388 (1975).

133. Cox, B. and Roy, C.; Electrochemical Technology, 4, 121 (1966).

134. Lees, D. C.; Calvert, J. M. and Derry, D. J.; Proceeding of the Thomas Graham Memorial Symposium, University of Strathclude (1971).

135. Rawal, B. S.; M. S. Thesis, Case Western Reserve University (1973) unpublished.

136. Barnard, R. S.; M. S. Thesis, Case Western Reserve University (1974) unpublished.

137. Reddy, K. P. R.; M. S. Thesis, Case Western Reserve University (1977) unpublished.

138. Turos, A.; Wielunski, L.; Barcz, A. and Olenski, J.; Journal of Radioanalytical Chemistry, 16, 627 (1973).

139. Cherki, C. and Siejka, J.; Journal of the Electrochemical Society, 120, 784 (1973).

140. Cohen, B. L.; Fink, C. L. and Degnan, J. H.; Journal of Applied Physics, 43, 19 (1972).

141. Coetzee, P. P.; Pretorius, R. and Piesach, M.; The Journal of the South African Chemical Institute, 28, 104 (1975).

142. Coetzee, P. O.; Pretorius, R. and Piesach; Nuclear Instruments and Methods, 131, 299 (1975).

143. Shabason, L. and Choyke, W. J.; Nuclear Instruments and Methods, 138, 533 (1976).

144. Evans, R. D.; The Atomic Nucleus; McGraw Hill, New York (1955).

145. Pierce, T. B. and Huddleston, J.; Nuclear Instruments and Methods, 144, 231 (1977).

146. Mayer, J. W. and Turos, A.; Thin Solid Films, 19, 1 (1973).

147. Musket, R. G. and Baver, W.; Thin Solid Films, 19, 69 (1973).

148. Evans, Jr., C. A.; Analytical Chemistry, 47, 818A (1975).

149. Musket, R. G.; Nuclear Instruments and Methods, 144, 241 (1977).

150. Schardt, A.; Fowler, W. A. and Lauritsen, C. C.; Physical Review, 86, 527 (1952).

AD-A069 004 CASE WESTERN RESERVE UNIV CLEVELAND OHIO DEPT OF MET--ETC F/G 11/2
USE OF NUCLEARMICROANALYSIS. PART II. NUCLEAR MICROANALYSIS OF --ETC(U)
AUG 78 A R COOPER, L D MAJOR F33615-74-C-4029

UNCLASSIFIED AFML-TR-78-119-PT-2 NL

3 OF 3
AD
A069004

END
DATE
FILMED
7-79
DDC

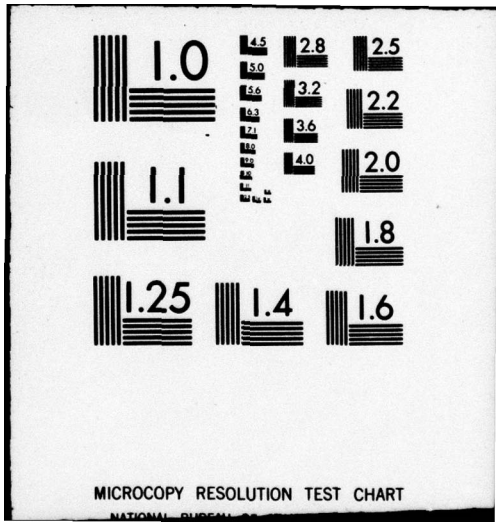
1.0
4.5
5.0
5.6
6.3
7.1
8.0
9.0
2.8
3.2
3.6
4.0
2.5
2.2
2.0
1.8
1.1
1.25
1.4
1.6
MICROCOPY RESOLUTION TEST CHART

151. Kraus, Jr., A. A.; French, A. P.; Fowler, W. A. and Lauritsen, C. C.; Physical Review, 89, 299 (1953).

152. Cohen, A. V. and French, A. P.; The Philosophical Magazine, 44, 1259 (1953).

153. Bashkin, S. and Carlson, R. R.; Physical Review, 106, 261 (1957).

154. Hagedern, F. B. and Marion, J. B.; Physical Review, 108, 1051 (1957).

155. Bashkin, S.; Carson, R. R. and Douglas, R. A.; Physical Review, 114, 1543 (1959).

156. Hebbard, D. G.; Nuclear Physics, 15, 289 (1960).

157. Ad'yasevich, B. P.; Antonenke, V. G.; Juznetsov, D. A.; Polunin, Yu. P. and Fomenko, D. E.; Soviet Journal of Nuclear Physics, 3, 290 (1966).

158. Cloud, S. D. and Ophel, T. R.; Nuclear Physics, A136, 592 (1969).

159. Rolfs, S. and Rodney, W. S.; Nuclear Physics, A235, 450 (1974).

160. Bethe, H. A.; Physical Review, 55, 103 (1939).

161. Bethe, H. A.; Physical Review, 55, 434 (1939).

162. Blatt, J. M. and Biedenharn, L. C.; Reviews of Modern Physics, 24, 258 (1952).

163. Bloch, I.; Hull, Jr., M. H.; Broyles, A. A.; Bouricius, W. G.; Freeman, B. E. and Breit, G.; Reviews of Modern Physics, 23, 147 (1951).

164. Ajzenberg-Selove, F.; Nuclear Physics A, A281, 46 (1977).

165. Biedenharn, L. C.; Tables of Racah Coefficients; ORNL 1098 (1952).

BIBLIOGRAPHY

Ad'yasevich, B. P.; Antonenke, V. G.; Juznetsov, D. A.; Polunin, Yu. P. and Fomenko, D. E.; Soviet Journal of Nuclear Physics, 3, 290 (1966).

Ahlberg, M.; Nuclear Instruments and Methods, 131, 381 (1975).

Ajzenberg-elove, F.; Nuclear Physics A, A281, 46 (1977).

Amsel, G.; Beranger, G.; de Gelas, B. and Lacombe, P.; Journal of Applied Physics, 39, 2246 (1968).

Amsel, G.; Nadai, J. P.; D'Artemure, E.; David, D.; Girard, E. and Moulin, J.; Nuclear Instruments and Methods, 92, 481 (1971).

Amsel, G. and Samuel, D.; Analytical Chemistry, 39, 1689 (1967).

Anderson, R. L.; D. Sc. Dissertation, Massachusetts Institute of Technology, (1967).

Atkinson, A.; Leatt, P. J. and Moulson, A. J.; Proceedings of the British Ceramic Society, 22, 253 (1973).

Barnard, R. S.; M.S. Thesis, Case Western Reserve University (1974) unpublished.

Bart, R,; Private Communication.

Bashkin, S. and Carlson, R. R.; Physical Review, 106, 261 (1957).

Bashkin, S.; Carlson, R. R. and Douglas, R. A.; Physical Review, 114, 1543 (1959).

Batha, D. and Whitney, E. D.; Journal of the American Ceramic Society, 56, 365 (1973).

Benka, O.; Geretschlager, M. and Paul, H.; Nuclear Instruments and Methods, 142, 83 (1977).

Bethe, H. A.; Physical Review, 55, 103 (1939).

Bethe, H. A.; Physical Review, 55, 434 (1939).

Bevington, P. R.; Data Reduction and Error Analysis for the Physical Sciences; McGraw Hill, New York (1969) p. 54-65, 92-118.

Biedenharn, L. C.; Tables of Racah Coefficients; ORNL 1098 (1952).

Birks, L. S.; Analytical Chemistry, 49, 1505 (1977).

Blakely, J. M.; Introduction to the Properties of Crystal Surfaces; Pergamon Press, New York (1973).

Blatt, J. M. and Biedenharn, L. C.; Reviews of Modern Physics, 24, 258 (1952).

Bloch, I.; Hull, Jr., M. H.; Broyles, A. A.; Bouricius, W. G.; Freeman, B. E. and Breit, G.; Reviews of Modern Physics, 23, 147 (1951).

Borisov, V. G. and Lyubov, B. Y.; Fiz Metallev I Metallevedenie, 1, 298 (1958).

Brook, R. J.; Carruthers, T. G.; Bowen, L. J. and Weston, R. J.; NATO ASI-Nitrogen Ceramics, Canterbury, England (August 1976).

Brown, F. and Mackintosh, W. D.; Journal of the Electrochemical Society, 120, 1096 (1973).

Carnera, A.; Della Mea, G.; Drigo, A. V.; LoRusso, S. and Mazzoldi, P.; Journal of Noncrystalline Solids, 23, 123 (1977).

Ceramics for High Performance Application; edited by Burke, J. J.; Gorum, A. E. and Katz, R. N.; Brook Hill, New York (1974).

Cherki, C. and Siejka, J.; Journal of the Electrochemical Society, 120, 784 (1973).

Chou, S.; Davidson, L. A. and Gibbons, J. F.; Applied Physics Letter, 17, 23 (1970).

Choudhury, A.; Palmer, D. W.; Amsel, G.; Gurien, H. and Baruch, P.; Solid State Communications, 3, 119 (1965).

Brown, F. and Mackintosh, W. D.; Journal of the Electrochemical Society, 120, 1096 (1973).

Chu, T. C.; Navarrette, V. R.; Kaji, H.; Izawa, G.; Shiokawa, T.; Ishii, K.; Morita, S. and Tawara, H.; Journal of Radioanalytical Chemistry, 36, 195 (1977).

Chu, W. K.; New Uses of Ion Accelerators; edited by Ziegler, J. F.; Plenum, New York (1975) p. 135-158.

Cloud, S. D. and Ophel, T. R.; Nuclear Physics, A136, 592 (1969).

Coble, R. L.; Journal of Applied Physics, 41, 4798 (1970).

Coetzee, P. P.; Pretorius, R. and Peisach, M.; The Journal of the South African Chemical Institute, 28, 104 (1975).

Coetzee, P. P.; Pretorius, R. and Peisach, M.; Nuclear Instruments and Methods, 131, 299 (1975).

Cohen, A. V. and French, A. P.; The Philosophical Magazine, 44, 1259 (1953).

Cohen, B. L.; Fink, C. L. and Degnan, J. H.; Journal of Applied Physics, 43, 19 (1972).

Condit, R. H.; Holt, J. B. and Himmel, L.; Journal of The Electrochemical Society, 114, 1100 (1967).

Cox, B. and Roy, C.; Electrochemical Technology, 4, 121 (1966).

Crank, J.; The Mathematics of Diffusion; Oxford (1970) p. 326.

Croset, M.; Petreanu, E.; Samuel, D.; Amsel, G. and Nadai, J. P.; Journal of the Electrochemical Society, 118, 717 (1971).

David, D.; Amsel, G.; Boiset, P. and Beranger, G.; Journal of the Electrochemical Society, 122, 388 (1975).

Davis, J. A.; Jackson, D. P.; Mitchell, J. B.; Norton, P. R. and Tapping, R. L.; Nuclear Instruments and Methods, 132, 603 (1976).

Deconninck, G.; Nuclear Instruments and Methods, 142, 275 (1977).

Din, G. U.; AEC AT(11-1)-1120 (1966).

Evans, Jr., C. A.; Analytical Chemistry, 47, 818A (1975).

Evans, R. D.; The Atomic Nucleus; McGraw Hill, New York (1955).

Feldman, L. C. and Appleton, B. R.; Applied Physics Letters, 15, 305 (1969).

Finger, U.; Gartner, K.; Koch, H. D. and Trippensee, W.; Journal of Radioanalytical Chemistry, 28, 49 (1975).

Fisher, J. C.; Journal of Applied Physics, 22, 74 (1951).

Gass, J. and Muller, H. H.; Nuclear Instruments and Methods, 136, 559 (1976).

Gass, J. E.; Muller, H. H.; Schmied, H.; Jorissen, L. and Ziffermayer, G.; Nuclear Instruments and Methods, 106, 109 (1973).

Greiger, H. and Marsden, E.; Proceedings of the Royal Society, 82, 495 (1909).

Hagedern, F. B. and Marion, J. B.; Physical Review, 108, 1051 (1957).

Harvey, B. G.; Introduction to Nuclear Physics and Chemistry; 2nd Edition; Prentice-Hall, New Jersey (1969) p. 236.

Hasselmann, I.; Koenig, W.; Richter, F. W.; Steiner, V.; Watjen, V.; Bode, J. C. and Ohta, W.; Nuclear Instruments and Methods, 142, 163 (1977).

Hirvonen, J.; Revesz, A. G. and Kinskendale, T. D.; Thin Solid Films, 33, 315 (1976).

Hofman, S. and Gauckler, L. J.; Powder Metallurgy International, 6, 90 (1974).

Holt, J. B. and Almassy, M. Y.; Journal of the American Ceramic Society, 52, 631 (1969).

Inomata, Y. and Vemura, Y.; Yogyo-Kyokai-Shi, 85, 244 (1975).

Jack, K. H.; Journal of Materials Science, 11, 1134 (1976).

Jackson, D. P.; Nuclear Instruments and Methods, 132, 603 (1976).

JANAF Thermochemical Tables; 2nd Edition; NSRDS-NBS 37 (June 1971).

JoJohansson, S.A.E. and Johansson, T. B.; Nuclear Instruments and Methods, 137, 473 (1976).

Johansson, T. B.; Akelsson, R. and Johansson, S.A.E.; Nuclear Instruments and Methods, 84, 141 (1970).

Katsanos, A.; Xenoulis, A.; Jadjiantoniou, A. and Fink, R. W.; Nuclear Instruments and Methods, 137, 119 (1976).

Kemp, K. and Jensen, F. P.; Nuclear Instruments and Methods, 142, 101 (1977).

Kingery, W. D.; Introduction to Ceramics; John Wiley and Sons, New York (1960) p. 376.

Kijima, K. and Shirasaki, S.; Journal of Chemical Physics, 65, 2668 (1976).

Kirvan, V.; Swindle, D. L. and Schweikert, E. A.; Analytical Chemistry, 46, 1626 (1974).

Kofstad, P.; Nonstoichiometry, Diffusion, and Electrical Conductivity in Binary Metals Oxides; John Wiley and Sons, New York (1972).

Kossowsky, R.; Journal of Materials Science, 8, 1603 (1973).

Kraus, Jr., A. A.; French, A. P.; Fowler, W. A. and Lauritsen, C. C.; Physical Review, 89, 299 (1953).

Krautle, H.; Nuclear Instruments and Methods, 137, 553 (1976).

Kregar, M.; Muller, J.; Rupnik, P. and Spiler, F.; Nuclear Instruments and Methods, 142, 495 (1977).

Dropf, A.; Nuclear Instruments and Methods, 142, 79 (1977).

Kuin, P. N. and Reynders, J. P.; Journal of Radioanalytical Chemistry, 16, 403 (1973).

LeClaire, A. D.; British Journal of Applied Physics, 14, 351 (1963).

Lees, D. C.; Calvert, J. M. and Derry, D. J.; Proceeding of the Thomas Graham Memorial Symposium, University of Strathclude (1971).

Levine, H. S. and MacCallum, C. J.; Journal of Applied Physics, 31, 595 (1960).

Lightowlers, E. C.; North, J. C.; Jordan, A. S.; Derick, L. and Merz, J. L.; Journal of Applied Physics, 44, 4758 (1973).

Lindstrom, W. W. and Heuer, A. H.; Nuclear Instruments and Methods, 115, 1 (1974).

Lou, V.; Private Communication

Lou, V.; Mitchell, T. E. and Heuer, A. H.; Bulletin of the American Ceramic Society (to be published).

Lundy, T. S. and Federer, J. I.; Transactions of the Metallurgical Society of AIME, 224, 1285 (1962).

Mackenzie, C. D. and Armitage, B. H.; Nuclear Instruments and Methods, 133, 489 (1976).

Mackintosh, W. D.; Journal of Radioanalytical Chemistry, 17, 45 (1973).

Mackintosh, W. D. and Plattner, H. H.; Journal of the Electrochemical Society, 124, 396 (1977).

Major, Jr., L. D.; M.S. Thesis, Case Western Reserve University (1975) unpublished.

Mangelson, N. F.; Hill, M. W.; Nielson, K. K. and Ryder, J. F.; Nuclear Instruments and Methods, 142, 133 (1977).

Mansour, N. A.; Saad, H. R.; Saleh, Z. A.; Sayed, E. M.; Zaloubvsky. I. I. and Gontcher, V. I.; Nuclear Physics, 65, 433 (1965).

Mayer, J. W. and Tu, K. N.; Journal of Vacuum Science and Technology, 11, 86 (1974).

Mayer, J. W. and Turos, A.; Thin Solid Films, 19, 1 (1973).

Mayer, J. W. and Ullrich, B. M.; New Uses of Ion Accelerators; edited by Ziegler, J. F.; Plenum, New York (1975) p. 105-134.

Mitchell, I. V.; Kamoshida, M. and Mayer, J. W.; Journal of Applied Physics, 42, 4378 (1971).

Mittler, A.; Barnes, B. K.; Litman, R.; Holton, F. and Barry, E. F.; Analytical Chemistry, 49, 432 (1977).

Moller, W.; Hufschmidt, H. and Kamke, D.; Nuclear Instruments and Methods. 140, 157 (1977).

Morgan, D. V.; Journal of Physics D: Applied Physics, 7, 653 (1974).

Morgan, D. V. and Gittins, R. P.; Physica Status Solidi (a), 13, 517 (1972).

Moseley, H.G.J.; Philosophical Magazine, 26, 1024 (1963).

Musket, R. G. and Baver, W.; Thin Solid Films, 19, 69 (1973).

Neild, D. J.; Wise, P. J. and Barnes, D. G.; Journal of Physics D: Applied Physics, 5, 2292 (1972).

North, J. C. and Lightowlers, E. C.; Journal of the Electrochemical Society, 121, 593 (1974).

Oishi, Y.; Terai, R. and Veda, H.; Mass Transport Phenomena in Ceramics; edited by Cooper, A. R. and Heuer, A. H., Plenum Press, New York (1975) p. 297-310.

Olivier, C.; Peisach, M. and Pierce, T. B.; Journal of Radioanalytical Chemistry, 32, 71 (1976).

Ollerhead, R. W.; Almquist, E. and Kuehner, J. A.; Journal of Applied Physics, 37, 2440 (1966).

Palmer, D. W.; Nuclear Instruments and Methods, 38, 187 (1965).

Patnaik, B. K. and Dhere, N. G.; Nuclear Instruments and Methods, 131, 503 (1975).

Persigehl, M.; Schicha, H.; Kasperek, K. and Feinendegen, L. E.; Journal of Radioanalytical Chemistry, 37, 611 (1977).

Picrauz, S. T.; New Uses of Ion Accelerators; edited by Ziegler, J. F.; Plenum, New York (1975) p. 229-281.

Pieraux, S. T. and Vook, F. L.; Applied Physics Letters, 18, 191 (1971).

Pierce, T. B. and Huddleston, J.; Nuclear Instruments and Methods, 144, 231 (1977).

Powell, B. D. and Drew, P.; Journal of Materials Science, 9, 1987 (1974).

Quere, Y.; Journal of Nuclear Materials, 53, 262 (1974).

Quere, Y.; Radiation Effects, 28, 253 (1976).

Rawal, B. S.; M.S. Thesis, Case Western Reserve University (1973) unpublished.

Reddy, K.P.R.; M.S. Thesis, Case Western Reserve University (1977) unpublished.

Rickards, J. and Ziegler, J. F.; Applied Physics Letters, 27, 707 (1975).

Rimini, E.; Haskell, J. and Meyer, J. W.; Applied Physics Letters, 20, 237 (1972).

Robin, R. C.; Ph.D. Dissertation, Case Western Reserve University (1971).

Robin, R.; Cooper, A. R. and Heuer, A. H.; Journal of Applied Physics, 44, 3770 (1973).

Rulfs, S. and Rodney, W. S.; Nuclear Physics, A235, 450 (1974).

Rutherford, E.; The Philosophical Magazine, 21, 669 (1911).

Samsonov, G. B.; Nometallic Nitrides (Metallurgia Moscow 1969).

Schardt, A.; Fowler, W. A. and Lauritsen, C. C.; Physical Review, 86, 527 (1952).

Schmid, K. and Ryssel, H.; Nuclear Instruments and Methods, 119, 287 (1974).

Schulte, R. L.; Nuclear Instruments and Methods, 137, 251 (1976).

Seaman, G. G. and Shane, K. C.; Nuclear Instruments and Methods, 126, 473 (1975).

Sellschop, J.P.F.; Reddy, R. J.; Mingay, D. W.; Renan, M. J. and Schuster, D. G.; International Journal of Applied Radiation and Isotopes, 26, 6640 (1975).

Shabason, L. and Choyke, W. J.; Nuclear Instruments and Methods, 138, 533 (1976).

Shaudhri, M. A.; Burns, G.; Reen, E.; Rouse, J. L. and Spicer, B. M.; Journal of Radioanalytical Chemistry, 37, 243 (1977).

Shiokawa, T.; Chu, T. C.; Navarrette, V. R.; Kaji, H.; Izawa, G.; Ishii, K.; Morita, S. and Tawara, H.; Nuclear Instruments and Methods, 142, 199 (1977).

Silverman, F. J. and Schwartz, N; Journal of the Electrochemical Society, 121, 550 (1974).

Sioshansi, P.; Lodhi, A. S. and Payrouan, H.; Nuclear Instruments and Methods, 142, 285 (1977).

Smeltzer, W. W. and Desmaison, J. C.; Invited Review, NATO ASI-Nitrogen Ceramics, Canterbury, England (August 1976).

Stark, J. and Wendt, G.; Annal de Physique, 38, 921 (1912).

Sundquist, B.; Gonzi, L.; Koersner, I.; Bergman, R. and Lindhj, U.; International Journal of Applied Radiation and Isotopes, 27, 273 (1976).

Suzuoka, T.; Transactions of the Japanese Institute of Metals, 2, 25 (1961).

Turkenburg, W. C.; Soszka, W.; Saris, F. W.; Kersten, H. H. and Colenbrander, B. G.; Nuclear Instruments and Methods, 132, 587 (1976).

Turkevich, A.; Franzgrate, E. and Patterson, J. H.; Science, 158, 635 (1967).

Turkevich, A.; Knelle, K.; Emmert, R. A.; Anderson, W. A.; Patterson, J. H. and Franzgate, E.; Review of Scientific Instruments, 37, 1681 (1966).

Turos, A.; Wielunski, L. and Barez, A.; Nuclear Instruments and Methods, 111, 605 (1973).

Turos, A.; Wielunski, L.; Barcz, A. and Olenski, J.; Journal of Tadioanalytical Chemistry, 16, 627 (1973).

Turos, A.; Wielunski, L. and Jelinska, J.; Acta Physica Polonica, A43, 657 (1973).

Turos, A.; Wielunski, L. and Olenski, J.; Physica Status Solidi (a), 16, 211 (1973).

Valkovic, V.; Contemporary Physics, 14, 415 (1973).

Valkovic, V.; Nuclear Instruments and Methods, 142, 151 (1977).

Van Rinsvelt, H. A.; Lear, R. D. and Adams, W. R.; Nuclear Instruments and Methods, 142, 171 (1977).

Vis, R. D.; VanderKam, P.M.A. and Verheul, H.; Nuclear Instruments and Methods, 142, 159 (1977).

Wagner, Jr., J. B.; Mass Transport in Oxides; edited by Watchman, Jr., J. B. and Franklin, A. D.; National Bureau of Standards Special Publication, 296, Washington.

Walter, R. L.; Willis, R. D.; Gutnecht, W. F. and Shaw, Jr., R. W.; Nuclear Instruments and Methods, 142, 181 (1977).

Wenz, R. P.; Ph.D. Dissertation, Case Western Reserve University (1977).

Wenz, R. P. and Hoffman, R. W.; Proceedings 7th International Vacuum Congress and 3rd International Conference on Solid Surfaces, Vienna (1977).

Whipple, R.T.P.; The Philosophical Magazine, 45, 1225 (1954).

Williams, J. S.; Nuclear Instruments and Methods, 126, 205 (1975).

Williamson, C. F.; Boujot, J. P. and Picard, J.; CEA-R 3042 (1966).

Wise, P. J.; Barnes, D. G. and Neild, D. J.; Journal of Physics D: Applied Physices, 7, 1475 (1974).

Wuensch, B. J. and Vasiles, T.; NOOOk4-73-C-0212 (December 1975).

Yatsurugi, Y.; Akiyama, N.; Endo, Y. and Nozaki, T.; Journal of The Electrochemical Society, 120, 975 (1973).

Ziegler, J. F. and Baglin, J.E.E.; Journal of Applied Physics, 42, 2031 (1971).

*U.S.Government Printing Office: 1979 — 657-002/552